2013

Endogenous and exogenous modulation of regulator of G-protein signaling 4

Carlos Aaron Monroy
University of Iowa

ENDOGENOUS AND EXOGENOUS MODULATION OF REGULATOR OF G-PROTEIN SIGNALING 4

by

Carlos Aaron Monroy

A thesis submitted in partial fulfillment of the requirements for the Doctor of Philosophy degree in Pharmacy (Medicinal and Natural Products Chemistry) in the Graduate College of The University of Iowa

August 2013

Thesis Supervisor: Assistant Professor David L Roman

Graduate College
The University of Iowa
Iowa City, Iowa

CERTIFICATE OF APPROVAL

PH. D. THESIS

This is to certify that the Ph. D. thesis of

Carlos Aaron Monroy

has been approved by the Examining Committee for the thesis requirement for the Doctor of Philosophy degree in Pharmacy (Medicinal and Natural Products Chemistry) at the August 2013 graduation.

Thesis Committee:

David L Roman, Thesis Supervisor

Jonathan A Doorn

Michael W Duffel

Rory A Fisher

Robert J Kerns

To my loving parents, Carmen and Carlos, and my sister, Candice, for always believing in me

ACKNOWLEDGMENTS

I would like to thank several people for their help throughout my graduate career. First I would like to thank my lab mates Chris Bodle, Michael Hayes, Colin Higgins, and Duncan Mackie for their supportive insight into my own work and the field we study. I would also like to thank the lab's technician Michelle Kroc for keeping and maintaining the lab.

Outside my department I also had the benefit of receiving help in learning new techniques and methodologies to expand my research. Dr DJ Murry and Armando Colorado were both instrumental in my understanding of mass spectrometry. Additionally, I would like Dr Jon Houtman for training me in isothermal titration calorimetry.

I thank The College of Pharmacy for accepting me to the program. And finally, I would like to thank Dr David Roman for accepting me into his lab and taking me on as his first graduate student.

TABLE OF CONTENTS

LIST OF TABLES

LIST OF FIGURES

LIST OF ABBREVIATIONS

1-methyl-4-phenyl-1,2,3,6-tetradropyridine	(MPTP)
3,4-Dihydroxyphenylacetaldehyde	(DOPAL)
4-Hydroxy-2-Nonenal	(4HNE)
6-hydroxydopamine	(6-OHDA)
Assay Buffer	(AB)
Bovine Serum Albumin	(BSA)
cAMP-responsive Element Binding Protein 1	(CREBP1)
CCAAT / Enhancer Binding Protein ß	(CEBPB)
Developing Solution	(DS)
Disheveled-EGL_{10}-Pleckstrin Homology	(DEP)
G-protein Coupled Receptor	(GPCR)
Gɣ Like	(GGL)
GTPase Accelerating Protein	(GAP)
guanosine diphosphate	(GDP)
guanosine triphosphate	(GTP)
High-Throughput Screening	(HTS)
Human Zinc Finger Protein	(ZF35)
Immunoblot	(IB)
Immunoprecipitation	(IP)
Interferon-Stimulated Response Element	(ISRE)
Ischemia / Reperfusion Injury	(IRI)

Isothermal Titration Calorimetry	(ITC)
Leucine-rich Repeat Kinase 2	(LRRK2)
Malachite Green Assay Buffer	(MGB)
Maltose Binding Protein	(MBP)
Mass Spectrometry	(MS)
Parkinson Protein 7	(DJ-1)
Parkinson's Disease	(PD)
PTEN-induced Putative Kinase 1	(PINK1)
PSD95/Dlg1/zo-1	(PDZ)
Reactive Oxygen Species	(ROS)
Regulator of G-protein Signaling	(RGS)
RGS Homology	(RH)
Steroidogenic Factor 1	(SF1)
Terrific Broth	(TB)
Tobacco Etch Virus	(TEV)
Transient Receptor Potential Anrkyrin 1	(TRPA1)
Tyrosine Hydroxylase	(TH)
Vesicular Monoamine Transporter 2	(VMAT2)

CHAPTER 1

INTRODUCTION

Parkinson's disease (PD) is a progressive neurodegenerative disorder mainly affecting elderly patients. PD is the second most common neurodegenerative disorder, affecting 2% of the world population over 50 years old, about 6 million worldwide [1]. PD was first identified in 1817 by James Parkinson as a shaking palsy, "an involuntary tremulous motion with lessened muscular power." [2]. The clinical characterization of this disease has been expanded to include the motor symptoms originally described such as resting tremor, bradykinesia, rigidity, and postural instability as well as cognitive deficits including anxiety, depression and memory deficits. The cognitive deficits are believed to be the result of Lewy body formation [3]. Lewy bodies are inclusions, primarily consisting of α-synuclein, that form within the cytoplasm and neuronal processes of the substantia nigra, as well as other parts of the brain, and are a hallmark of PD progression [4]. The death of dopaminergic neurons in the substantia nigra pars compacta and subsequent loss of dopaminergic signaling results in the motor deficits [5]. The motor symptoms begin to manifest after the loss of 40 - 60% of the dopaminergic signaling in the striatum [6]. This loss is thought to be the combination of multiple environmental and genetic risk factors. The most prevalent risk factor for PD development is age [5]. It is thought that age-

dependent changes in neuronal homeostasis may initiate or exacerbate neurodegeneration. 10 - 20% of patients posses some family history of PD [7]. Evaluation of these cases for linked genetic mutations has revealed six genes to be risk factors for PD: α-synuclein, ubiquitin C-terminal hydrolase, parkin, leucine-rich repeat kinase 2 (LRRK2), PTEN-induced putative kinase 1 (PINK1) and parkinson protein 7 (DJ-1) [8-13]. In the remaining sporadic cases, this loss is thought to be the result of a substantial oxidative stress insult from a variety of environmental toxins, such as 1-methyl-4-phenyl-1,2,3,6-tetradropyridine (MPTP) and select pesticides [14]. The prevalence of PD as well as the severity of its symptoms has lead to a substantial investment in understanding the pathology and developing treatments for the disease.

Parkinson's Disease: Identification of a New Therapeutic Target

To evaluate PD at the whole organism level, a variety of animal models have been devised. Direct study of mutations prevalent in PD patients has led to the development of several mouse models. These models include mutations in either autosomal dominant PD (α-synuclein and LRRK2), or autosomal recessive PD (PINK1, parkin and DJ-1) [15-17]. Mutations in α-synuclein, parkin, and ubiquitin C-terminal hydrolase contribute to PD

through Lewy body formation through protein misfolding or disruption of ubiquitin ligase activity [18-19,9]. Mutations in DJ-1 and PINK1 function through oxidative stress mechanisms, specifically by deletion of a strong antioxidant (DJ-1) or disruption of normal mitochondrial function [20,12]. The mechanism of LRRK2 induction of PD symptoms is not well understood. These mutations correspond to only about 10% of the reported cases of PD and are therefore less interesting than neurotoxic models of PD [21]. Of the neurotoxic models their are two modes of induction: reversible and irreversible. The reversible model commonly uses methyl(1R,15S,17R,18R, 19S,20S)-6,18-dimethoxy-17-(3,4,5-trimethoxybenzoyl)oxy-1,3,11,12,14,15,16, 17,18,19,20,21-dodecahydroyohimban-19-carboxylate (reserpine), a vesicular monoamine transporter 2 (VMAT2) inhibitor [22]. Inhibition of VMAT2 blocks packaging of dopamine, serotonin, and norepinephrine in vesicles for later release into the synapse, mimicking dopamine depletion in PD [23]. In the irreversible model of PD, mice are treated with MPTP, 6-hydroxydopamine (6-OHDA), or rotenone. Each of these compounds generate reactive oxygen species (ROS) as a critical component of their mechanism of action [24-27]. Of these models, the irreversible model using 6-OHDA lesioning remains one of the most popular models for evaluating PD.

The model for 6-OHDA is generated by direct injection into either the substantia nigra pars compacta, the median forebrain bundle, or the striatum for the targeted destruction of dopaminergic neurons. Location of injection is

usually selected based on the desired avoidance of mechanical damage to various regions of the brain but the substantia nigra pars compacta is most commonly chosen due to the use of a single injection site for both toxin and drug treatment [28]. 6-OHDA is typically dosed with a selective noradrenaline reuptake inhibitor to protect noradrenergic neurons from 6-OHDA induced toxicity [29]. Following injection, 6-OHDA selectively destroys catecholaminergic neurons through significant ROS production within those cells. This depletes the affected area of about 60% of tyrosine hydroxylase (TH) positive cells, a key marker of dopaminergic neurons, as well as eliminating TH positive terminals from the striatum [25]. In a recent study investigating potential pathways for the development of the motor symptoms of PD, regulator of G-protein signaling (RGS) 4 was identified as a critical mediator of these symptoms in a 6-OHDA lesion model [30].

RGS Proteins: Temporal Modulators of G-Protein Signaling

RGS proteins are modulators of G-protein coupled receptor (GPCR) signaling. GPCRs are a class of seven-transmembrane proteins which represent about 4% of the total protein coding human genome [31]. This diverse group of receptors signal through coupling to a heterotrimeric G-protein complex, consisting of a G-α, -ß, and -ɣ proteins. GPCR activation

typically occurs when a ligand binds to the receptor or a bound ligand is induced to the active confirmation, such as light catalyzed cis-to-trans isomerization of (2E,4Z,6E,8E)-3,7-dimethyl-9-(2,6,6-trimethylcyclohexen-1-yl)nona-2,4,6,8-tetraen-1-ol (retinol) activation of rhodopsin, and induces the active confirmation of the receptor [32]. Upon GPCR stimulation, the receptor facilitates the exchange of guanosine diphosphate (GDP) for guanosine triphosphate (GTP) within the Gα subunit. This causes the disassociation of the heterotrimer from the GPCR as well as the separation of the Gα subunit from the heterodimer, Gβɣ, and both go on to affect their various downstream targets. Signaling terminates upon hydrolysis of GTP within the Gα subunit and subsequent reasssociation of the Gα and Gβɣ subunits. In the initial study of GPCR signaling, using rhodopsin as a model, $G\alpha_t$ was found to have a GTPase rate of 1 - 2 min^{-1}, but in rod cells the signal returns to baseline in under 200 ms [33]. To explain this discrepancy, there must be a GTPase accelerating protein (GAP) involved in normal neuronal signaling. RGS9 was identified as a specific GAP for $G\alpha_t$ and confirmed RGS protein necessity in GPCR signaling, illustrated in Figure 1.1 [34].

RGS proteins temporally modulate GPCR signaling through their GAP activity. RGS proteins have poor affinity for both the GDP and GTP bound forms of the Gα subunit, but have a substantially greater affinity, 50 fold over the basal rate, for the transition state mimic using GDP-AlF_4^- [35]. RGS proteins GAP activity is the product of this high affinity for the

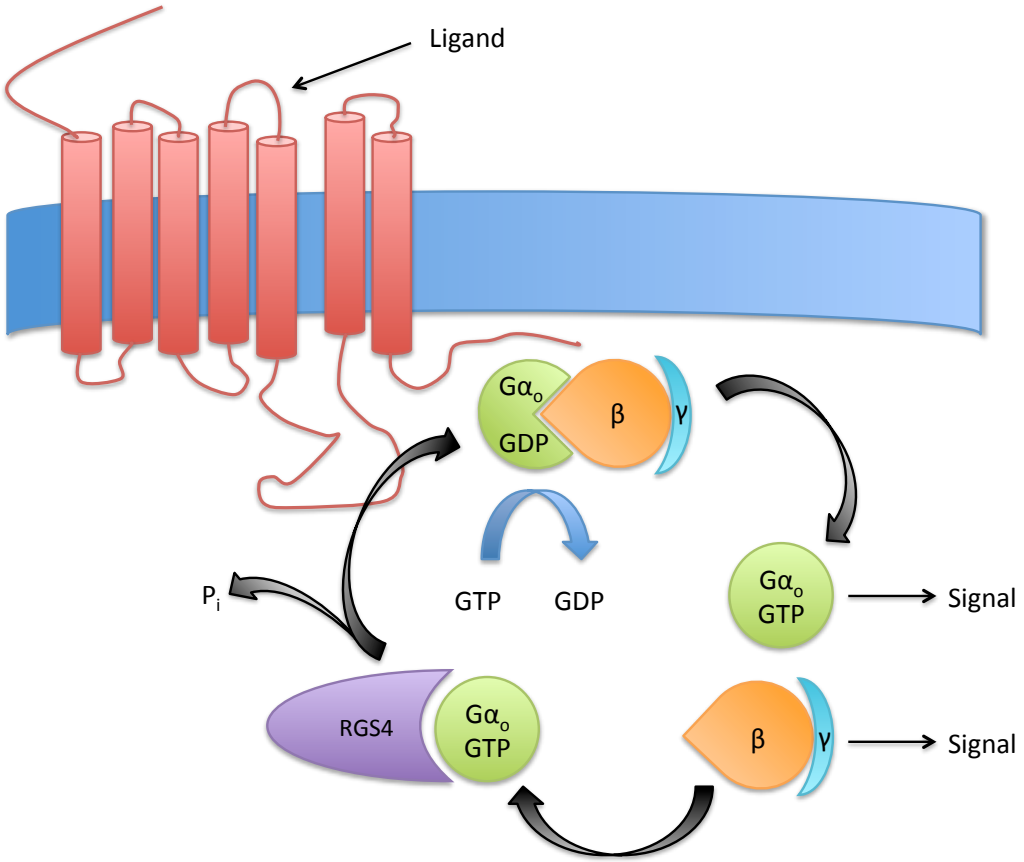

Figure 1.1 The G-Protein Cycle. Upon binding of a ligand to a GPCR, GDP is exchanged for GTP within the Gα subunit. This results in disassociation of the heterotrimeric complex from the GPCR and separation of the Gα from the Gß/ɣ subunits. This signal is terminated by hydrolysis of GTP to GDP, which may be accelarated by the introduction of an RGS protein, and reassociation of the hetertrimeric G-protein complex.

transition state of the Gα subunit, through interaction with key residues of the Gα subunit known as the switch I, II, and III regions [36]. These switch regions are integrally involved in the GTP hydrolysis activity of Gα subunit and interact with residues highly conserved among RGS proteins, in RGS4 these residues are identified as serine 85, glutamate 87, asparagine 88, leucine 159, aspartate 163, serine 164. and arginine 167 [36].

While extremely diverse, all RGS proteins contain a 125 amino acid domain termed the RGS homology (RH) domain [37]. This highly conserved RH domain represents the identifying component of this diverse group of negative regulators of Gα signaling with between 25 -85% sequence identity between members [38]. This family of proteins interacts with inhibitory Gα subunits, including $G\alpha_i$ and $G\alpha_o$, and $G\alpha_q$, but not the stimulatory $G\alpha_s$ [39]. RGS proteins are divided into several subfamilies, R4, R7, R12, and RZ, based on sequence identity within their RH domain [40]. R4 family members are the smallest of any of the subfamilies, except of RGS3, consisting of little more than the RH domain and a small N-terminal and C-terminal flanking regions, except for RGS3. RGS3, identified through high sequence similarity to RGS2, contains a PSD95/Dlg1/zo-1 (PDZ) domain [41]. Despite the relatively small size (20 - 30kDa), R4 subfamily members interact with a variety of proteins including receptors, adenylate cyclase, and phospholipase Cß [42]. R4 members are similarly promiscuous among Gα subunits, interacting with $G\alpha_i$, $G\alpha_o$, and $G\alpha_q$. The amphipathic α-helix in the N-terminus provides plasma membrane localization [43]. The R7 subfamily of RGS proteins are described as containing a disheveled-EGL_{10}-Pleckstrin homology (DEP) domain required for R7 binding protein association, used for membrane association [44]. Another component of R7 subfamily members is the Gγ-like (GGL) domain which allows for association of R7 members and $G\beta_5$ subunits. The R12 subfamily contain GoLoco domains which can prevent

the exchange of GDP for GTP within the Gα subunit as well as prevent association of the Gß/ɣ [45-46]. The RZ subfamily is the least well-studied group of RGS proteins whose members all contain a characteristic polycysteine string [47]. This N-terminal motif is a target for palmitoylation which may be used for subcellular trafficking as well as protein stability. These effectors are enticing targets for modulating signaling pathways, including the previously identified PD target RGS4.

RGS4 and Drug Development

RGS4 is a member of the R4 subfamily of RGS proteins. Often used as the prototypic RGS protein it contains little more than an RGS domain, shown in Figure 1.2a. The RGS4 gene contains five splice variants. Isoforms 1 and 2, despite different first exons code for the same 205 amino acid protein. Isoform 3 codes for a long N-terminus, adding an additional 97 amino acids. Isoform 4 codes for a truncated form of RGS4, lacking the majority of the RH domain. Isoform 5 is another truncated isoform that lacks the first 18 amino acids [48]. RGS4 is predominantly expressed in the heart and brain [49-50]. In failing hearts, RGS4 expression increases in response to hypertrophy [51]. The high expression of RGS4 in most cortical neuron layers has lead to an investigation into the physiological role of RGS4 in the brain,

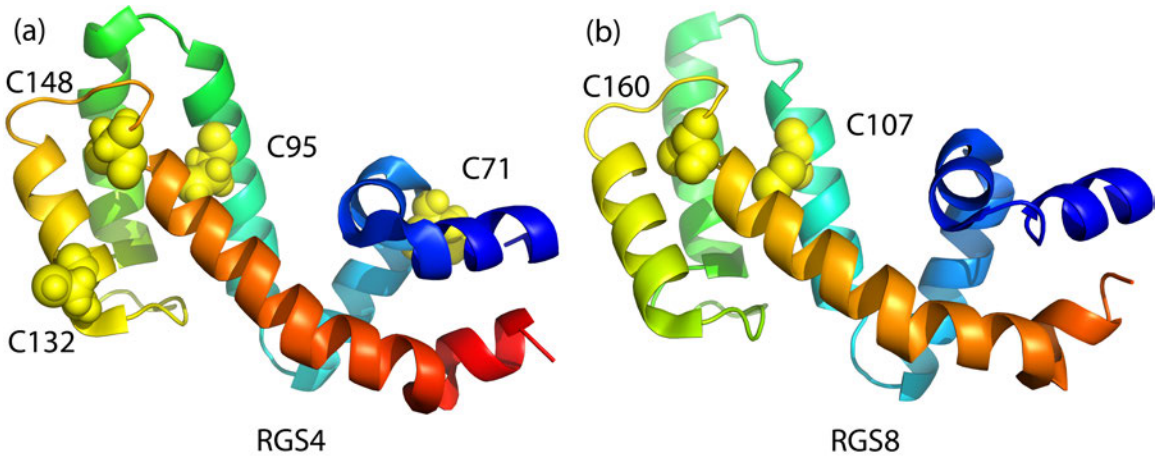

Figure 1.2 Comparison of RGS4 and RGS8. Both structures extracted from Protein Data Bank: entries 1AGR and 2IHD respectively [36,52]. (a) Structure of RGS4 with cysteine residues highlighted. (b) Structure of RGS8 with cysteine residues highlighted. RGS8 cysteine residues are analogous to C148 and C95.

which has been revealed to include opioid, serotinergic, and cholinergic signaling modulation. RGS4 is believed to play a role in opioid tolerance due to RGS4 induction in rat locus coeruleus in response to morphine treatment, and diminishes rapidly after withdrawal [53]. RGS4 activity has also been shown to modulate 5HT-1A signaling in a rat model of schizophrenia [54]. Of particular interest is the effect of RGS4 on cholinergic signaling identified in a PD model. RGS4 induction, in response to reserpine treatment, radically affected cholinergic autoreceptor signaling, yielding aberrant cholinergic signaling and a potential mechanism for the motor symptoms of PD [55]. The role of RGS4 in various disease states has lead to the development of pre-therapeutic compounds.

Initial development of RGS4 inhibitors sought to interrupt the interaction between RGS4 and its endogenous binding partner, the Gα subunit [56]. The interaction is transient and therefore difficult to measure. This was overcome by using of GDP-AlF_4^- to trap the GTP hydrolysis transition state of the Gα subunit, creating an interaction 50 fold more stable than the basal interaction [35]. The first attempt to discover RGS4 inhibitors

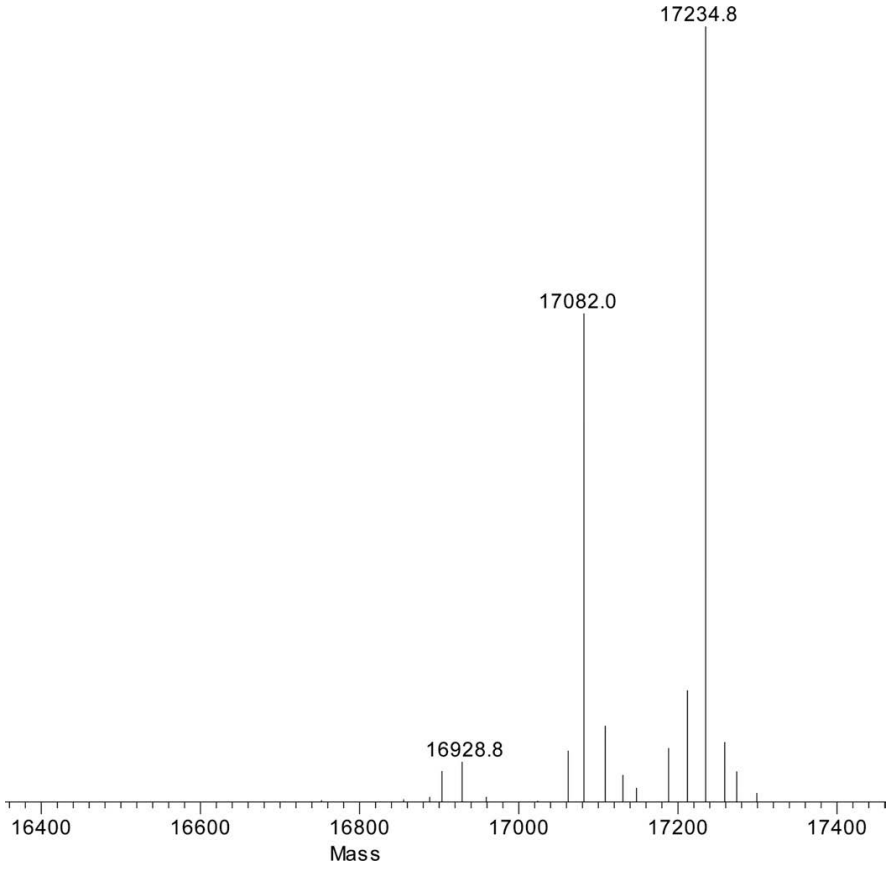

Figure 1.3 Mass Spectrometry Analysis of CCG-4986 Treated RGS8. MS analysis reveals that CCG-4986 covalently modifies RGS8 at both cysteine residues. The three predominant peaks identified in the deconvoluted spectrum inculde the unadducted (16928.8), singly adducted (17082.0), and doubly adducted (17234.8).

in a high throughput screening fashion yielded covalent inhibitors, both a small molecule and a peptide [57-58]. The small molecule, CCG-4986, was found to covalently modify and inhibit RGS4 at cysteine residues 132 (C132) and 148 (C148). The mechanism of action for inhibition of RGS4 at C132 relys on occlusion of the binding site for the Gα subunit. Interestingly, CCG-4986 was far more potent through C148 modification than C132 [59]. The closest homologue of RGS4 is RGS8, which contains an analogous cysteine residue to C148, as shown in Figure 1.2. RGS8 was not inhibited by CCG-4986; however, CCG-4986 is capable of modifying RGS8 as shown by mass spectrometry (MS) in Figure 1.3 [59]. C148 is located away from the Gα interaction face. Inhibition by modification at this site must cause a conformational change in the protein to impair G-protein binding. This novel binding site on RGS4 represents a unique allosteric modulation site, distinct from even its nearest homologue, RGS8. The discovery of this allosteric site represents an opportunity to refine the development of RGS4 inhibitors by targeting a unique allosteric site to inhibit RGS4 selectively over other RGS proteins.

Rationale for Further RGS4 Analysis

The evidence for RGS4 involvement in mediating motor symptoms in neurological diseases is mounting. RGS4 is highly expressed in the striatum

and RGS4 has been implicated in PD through actions in the striatum [60,30,55]. Using reserpine to deplete dopamine signaling, RGS4 expression is induced in D_2 receptor containing cholinergic interneurons [55]. D_2 receptor activation down-regulates RGS4 expression at the transcriptional level [61]. This increased RGS4 expression within cholinergic neurons negatively regulates the M_4 muscarinic autoreceptor, resulting in the disruption of the auto-inhibitory pacemaking of the cholinergic interneurons [55]. These cholinergic neurons act to regulate medium spiny neurons by direct activation of the M_1 muscarinic receptor and prevent excitation [62]. The suppression of medium spiny neurons translates into the negative motor symptoms of PD. Suppressing dopamine signaling in an animal model, using 6-OHDA to selectively destroy dopaminergic neurons, would support this mechanism for PD symptom development, summarized in Figure 1.4. RGS4 mediation of these motor symptoms was shown in a mouse model for PD using 6-OHDA. Deletion of RGS4 completely removed the motor symptoms resulting from 6-OHDA treatment [30]. Of interest when targeting RGS4 as a potential therapeutic target is the phenotype without RGS4. In genetic knockouts of RGS4 in mouse models, the positive symptoms associated with RGS4 knockout were mild and consisted of lower body weight and poorer sensorimotor coordination [63]. Poorer sensorimotor coordination in particular is mild; RGS4 mice performed as well as negative controls in a variety of motor tests such as a rotorod test [30]. The potentially mild side-

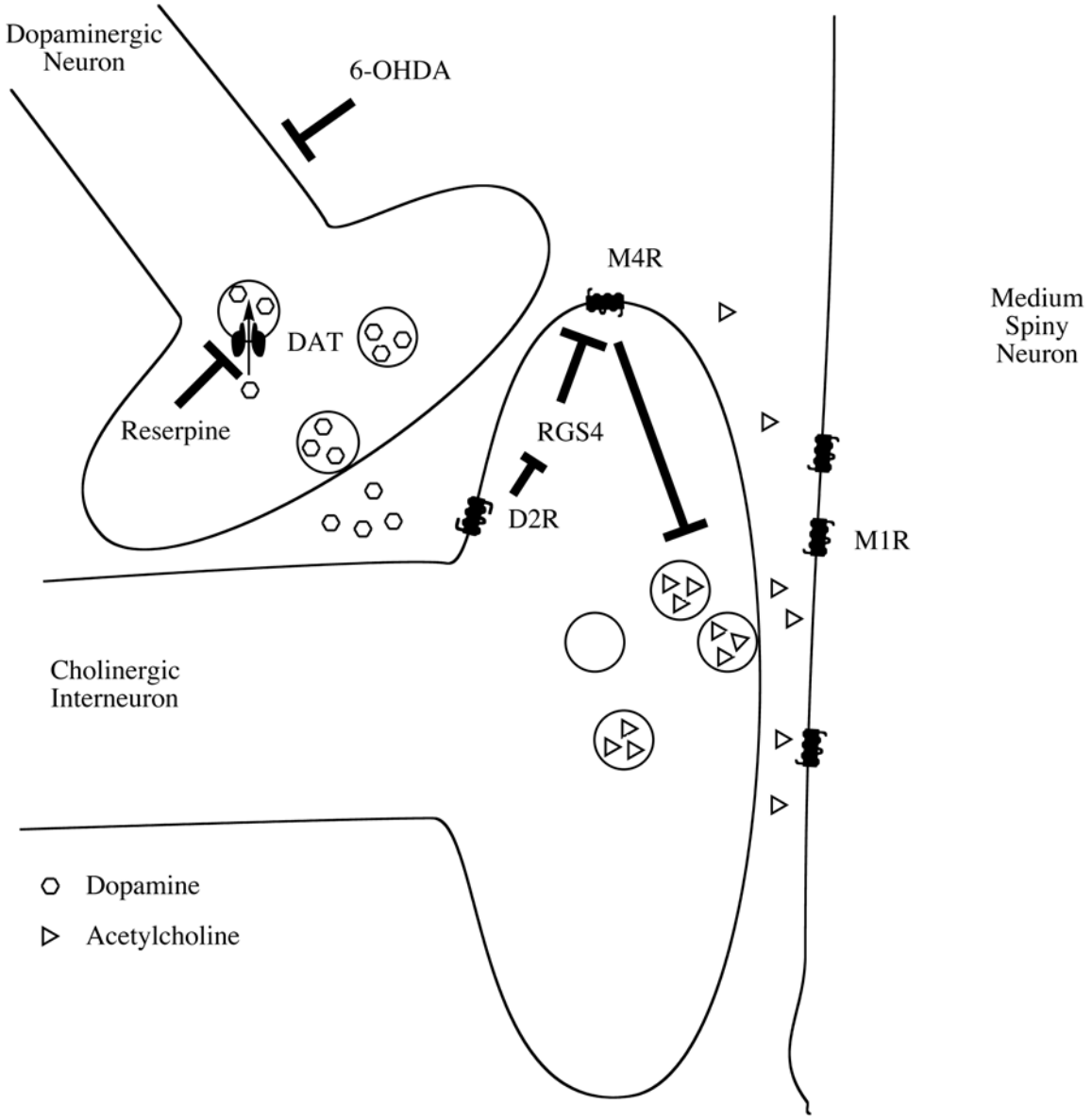

Figure 1.4 Proposed Involvement of RGS4 in Parkinsonian Motor Symptoms. RGS4 expression is directly regulated by the D2 dopamine receptor (D2R). 6-OHDA eliminates dopamine signaling by destroying dopaminergic neurons and reserpine eliminates dopamine signaling by preventing dopamine vesicle formation by inhibiting the dopamine transporter (DAT). Following D2R antagonism, RGS4 expression is increased and acts to negatively regulate the M4 muscarinic autoreceptor (M4R). This disrupts the autonomous pacemaking of the cholinergic interneurons resulting in aberrant signaling to medium spiny neurons and the characteristic motor symptoms of PD.

effects of RGS4 inhibition, coupled with the novel allosteric site (centered at C148) specific to RGS4, makes for an appetizing target for the treatment of PD through small molecule inhibition.

Statement of Hypothesis

RGS4 has been implicated in mediating the motor symptoms PD through increased expression, in comparison to healthy patients, in the striatum [55]. Another major component of PD is oxidative stress through both endogenous and exogenous sources. Within the neurons, deregulation of cellular processes due to age can result in oxidative stress, compounding the higher oxidative load in dopaminergic cells [64]. Toxic insult from a variety of pesticides and natural toxins also serve to induce oxidative stress in the brain [65-66]. A common product of oxidative stress at cell membranes is the formation of lipid peroxidation products. These products may covalently modify a variety of nucleophilic sites, such as cysteine residues, on proteins. We hypothesize that oxidative stress plays an important role in modulating RGS4 expression and the RGS4 specific allosteric site represents an endogenous regulatory mechanism for inhibition by lipid peroxidation products.

A major component of PD pathology is oxidative stress. The unique modulation site on RGS4 may be a site for endogenous regulation by lipid

peroxidation products, such as 4-hydroxy-2-nonenal (4HNE). In support of the hypothesis, we have determined whether RGS4 modification occurs within cells stressed with 4HNE. In addition to confirmation of RGS4 modification in cells, 4HNE adducts were determined to be stable cysteine residue Michael adducts, as determined by MS. Modification was determined to occur predominately at three residues, C71, C148, and C183. This modification results in inhibition of RGS4, but not a cysteine null construct (Unpublished data, Monroy et al). This inhibition represents the first evidence of an endogenous regulatory function for the allosteric site of RGS4.

To expand the tools for analyzing RGS proteins, more direct methods of analysis are required. While measuring the interaction between the RGS protein and the transition state of the Gα subunit, mimicked by GDP-AlF_4^-, may provide valuable insight into the interaction between the two, this methodology does not adequately interrogate the actual activity of the RGS protein. Current methods to interrogate the GAP activity of RGS proteins directly either rely on expensive antibodies, Transcreener, or the exceedingly low throughput and hazardous ^{32}P labeled GTP single turnover and steady state assays [67-68]. To develop a simple method for RGS4 analysis, we successfully adapted the well known malachite green assay to measure GAP activity in a steady state fashion. This assay has been demonstrated for use in a high throughput screening application to 1536-well format. Additionally, four compounds were identified in a pilot screen as novel RGS4 inhibitors

[69]. The development of this simple and cheap assay can be adapted for usage with a variety of RGS proteins with little work to interrogate other pathways and identify novel RGS modulators.

Finally, expansive study of PD and schizophrenia have linked oxidative stress to the pathology of both diseases. What has not been discerned is the potential relationship between oxidative stress and the induction of RGS4. In support of the hypothesis, we evaluated the potential relationship between oxidative stress and RGS4 expression. This was accomplished by evaluating two neuron like cell lines, the neuro blastoma cell line SH-SY5Y and the cultured human cortical neuron cell line HCN-1A. Hydrogen peroxide (H_2O_2) stressed cells were evaluated for RGS4 induction. Both cell lines showed increased RGS4 in response to oxidative stress. This response is not however related to mRNA expression, indicating this change is most likely an adjustment of proteasomal regulation of RGS4. This phenomenon may explain the rapid onset of Parkinsonian motor symptoms in reserpine treated animal models of PD, as excess dopamine in the cytoplasm may be rapidly metabolized to reactive products.

CHAPTER II

MODIFICATION AND FUNCTIONAL INHIBITION OF RGS4 BY 4-HYDROXY-2-NONENAL

The data presented in this chapter have been submitted for publication.

Introduction

Oxidative stress has been suggested as an important component of several pathologies including ischemia/reperfusion injury (IRI) and neurodegenerative diseases such as Parkinson's disease (PD) and schizophrenia [21,70-71]. Oxidative stress is the result of an imbalance in reductive and oxidative reactions in the cell leading to the production of reactive oxygen species (ROS). Cellular oxidative stress processes produce a wide array of reactive biomolecules, such as the lipid peroxidation product 4-hydroxy-2-nonenal (4HNE). 4HNE is one of the most prevalent and well-studied lipid peroxidation products. Basal levels of 4HNE are typically around 0.1 μM in plasma but increase to 1 μM in pathological conditions [72]. In response to oxidative stress, previous research has suggested that 4HNE can accumulate in stressed membranes at concentrations of 10 μM to 5 mM [73]. 4HNE is capable of modifying a variety of intracellular targets at cysteine, histidine and lysine residues. Of these, cysteine modification is

considered to be the most relevant modification for modulation of enzymes. 4HNE has also been shown to modulate G-protein coupled receptor (GPCR) signaling through direct modification of $G\alpha_{q/11}$ [74].

While many enzymes involved in xenobiotic metabolism, such as glutathione S-transferase and some cytochrome P450s, have been intensely studied for the effect of 4HNE on modification, other important cellular systems have remained under-investigated for modulation by lipid peroxidation products. In this report, we focus on Regulator of G-protein signaling 4 (RGS4), a modulator of G-protein signaling. GPCRs are a class of receptors containing seven trans-membrane helices. When activated, these receptors facilitate the release of GDP, to allow for the binding of GTP, in the Gα subunit, one of the components of the heterotrimeric G-protein. This exchange of nucleotide results in the dissociation of both the α- and βɣ-heterodimer subunits from the receptor, and each modulates a variety of downstream targets. Termination of G-protein signaling is dependent upon hydrolysis of GTP to GDP, via intrinsic GTPase activity of the Gα-subunit, followed by association of both the Gα and βɣ subunits [75]. The rate of intrinsic hydrolysis of GTP to GDP in this system occurs too slowly to account for normal cellular signal transduction. These GTPase accelerating proteins (GAPs) function on inhibitory G-proteins, including $G\alpha_o$, $G\alpha_i$ and $G\alpha_q$ but not on the stimulatory $G\alpha_s$. RGS proteins maintain this GAP activity through a highly conserved, 120 amino acid alphahelical RGS domain. RGS4, in

particular, is a relatively small RGS protein containing a short N-terminal amphipathic helix and a RGS domain. Palmitoylation of RGS4 is used to direct the protein to the plasma membrane [43]. This membrane-associated protein has been the target of several high-throughput screens to develop inhibitors [57,69,76-77]. These studies have identified several small molecule inhibitors of RGS4 some of whose mode of inhibition is the covalent modification at two cysteine residues, C132 and C148, with the latter affording a greater degree of inhibition [57].

RGS4 has emerged as an interesting drug target due to its role in several pathologies. Increased RGS4 activity has been linked with improved renal function after induced renal IRI [78]. RGS4 modulation of cholinergic

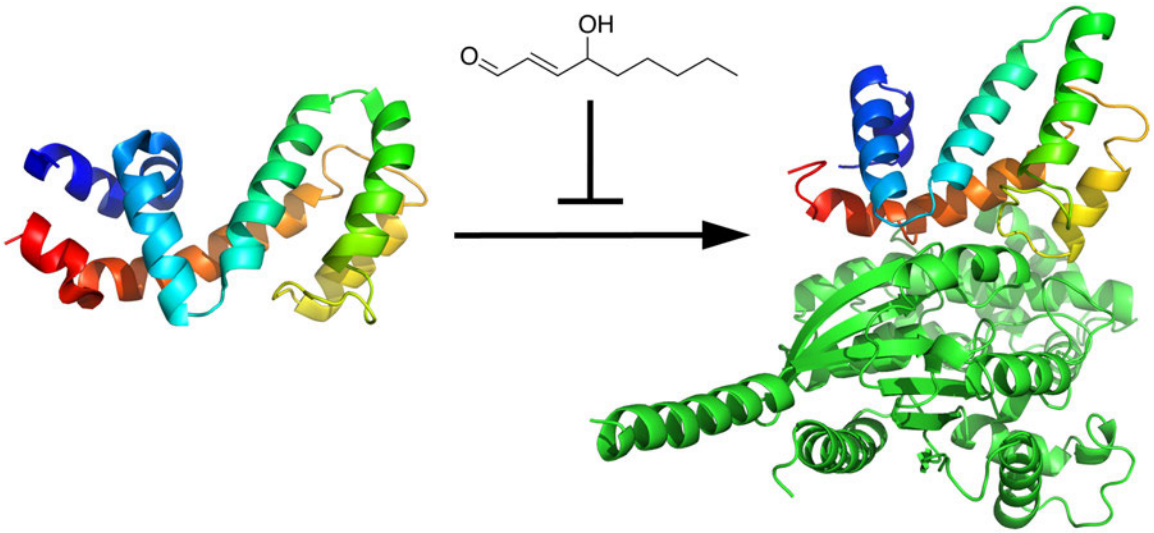

Figure 2.1 4HNE Inhibition of RGS4 Scheme. RGS4 acts as a GAP by interacting with the switch regions of the Gα subunit. 4HNE modification can inhibit this interaction.

signaling by regulation of M4 muscarinic autoreceptors has been implicated in the motor symptoms of PD [55]. Further interrogation of RGS4 in PD has revealed that deletion of RGS4 ablates motor deficits in 6-hydroxydopamine treated mice [30]. RGS4 has been implicated as a susceptibility gene in schizophrenia, although its importance is controversial [79]. With the known roles of oxidative stress in each of these disease states, we set out to investigate the role of oxidative stress in modulating RGS4 activity, using 4HNE as a model. We hypothesized that the sensitivity of RGS4 inhibition by exogenous small molecules with mechanisms of action being cysteine modification may be recapitulated by modification of those cysteine residues by reactive biomolecules generated during oxidative stress, as described in Figure 2.1. This could also reveal an important role, in normal physiology (or pathology) for these cysteine residues in modulating RGS4 activity.

In this study, we investigated the sensitivity of RGS4 to 4HNE modification. This study represents the first attempt to evaluate 4HNE as a potential modulator of RGS activity. When cells transiently expressing RGS4 were exposed to 4HNE, RGS4 modification by 4HNE was readily detectable using immunoprecipitation. When compared to the cysteine null mutant (designated henceforth as Δ7) in both western blot and mass spectrometry (MS), only the wild type construct (WT) contained detectable adducts. The RGS4(Δ7) construct has been previously characterized and been found to be similar to RGS4(WT) in both activity and association with its native binding

partner $G\alpha_o$ [77]. Further examination of RGS4(WT), by tryptic digest / MS revealed modification occurred at C71, C148, and C183. When challenged in a steady-state malachite green based activity assay, 4HNE was found to inhibit RGS4 at concentrations of 4HNE observed during oxidative stress. We propose that lipid peroxidation products inhibit RGS4 during oxidative stress through cysteine residues.

Experimental Procedures

Cell Culture and Treatment.

Human embryonic kidney cells transfected with the SV40 large T antigen (HEK293T) were obtained from ATCC (Manassas, VA). The cells were grown as an adherent monolayer in T-75 tissue culture flasks in high glucose DMEM (Life Technologies; Grand Island, NY) supplemented with 10% fetal bovine serum (Fisher Scientific; Waltham, MA) and 1% penicillin / streptomycin (Life Technologies; Grand Island, NY). Following transfection, HEK293T cells were treated with increasing concentrations of 4HNE (Cayman Chemical; Ann Arbor, MI), 1 μM, 5 μM, and 10 μM. Following a 10 min incubation at 37°C, stressing media was removed and cells were washed with PBS. Cells were lysed in Lysis Buffer (10 mM KH_2PO_4 pH 7.5 and 0.1% Triton X-100) and homogenized using a Sonic Dismembrator (Fisher Scientific; Waltham, MA). Samples were cleared by centrifugation at 13 000 x

g for 15 min and the supernatant was collected. Crude protein concentration was determined by DC protein assay (Bio-Rad; Hercules, CA) for use in later experiments.

Plasmid Construct and Transfection.

A construct containing a N-terminal HA tagged RGS4, with cysteine 2 mutated to serine to avoid degradation, (C2S) in pCDNA3.1+ was used for transfection [80]. First, cells were plated into 12-well dishes at 2 x 10^5 cells/ well. Cells were transfected the following day using Lipofectamine 2000 (Life Technologies; Grand Island NY) according to manufacturer's protocol. After 6 h, media was exchanged with fresh media and allowed to incubate for 48 h before being stressed with 4HNE.

Immunoprecipitation.

4 μg of a goat anti-4HNE modification antibody, ab46544 (Abcam; Cambridge, MA) was added to 500 μg of protein sample and was diluted to 500 μL for a final concentration of 1mg/mL sample. The sample was incubated for 16 h at 4°C under light agitation using a HULA Shaker (Life Technologies; Grand Island, NY). 50 μL of Protein-G Magna Beads (Life Technologies; Grand Island, NY) were added to each sample and incubated for 2 h at 25°C. Beads were washed three times for 5 min in PBS. Beads were

then suspended in 30 µL Denaturation Buffer (200 mM Glycine pH 2.6) and incubated for 10min at 55°C.

Protein Expression and Purification.

Tobacco etch virus (TEV) protease was expressed and purified as a His-tagged protein in E. Coli, BL21-pRIL (Stratagene; La Jolla, CA), in the pRK793 vector as previously described [81]. Rat RGS4, sharing 97% sequence identity with human RGS4, (WT) and the cysteine to alanine (Δ7) mutant was expressed as fusion proteins of maltose binding protein (MBP), a 10x His tag, and a TEV protease recognition site to the N-terminus of an RGS4 construct lacking the first 51 amino acids, in the vector pMALC2H10T [82]. The fusion protein was induced using 100 µM IPTG and expressed in LB at 37°C for 4 h. The bacteria was pelleted and suspended in RGS4 Buffer (50 mM HEPES at pH 8, 100 mM NaCl, 5 mM ß-mercaptoethanol). The cells were lysed using 0.5 mg of lysozyme (Fisher Scientific; Waltham, MA) for every 1 mL of pellet. The pellet was cleared of DNA by the addition of 1 mg of DNAase1 (Fisher Scientific; Waltham, MA) and incubated on ice until consistency became fluid. The samples were then centrifuged at 100 000 x g for 1 h to clear the sample. After centrifugation, the resulting supernatant was filtered (0.45µm) and loaded onto an amylose column (New England Biolabs; Ipswich, MA), 1.5 mL resin for every 1 L of culture. The protein of interest was eluted using 10 mM maltose, and analysis via SDS-PAGE

showed a fusion protein of >95% purity, with the minor contaminant being free MBP. Fractions containing the protein of interest were pooled and incubated with TEV protease at a molar ratio of 10 : 1 (fusion protein:TEV protease) overnight at 4°C. The cleaved Δ51-RGS4 was then isolated by purification over ANX column (GE Healthcare Life Sciences; Uppsala, Sweden) in 50 mM HEPES at pH 6.8 and 50 mM NaCl. The flow through, containing the Δ51-RGS4, was then collected and concentrated using a YM-10 centrifugal concentrator (Millipore; Billerica, MA). The rate-altered variant of Human $G\alpha_{i1}$ (R178M, A326S), described in literature, was expressed in Terrific Broth (TB) media as a 6 x His labeled protein in the pQE80 vector [67]. Protein expression was inducted at OD_{600nm} of 1.0 using 100 μM IPTG at 30°C. At 16 h after induction, the bacteria were pelleted at 3 600 x g for 15 min. Pellets were lysed, centrifuged, and filtered similar to as described for RGS4, but in $G\alpha_i$ Buffer (50 mM HEPES at pH 7.5, 500 mM NaCl, 1 mM β-mercaptoethanol, and 20 μM GDP). After loading onto a Ni-NTA column (Qiagen; Hilden Germany) containing 3 mL of resin for every 1 L media, the column was washed with 2 column volumes $G\alpha_i$ Buffer supplemented with 25 mM imidazole. The protein of interest was eluted from the column using $G\alpha_i$ buffer supplemented with 300 mM imidazole. Fractions containing $G\alpha_i$, as determined by SDS-PAGE, were pooled and dialyzed for 12 h against $G\alpha_i$ Dialysis Buffer (50 mM HEPES at pH 7.5, 25 mM NaCl, 1 mM β-mercaptoethanol, and 20 μM GDP). The pooled fractions were then loaded

onto a Q-sepharose column (GE Healthcare Life Sciences; Uppsala, Sweden) and eluted along a salt gradient from 50 mM NaCl to 1 M NaCl in $G\alpha_i$ Buffer. Fractions containing $G\alpha_i$, determined by SDS-PAGE, were pooled and concentrated using an Amicon stirred cell concentrator (Millipore; Billerica, MA) with a YM-10 filter (Millipore; Billerica, MA). $G\alpha_i$ activity was assayed using the [^{35}S] GTPγS binding assay [83].

4HNE Treatment of Purified RGS4.

Δ51-RGS4(WT) and Δ51-RGS4(Δ7) were treated with increasing concentrations of 4HNE for 30 min at 37°C. 2 μg of cleaved Δ51-RGS4 was treated with 0 μM, 6 μM, 60 μM, or 600 μM 4HNE, which corresponds to 1 : 0, 1 : 1, 1 : 10, and 1 : 100 molar ratios (RGS4:4HNE).

SDS-PAGE and Western Blotting.

Samples were then loaded into SDS-PAGE gels for analysis by western blot. After transfer of the samples to Immobilon-P transfer membrane (Millipore; Billerica, MA) according to manufacturer's protocol, the membrane was then blocked, overnight, using tris buffered saline Tween-20 (TBST; 50 mM Tris pH 7.4, 150 mM NaCl, 0.1% Tween-20) supplemented with 3% bovine serum albumin (BSA). To detect RGS4, samples were first probed for 4 h at 4°C using U1079 (rabbit anti-RGS4) at a 1 : 10 000 dilution in 3% BSA TBST. The blot was then probed using a 1 : 20 000 dilution of goat

anti-rabbit secondary, conjugated to horseradish peroxidase (Protein Biosystems; Pelham, Alabama), for 1.5 h at 25°C. The blot was developed using WestPico chemiluminescent substrate (Thermo Scientific, Waltham, MA) and imaged using a UVP Biospectrum Imaging system (Upland, CA). To detect 4HNE, the blot was probed using 0.1 μg/mL ab46544 anti-4HNE antibody (Abcam, Cambridge, MA) for 4 h at 4°C and subsequently detected utilizing an anti-Goat HRP conjugated secondary (ab753, Abcam, Cambridge, MA), at a dilution of 1 : 20 000, for 1.5 h at 25°C. The blot was developed using WestPico chemiluminescent substrate (Thermo Scientific, Waltham, MA) and imaged using a UVP Biospectrum Imaging system (Upland, CA).

LC/MS Analysis of RGS4.

Δ51-RGS4(WT) and Δ51-RGS4(Δ7) were treated for 30 min at 37°C. 1.5 μg of RGS4 was treated with 50 μM 4HNE in a final volume of 15 μL in Reaction Buffer (50 mM HEPES pH 8.0, 100 mM NaCl). Following treatment the samples were diluted 1 : 100 in doubly de-ionized water and loaded into LC-ESI-IT-TOF (Shimadzu; Kyoto, JP) similarly to as described previously [59]. 10 μL of the diluted sample was injected onto a Jupiter C-18 column (Phenomenex; Torrance, CA) and eluted at a gradient of 20% - 80% acetonitrile in 0.05% formic acid over 30 min after a 5 min step at 20% acetonitrile to remove excess salt. The results were analyzed using MagTran software. To determine sites of modification RGS4 was treated with 10 fold

excess 4HNE, as described above, and digested to peptide fragments for MS analysis.

Following the 30 min incubation at 37°C, the samples were quenched using a 10 fold molar excess of cysteine, in Reaction Buffer. The samples were then digested 10 h at 25°C with trypsin (Sigma Alderich; St Louis, MO) at a ratio of 20 : 1 (RGS4 : trypsin) in Reaction Buffer. The sample was the diluted 1 : 100 as before and injected onto the LC-ESI-IT-TOF, utilizing the previously described protocol [59]. 10 μL of the diluted sample was injected onto a Jupiter C-18 column (Phenomenex; Torrance, CA) and eluted at a gradient of 5% - 90% acetonitrile in 0.05% formic acid over 30 min after a 5 min step at 5% acetonitrile to remove excess salt. The results were then analyzed using MagTran software.

Steady State GTPase Accelerating (GAP) Assay.

A steady state analysis of RGS4 GAP activity was performed largely as described previously [69]. In a 384-well plate, 10 μL of each component, except for cysteine quenching and $G\alpha_{i1}$ which each receive 5 μL, was added sequentially with a 5 min centrifugation at 100 x g after each addition. 4 x final concentrations of 4HNE at 4 mM (1 mM final) or vehicle treatment were prepared and added to appropriate wells. To each well, 800 nM RGS4 (200 nM RGS4) was added and allowed to incubate 30 min at 25°C. The reaction was quenched by the addition of 5μL of 80 mM cysteine and incubated for 5

min after centrifugation. 5 μL of 40 μM $G\alpha_{i1}$ (5 μM final) was added to each well. After a 5 min incubation, 600 μM GTP (150μM final) was added to each well. Developing solution (DS) was prepared on the day of use by creating a 50 : 12.5 : 1 ratio of the following: 0.12% malachite green (w/v) dissolved in 17% H_2SO_4 (v/v), 7.5% ammonium molybdate tetrahydrate, and 11% Tween-20 (v/v) [84]. After a 75 min incubation, DS was added to each well. After a 50 min incubation the plate was read using an EnVision plate reader (PerkinElmer; Waltham, MA).

Statistical Analysis.

Steady state assay data was analyzed using GraphPad Prism software (La Jolla, CA). Treated samples were compared to control samples using an unpaired t-test test for statistical significance. Values of $p < 0.05$ was considered significant.

Results

Detection of RGS4 Modification in HEK293T Cells.

Initially, we set out to identify whether RGS4, known to be sensitive to cysteine modification, was capable of being modified in cells [59]. 48 h After transient transfection of HA-RGS4(C2S), cells were treated with 0 – 10 μM 4HNE for 10 min and analyzed for 4HNE modification of HA-RGS4(C2S) by

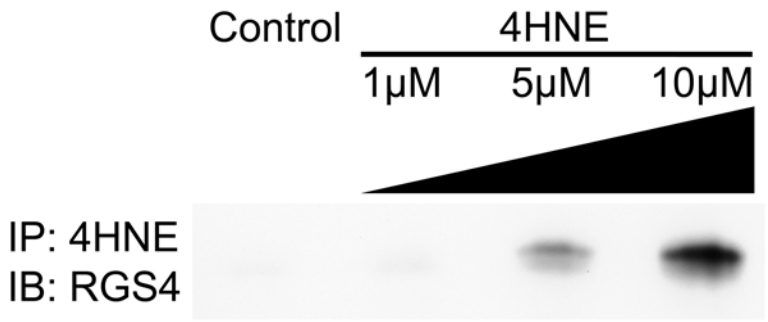

Figure 2.2 Immuno-precipitation of 4HNE-Modified RGS4. Immunodetection of RGS4 via western blot after immunoprecipitation (IP) of 4HNE labeled protein. HEK293T cells, transfected with HA-(C2S)RGS4, were treated with increasing concentrations of 4HNE from 0 – 10 μM. The samples were then immunoblotted (IB) for RGS4. No detectable RGS4 was seen at 0 μM but a faint band appears at 1 μM and significantly increases at 5 μM. Image shown is representative of n=3 experiments.

immunoprecipitation. While no modification was determined for 1 μM, a significant amount of 4HNE-modified RGS4 was detected at 5 μM as quantified by densitometry. Nearly twice as much modified RGS4 was detected when the cells were exposed to 10 μM 4HNE versus 5 μM 4HNE, as shown in Figure 2.2.

RGS4 Treatment with 4HNE and Detection of Products.

2 μg of Δ51-RGS4(WT) and Δ51-RGS4(Δ7) were treated with variable amounts of 4HNE and a western blot was performed to determine whether modification occurs on either construct. Increasing concentrations of 4HNE resulted in extensive protein modification by 4HNE as shown by the increasing intensity of the band corresponding to 4HNE modified protein in

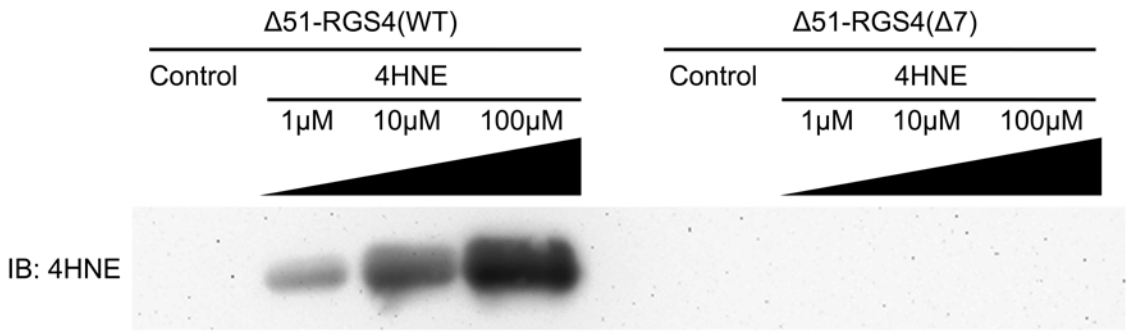

Figure 2.3 Immunodetection of 4HNE-Modified Δ51-RGS4(WT) and Δ51-RGS4(Δ7). Purified protein exposed to increasing ratios of 4HNE, from 0 – 100 fold. Δ51-RGS4(WT) was clearly detected by western blot at even 1 : 1 ratio of 4HNE, while Δ51-RGS4(Δ7) was not detected even at ratios of 1 : 100 4HNE. Image shown is representative of n=3 experiments.

Figure 2.3. While the modification was detectable at even the 1 : 1 molar ratio in the Δ51-RGS4(WT), no modification was detected on the Δ51-RGS4(Δ7) construct, even at molar ratios of 1 : 100.

MS Quantification of 4HNE Adducts on RGS4.

Δ51-RGS4(WT) and Δ51-RGS4(Δ7) were treated with 4HNE and separated by HPLC using a C18 column with a gradient from 20% - 80% ACN in 0.5% formic acid. The Δ51-RGS4 constructs eluted at 10-11 minutes in the protocol described in the methods. The unadducted Δ51-RGS4(WT) species was detected with a deconvoluted m/z of 18090.8, as shown in Figure 2.4a. In treated samples, another peak coeluting with the unmodified protein contained a protein with a deconvoluted mass of 18558.1. The difference in

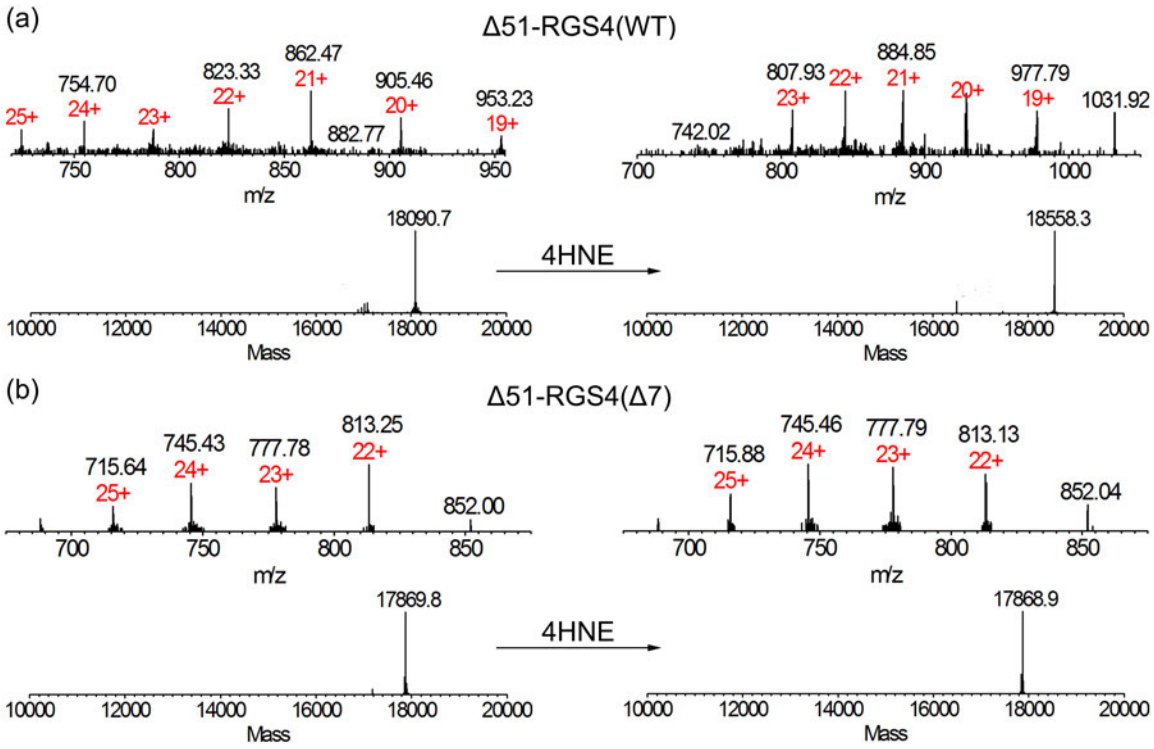

Figure 2.4 MS Detection of 4HNE Modification in Δ51-RGS4(WT) and Δ51-RGS4(Δ7). (a) Injection of 10 µL of RGS4, about 0.7 pmol, was analyzed by LC-ESI-IT-TOF. Expected MW for the deconvoluted singly charged molecular weight was 18090.7 and a detected deconvoluted signal was 18090.8. Treatment with 4HNE revealed a deconvoluted mass was 18558.1. The calculated difference in the mass, 467.3, accounts for 3 adduction sites for 4HNE. (b) Expected MW for the deconvoluted Δ51-RGS4(Δ7). singly charged molecular weight was 19075.0, as detected. After 4HNE treatment, the detected deconvoluted mass was 19075.0, indicating no detectable modification. Data shown are representative of n=3 experiments.

the mass, 467.3 (3 x 155.8), corresponds to Michael addition of 3 4HNE molecules. In similarly treated Δ51-RGS4(Δ7) protein shown in Figure 2.4b, untreated samples produced a distribution of peaks that deconvoluted to m/z of 19075.0. In samples treated with 4HNE, the unadducted mass continues to be the only detectable species had a deconvoluted mass of 19075.0,

corresponding to unadducted protein. These results confirm that Cys residues are being preferentially modified on RGS4.

Table 2.1 Tryptic Digest of Δ51-RGS4(WT) Construct.

Fragment Position	Sequence	Position	Predicted Mass	Experimental Mass	Adducted Mass
1	SQEEVK	52 - 57	719.77	719.82	--
2	WAESLENLIN HECGLAAFK	59 - 77	2146.44	2145.87	2303.98
3	SEYSEENIDF WISCEEYK	82 - 99	2272.42	2272.76	--
4	IYNEFISVQA TK	114 - 125	1413.62	1413.63	--
5	EVNLDSCTR	126 - 134	1037.14	1037.40	--
6	NMLEPTITCF DEAQK	140 - 154	1741.00	1740.66	1897.77
7	IFNLMEK	156 - 162	895.12	895.40	--
8	FYLDLTNPSS CGAEK	173 - 187	1645.84	1646.64	1802.74
9	SSADCTSLVP QCA	193 - 205	1282.44	1281.77	--

Tryptic Digest/MS Analysis of 4HNE Adduction.

Tryptic digest of RGS4 yields a manageable 9 detectable tryptic fragments containing no more than 2 Cys residues per peptide shown in Table 2.1. After treatment with 1:10 molar excess 4HNE (5 μM RGS4 to 50

μM 4HNE), Δ51-RGS4(WT) was digested with trypsin and the resulting fragments were analyzed by MS. Initial analysis of the tryptic fragments revealed the expected sequence coverage of 75%, due predominantly to many tryptic fragments less then 4 amino acids in length as shown in Figure 2.5a. In the total ion chromatogram, the adducted fragments were detected as

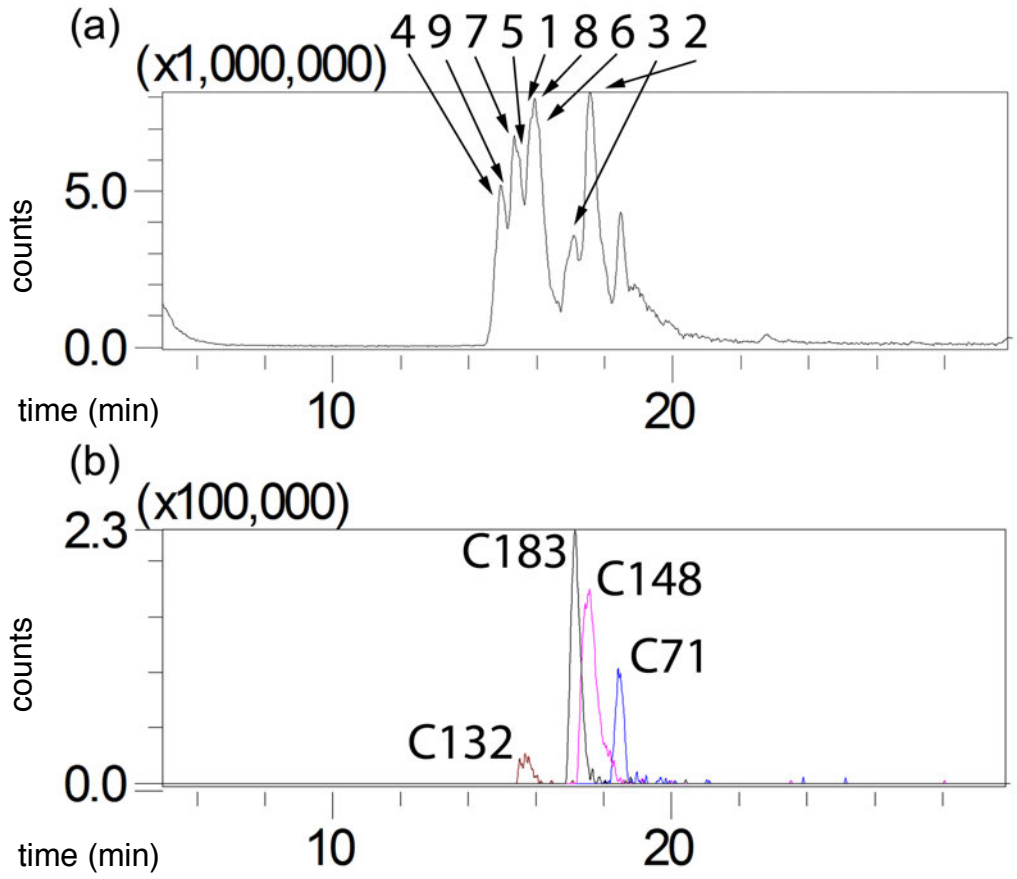

Figure 2.5 MS Detection of 4HNE Treated Δ51-RGS4(WT) Tryptic Digest. The elution gradient of 5 – 90% ACN allowed for separation of tryptic peptides for analysis. (a) Outlined is the total ion chromatogram as well as the base peak for each fragment. Peaks are identified according to fragment number from Table 2.1. (b) The elution peak for each of the adducted fragments. Image shown is representative of n=3 experiments.

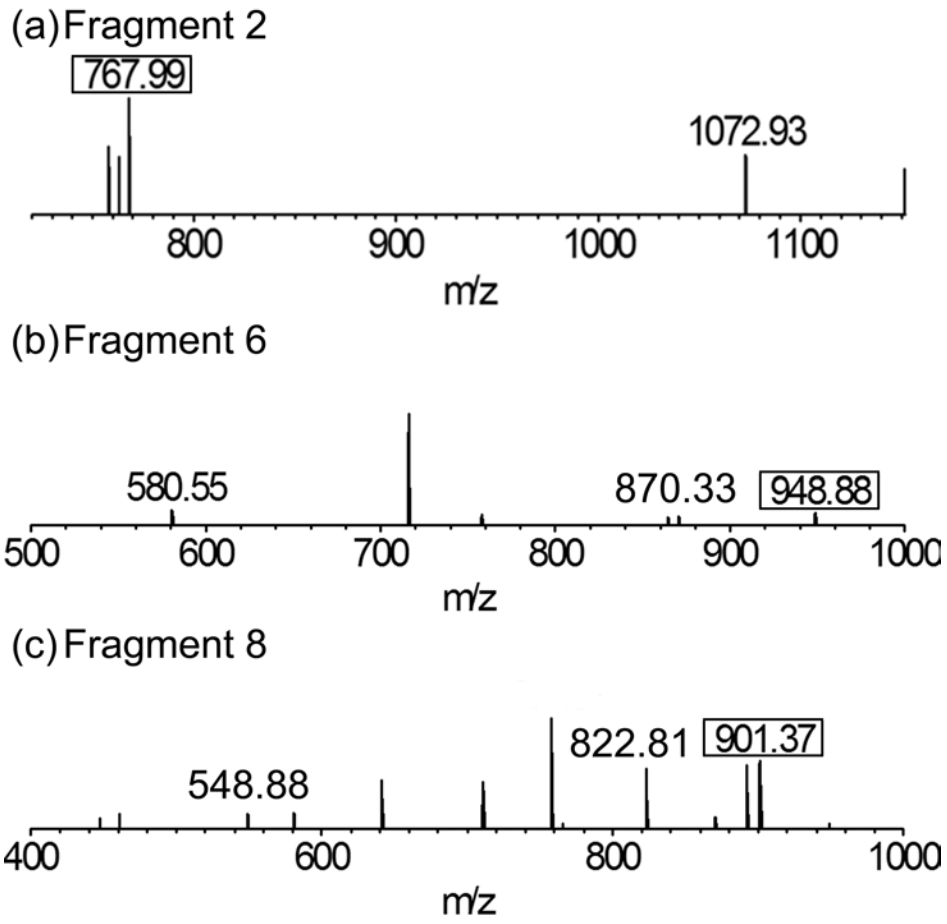

Figure 2.6 MS Detection of Adducted Δ51-RGS4(WT) Tryptic Fragments. (a) Fragment 2, corresponding to C71, was detected containing a 4HNE adduct. The adducted fragment was detected as a triply charged species with an m/z of 767.99. (b) Fragment 6, corresponding to C148, was detected containing a 4HNE adduct. The adducted fragment was detected as a doubly charged species with an m/z of 948.88. (c) Fragment 8, corresponding to C183, was detected containing a 4HNE adduct. The adducted fragment was detected as a doubly charged species with an m/z of 901.37. Image shown is representative of n=3 experiments.

either doubly or triply charged species eluting later than their unadducted counterparts (Figure 2.5b). For Fragment 2 (WAESLENLIN HECGLAAFK), the adducted fragment was detected as a triply charged species with a m/z of 767.99, shown in Figure 2.6a. For fragment 6 (NMLEPTITCF DAEQK) and 8

(FYLDLTNPSS CGAEK), both were detected as doubly charged species with a m/z of 948.88, in Figure 2.6b, and 901.37, in Figure 2.6c respectively. These adducted fragments correspond to the 3 adduct sites on RGS4 identified in the whole protein MS analysis. Fragments 2, 6, and 8 correspond to specific cysteine residues within RGS4: C71, C148 and C183 respectively.

Steady State Analysis of 4HNE Modified RGS4.

4HNE modulation of RGS4 activity was evaluated using the malachite green based steady state GAP activity assay. In Figure 2.7, we show 1 mM 4HNE inhibits Δ51-RGS4(WT). In contrast, Δ51-RGS4(Δ7) was not inhibited by 4HNE.

Discussion

4HNE is a common lipid peroxidation product and a signal of oxidative stress at the cell membrane. Oxidative stress has been implicated as an important component of the pathology of various neurological disorders including Parkinson's disease [85]. In a disease with similar pathology, manganism, excess manganese is capable of activating microglia and stimulating the release of hydrogen peroxide [86]. The direct production of lipid peroxidation products at the plasma membrane can result in alteration of various signaling pathways. RGS4 plays a critical role in regulating M4

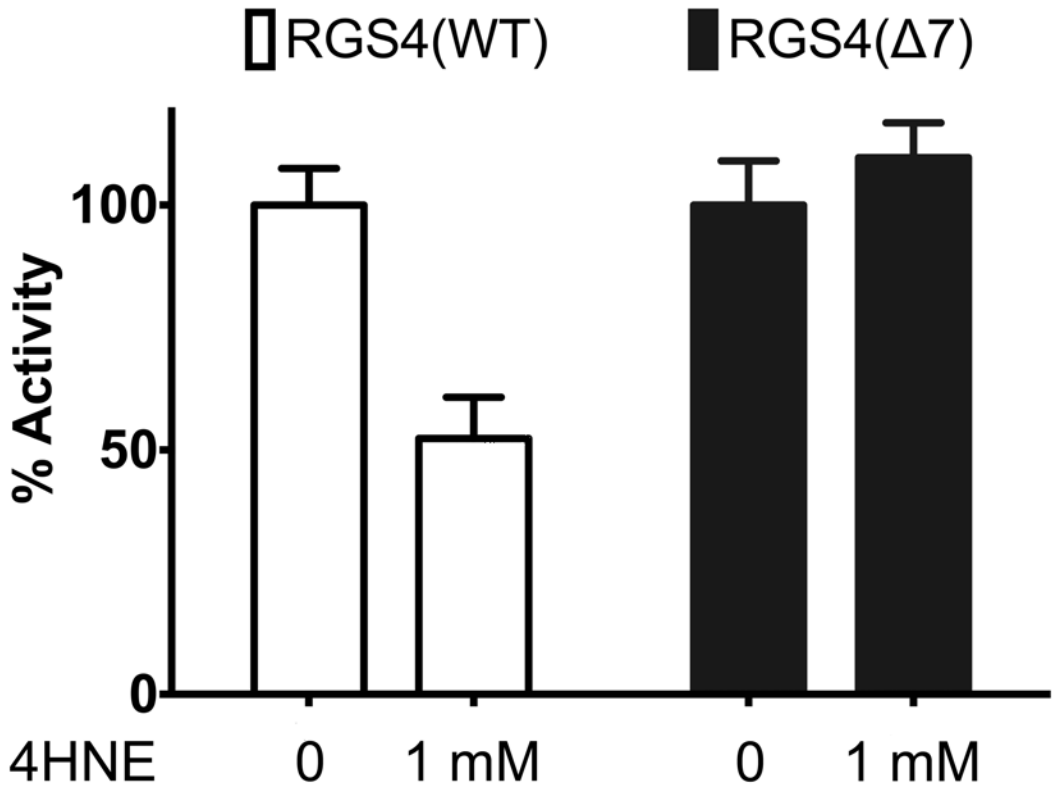

Figure 2.7 Steady State Analysis of 4HNE Modified Δ51-RGS4(WT) and Δ51-RGS4(Δ7). Steady state analysis of RGS4 GAP activity was evaluated using $G\alpha_{i1}$ as the GTPase. RGS4(WT) was inhibited 50% by 1 mM 4HNE, and RGS4(Δ7) was not inhibited at all by 4HNE under similar conditions. Image shown represents average of n=3 experiments.

autoreceptor activity in striatal neurons [55]. As a membrane associated protein, RGS4 is an interesting target for 4HNE modification during oxidative stress. 4HNE modification of RGS4 could alter signaling from stressed cells. Using a variety of techniques, we show that RGS4 can be modified by 4HNE, and the resulting modification can disrupt RGS4 activity.

Initially, we set out to detect whether RGS4 was modified by 4HNE within cells. Western blot analysis of RGS4 was used to determine whether

RGS4 modification by 4HNE was possible. In whole cell lysate, RGS4 was consistently modified by 4HNE in treated cells. This modification was expected due to high accumulation of 4HNE in the plasma membrane and the membrane association of RGS4 when modulating signaling pathways [73,43]. In PD, RGS4 activity is hypothesized to play a critical role in mediating the motor symptoms. Oxidative stress modulation of RGS4 signaling by covalent modification may act to attenuate this effect.

4HNE has been shown to modify cysteine, histidine and lysine residues [87]. In comparison to the cysteine-null mutant which did not show detectable modification in the western blot, Δ51-RGS4(WT) was modified by increasing concentrations of 4HNE. We did not expect to detect much modification at other residues due to the significantly increased reactivity of 4HNE to cysteine residues over both histidine and lysine residues [87]. The construct used contains 7 cysteine residues, 4 of which were within the RGS domain of RGS4 [36]. Mass spectrometry results indicate that Δ51-RGS4(WT) was readily modified by 4HNE, but not Δ51-RGS4(Δ7) mutant. This marks the first report of lipid peroxidation products, such as 4HNE, showing modification of an RGS protein. Based on the results from the previous experiments, we expected this to be the case. RGS4 has been previously shown to be sensitive to thiol modification at cysteine residues 132 and 148, suggesting those locations as modification sites for 4HNE as well [59]. Further analysis of Δ51-RGS4(WT) revealed consistent modification at tryptic

fragments corresponding to 3 residues: C71, C148, and C183. The detection of modification at C148 suggested a mode of inhibition of RGS4 by 4HNE similar to previously reported small molecule inhibitors, such as CCG-4986 [59].

In order to analyze modulation of RGS4 activity a label free activity assay was required. A steady state colorimetric assay was utilized to determine the effect of 4HNE on RGS4 GAP activity. At the concentrations examined, the free cysteine quenching of excess 4HNE protected $G\alpha_i$, allowing for the facile analysis of 4HNE modification on RGS4 activity. 4HNE was found to inhibit Δ51-RGS4(WT). 1 mM 4HNE inhibited Δ51-RGS4(WT) 50% of mock treated controls. The cysteine null mutant, Δ51-RGS4(Δ7), was not inhibited by 4HNE at similar concentrations. 4HNE failing to inhibit Δ51-RGS4(Δ7) indicates that cysteine modification accounts for the relevant modification of RGS4, similar to previously described mechanism of actions of known RGS4 inhibitors [59].

In conclusion, we have identified a potential target for 4HNE modification during oxidative stress. Specifically, in cultured cells exposed to 4HNE, RGS4 was readily identified as a target for modification. In this study, we show RGS4 is susceptible to modification at particular cysteine residues, including C148, which has been previously shown to be a target for covalent modification. With the identification of C148 as a modification target for 4HNE, this allows for the possibility for 4HNE to act as an internal control

for aberrant signaling due to excess RGS4 activity in a variety of pathologies where oxidative stress is a strong component, such as PD. Future studies will focus on determining the effects of 4HNE modification on RGS4, and other RGS proteins, on downstream signaling events critical to GPCR signal transduction.

CHAPTER III

A HIGH THROUGHPUT SCREEN FOR RGS PROTEINS UTILIZING STEADY STATE MONITORING OF FREE PHOSPHATE FORMATION

The data presented in this chapter has been published in PLoS One.[1]

Introduction

G-protein coupled receptors (GPCRs) are a diverse group of seven transmembrane-spanning receptors that represent targets for over 50% of drugs available on the market [88]. These receptors signal through the activation of a heterotrimeric G protein complex, consisting of Gα, Gß, and Gɣ subunits. Upon activation of a GPCR, bound guanosine-diphosphate (GDP) is exchanged for guanosine-triphosphate (GTP) in the Gα subunit. This causes a dissociation of the Gα subunit from both the receptor and Gßγ subunit complex, and both the Gα subunit and the Gßγ complex proceed to activate their respective signaling pathways. The signal is terminated by the hydrolysis of GTP to GDP in the Gα subunit [89]. The intrinsic, relatively

---

1. Monroy CA, Mackie DI, Roman DL (2013) A High Throughput Screen for RGS Proteins Using Steady State Monitoring of Free Phosphate Formation. PLoS ONE 8: e62247.

slow rate of hydrolysis of the Gα subunits in the $G\alpha_i$ and $G\alpha_q$ subfamily are temporally modulated by another superfamily of proteins, regulators of G-protein signaling (RGS) proteins, that increases the GTPase rate of a variety of Gα subunits, thus acting as GTPase activating proteins (GAPs) [90].

Due to their important role in regulating GPCR signaling, RGS proteins represent intriguing targets for drug development. In developing high-throughput screening (HTS) assays for RGS targets, methods have emerged for the targeting of the RGS-Gα protein-protein interaction, such as flow cytometry, Alpha Screen, fluorescence polarization, and time-resolved fluorescence resonance energy transfer [77,91,67,92]. These methods have been successfully used to detect the disruption of the protein-protein interaction and not the GAP functionality of the RGS proteins. Historically, the predominant method for determination of RGS protein activity is the use of ^{32}P labeled GTP in single turnover or steady-state assays [56,68]. While these ^{32}P assays provide a measure of RGS activity on GTPase activity, they are technically challenging, even in low throughput benchtop experiments which involve the use of radioactivity and require careful timing for reproducible results [93].

The limitations of these approaches have driven our group, and others, to develop simple, non-radioactive assays to measure RGS protein GAP function. Early work focused on the development of entire receptor / protein complexes contained within phospholipid vesicles [94]. This method is

laborious and does not extend well into development of HTS assays. In order to develop a viable HTS assay for measuring GAP function, two hurdles must be overcome. First, the catalytic activity of the Gα subunit must be slowed to allow for a larger time window. Second, the rate-limiting step of Gα subunit turnover must be shifted from GDP dissociation to GTP hydrolysis. Analysis of the Gα subunit resulted in the previous reports describing a point mutation at the catalytically critical arginine residue (R178C in $G\alpha_{i1}$) that results in a marked reduction in the intrinsic GTPase activity of the Gα subunit while maintaining sensitivity to the GAP activity of RGS proteins [56,95-96]. Another point mutation, A326S in $G\alpha_{i1}$, allows for a ~25 fold increase in $k_{off(GDP)}$ while maintaining normal GTPase activity [97-98]. These two point mutations have been used in the development of another HTS assay, the

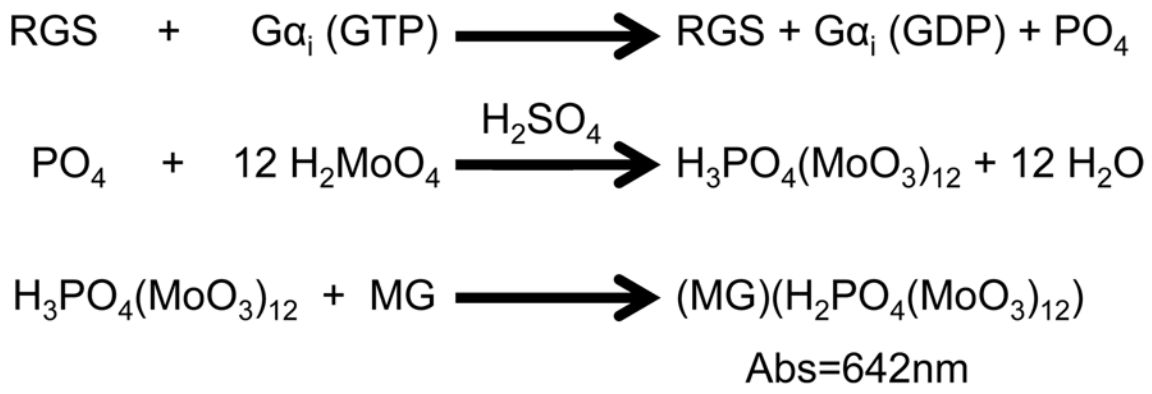

Figure 3.1 Scheme of Malachite Green Assay. RGS protein interacts with $G\alpha_i$ and induces the hydrolysis of GTP to GDP, releasing free phosphate. In the presence of acid, molybdate releases water and complexes with the free phosphate. Lastly, the phosphomolybdate complex associates with the malachite green to produce a strong absorbance peak at 642nm.

Transcreener assay (BellBrook Labs; Fitchburg, WI) to detect GDP generation [67]. The Transcreener assay relies on the usage of antibodies for the detection of generated GDP by fluorescence polarization. While this assay is well validated and commercially available, the use of antibodies in HTS assays can become prohibitively expensive. Therefore, we approached a very simple method previously used for detecting ATPase activity - the detection of free phosphate generation by a malachite green reagent [99]. As demonstrated in (Figure 3.1), free phosphate complexes with molybdate to form a phosphomolybdate complex called phosphomolybdic acid [100]. This phosphomolybdate complex then interacts with malachite green to develop an intense absorbance peak at 630nm [101]. A single step addition method of this assay is accomplished by using low pH to improve the solubility of malachite green [84].

In this study, we developed a malachite-based assay to measure GAP activity of a variety of RGS proteins. RGS4 was selected as the pilot RGS for this assay due to the results of recent RGS4 HTS campaigns and the availability of a small collection of control compounds [77,67,102,76,57-58]. While the majority of known RGS4 inhibitors act as irreversible cysteine modifiers (particularly at CYS148), our group, and others, seek the development of non-covalent RGS inhibitors [59]. The development of reversible inhibitors of RGS4 is of particular interest to the study of

Parkinson's disease (PD). Recent research has shown that RGS4 induction is an integral component of the progression of motor symptoms in mouse models of PD [30]. For this reason, in the development of the assay we include a counter screen against the cysteine null mutant of RGS4 (designated Δ7) to eliminate compounds that modify free thiols as their mode of inhibition [57]. This malachite green based assay allowed us to perform steady state analysis of RGS4, RGS8 and RGS17 activity readily in a plate based assay, acquiring data in as little as 40 min, with stability out to 2 h. After development, the absorbance remains stable for at least 30 min after, allowing for multiple reads of the same plate, such as scanning the fainter peak at 405 nm in order to evaluate compounds with strong absorbance at the principle peak of 630 nm [84]. Another benefit of this assay is the negligible reagent cost for this assay, at approximately $0.005 / well.

Experimental Procedures

Expression and Purification of Recombinant Protein.

Tobacco etch virus (TEV) protease was expressed and purified as a His-tagged protein in E. coli, BL21-pRIL (Stratagene; La Jolla, CA), in the pRK793 vector as previously described by the Waugh lab [81].

Rat RGS4, sharing 97% sequence identity with human RGS4, and the cysteine to alanine mutant were expressed as fusion proteins of maltose

binding protein (MBP), a 10 x His tag, and a TEV protease recognition site fused to the N-terminus of an RGS4 construct containing amino acids 51 – 205, in the vector pMALC2H10T in BL21-DE3 E. coli (Stratagene; Santa Clara, CA) [82]. The single cysteine-null Δ51-RGS4 construct was generated by site-directed mutagenesis as described previously [59]. Expression and purification were performed as described previously [59]. Purified protein was incubated with TEV protease at a molar ratio of 10 : 1 (fusion protein : TEV protease) overnight at 4°C. The cleaved Δ51-RGS4 was then isolated by purification over an ANX column (GE Healthcare; Fairfield, CT) in 50 mM HEPES at pH 6.8 and 50 mM NaCl. The flow through, containing the ~99% Δ51-RGS4 as determined by SDS-PAGE gel, was then collected and concentrated using a YM-10 centrifugal concentrator (Millipore; Billerica, MA). The concentration of Δ51-RGS4 was calculated based on the absorbance at 280 nm utilizing a Take-3 plate (Biotek; Winnoski, VT) in a Synergy 2 plate reader (Biotek; Winnoski, VT).

Human RGS8 expression and purification was performed similar to other RGS8 purifications previously reported [103]. An RGS8 truncated construct analogous to the RGS4(Δ51) construct described above, amino acids 60 – 198 with a C-terminal 6 x His tag in the pET28 vector was expressed in BL21-RIPL E. coli (Stratagene; Santa Clara, CA) cells cultured in Terrific Broth (TB) media. Cultures were induced with 200 μM IPTG at OD_{600nm} of 2.0 and cultured for 16 h at 18°C. Pellet was lysed, centrifuged, and filtered as

described above except in RGS8 Buffer (50 mM HEPES at pH 7.5, 500 mM NaCl, 0.5 mM β-mercaptoethanol). Samples were loaded onto a Ni-NTA column (Qiagen; Hilden, Germany), 3 mL for every 1 L media, and washed with RGS8 Buffer supplemented with 25 mM imidazole. The protein was eluted using 200 mM imidazole and fractions were analyzed by SDS-PAGE gel. Fractions containing RGS8 >95% purity were pooled and protein concentration was determined by 280 nm absorbance as previously described above.

Human RGS17 was expressed and purified as a His-tagged protein in E. coli BL21-DE3 (Stratagene; La Jolla, CA), in the pET28 vector as previously described [91].

Human $G\alpha_{i1}$ (R178M, A326S) rate-altered variant, was expressed in BL21-DE3 E. coli, grown in TB media, as a 6 x His labeled protein in the pQE80 vector [67]. Expression was induced, at OD_{600nm} of 1.0, with 100 μM IPTG at 30°C for 16 h. Pellets were lysed, centrifuged, and filtered as described above, but in $G\alpha_i$ Buffer (50 mM HEPES at pH 7.5, 500 mM NaCl, 1 mM β-mercaptoethanol, and 20 μM GDP). The sample was first loaded onto a Ni-NTA column (Qiagen; Hilden, Germany), containing 3 mL of resin for every 1 L of media. The column was first washed with $G\alpha_i$ Buffer supplemented with 25 mM imidazole. $G\alpha_i$ was then eluted from the column with $G\alpha_i$ buffer supplemented with 300mM imidazole. After analysis by SDS-PAGE gel, fractions that contained $G\alpha_i$ were pooled and dialyzed overnight

against $G\alpha_i$ Dialysis Buffer (50 mM HEPES at pH 7.5, 25 mM NaCl, 1 mM β-mercaptoethanol, and 20 μM GDP). The sample was then loaded onto a Q-sepharose column (GE Healthcare; Fairfield, CT) and eluted along a salt gradient from 50 mM NaCl to 1 M NaCl in $G\alpha_i$ Buffer. The resulting peaks were then analyzed by SDS-PAGE for fractions containing >99% $G\alpha_i$. The purified $G\alpha_i$ was then assayed for activity utilizing the $[^{35}S]GTP\gamma S$ binding assay [83].

Rat $G\alpha_o$ was expressed in LB media as a fusion protein of glutathione-S-transferase (GST), 6 x His, and $G\alpha_o$, in pQLinkGD vector. Expression was induced, at OD_{600nm} of 0.5, with 100 μM IPTG at 30°C for 16 h. Pellets were lysed, centrifuged, and filtered as described above, but in $G\alpha_o$ Buffer (50 mM HEPES at pH 8, 100 mM NaCl, 10 μM GDP, 1 mM tris (2-carboxethyl) phosphine). The protein was first purified over a nickel charged resin column, 1 mL resin for every 1 L culture. Prior to elution, the column was washed with 20 mM imidazole to clear weak binding contaminants from the sample. The fusion protein was eluted with 250 mM imidazole. Fractions were collected and analyzed by SDS-PAGE gel. Fractions containing the protein of interest were pooled and loaded onto glutathione sepharose column (GE Healthcare; Fairfield, CT), 1.5 mL resin for every 1 L culture. The protein was then eluted with 1 mM free glutathione and analyzed by SDS-PAGE gel. Fractions containing >99% pure protein were pooled for activity

determination. The purified $G\alpha_o$ was then assayed for activity utilizing the [^{35}S]GTPγS binding assay [83].

Malachite Green Assay.

Stock solutions of each of the 3 components of the developing solution were prepared, which are stable for long-term storage [84]. Malachite solution was prepared by first diluting concentrated sulfuric acid 1 : 5 in distilled water. Once the solution cooled to 25°C, malachite solution was prepared by dissolving 0.44 g of malachite green oxalate (Alfa Aesar; Ward Hill, MA) in 360 mL diluted acid and stored at 25°C. Molybdate solution, containing 7.5% ammonium molybdate tetrahydrate (Alfa Aesar; Ward Hill, MA), was prepared in distilled water and stored at 4°C. Tween-20 solution, used to maintain solubility of the phosphate-molybdate-malachite complex, was prepared as 11% (v/v) Tween-20 in distilled water. On the day of use, 2.5 mL molybdate solution and 0.2 mL Tween-20 solution were added to 10 mL of malachite solution and mixed quickly to avoid precipitation of malachite. The final ratio of the Developing Solution (DS) was 50:12.5:1 (malachite:molybdate:Tween-20). The peak absorbance was determined by a 2nm step wavelength scan, using 10 μM Na_3PO_4 at pH 7.5 as the negative control.

The malachite green assay involves 5 components, with a 1 min centrifugation at 100 x g between each addition. For time-course

experiments, the first component was 10 μL Malachite Green Assay Buffer (MGB; 50 mM HEPES at pH 7.5, 100 mM NaCl, 5 mM EDTA, 10 mM $MgCl_2$, 0.01% lubrol) into a clear 384-well plate (ThermoFisher Scientific; Waltham, MA) using a MultiDrop dispenser (PerkinElmer; Waltham, MA). The second component dispensed was 10 μL of a 4x stock of RGS4, typically 200 nM to 1.6 μM with the target final concentration of 50 nM to 400 nM, diluted in MGB. After a 30 min incubation, 10 μL of the third component, 4x stock of $G\alpha_i$ diluted in MGB, was dispensed (typically between 4 μM and 80 μM with a desired final concentration 1 μM to 20 μM). After a minimum of 5 min incubation, 10 μL of the fourth component, 4x GTP diluted in MGB, was added at 10 minute intervals from 1 – 110 minutes. The 0 min time point was excluded due to amount of time required to proceed from GTP addition to quenching with DS. 4x GTP concentrations varied between 0.2 mM and 2.4 mM, with a target final concentration of 50 μM to 600 μM. To terminate the reaction, 10 μL of DS was added to each well using a Microlab Star liquid handling robot (Hamilton Robotics; Reno, NV), to achieve a final ratio 4 : 1 (sample : developing solution). Following centrifugation, the plate was incubated for 25 min before being read at 642 nm for absorbance using an EnVision plate reader (PerkinElmer; Waltham, MA). RGS8 was evaluated similarly to as described for RGS4, with 4x stock concentrations from 20 nM and 800 nM. For each time-course, corresponding GTP only wells were included to account for spontaneous hydrolysis of GTP over time.

Time-course experiments for RGS17 were conducted using the 5 component mixture, with a 1 min centrifugation at 500 x g between each addition. The first component was 10 µL MGB into a clear 384-well plate as previously described. The second component dispensed was 10 µL of a 4 x stock of RGS17 ranging between 1 µM to 4 µM with the target final concentration of 500 nM to 1 µM, diluted in MGB. After a 30 min incubation, 10 µL of the third component, a 4x stock of $G\alpha_{i1}$ diluted in MGB, was dispensed at a concentration of 4 µM into each well with a final target concentration of 1 µM. This was incubated for a minimum of 5 min. Then 10 µL of the fourth component, 4x GTP at 1.2 mM diluted in MGB, was added at 10 min intervals from 1 - 110 minutes with a final concentration of 300 µM. Reaction was terminated as previously described using 10 µL of DS and absorbance was read at 642 nm.

Malachite green GAP Activity assay for compound activity and Z-factor analysis conducted in 384-well plates utilized optimized parameters as discerned from the time-course experiments. 10 µL of 4 x compound or MGB was dispensed into appropriate wells. For single point assay, 160 µM compound was used, and for dose-response assays a series of ½ log dilutions from 100 µM final to 316 pM final was used. 10 µL of the optimized 4 x RGS4 concentration, 0.8 µM in MGB, was dispensed into all wells. After centrifugation at 100 x g for 1 min, the assay plate was incubated at 25°C for 30 min. 10µL of the optimized $G\alpha_i$ concentration, 20 µM in MGB, was

dispensed to each well and incubated at 25°C for 5 min. 10 μL of the optimized 4x GTP, 600 μM in MGB, was then added to the samples. After centrifuging the samples at 100 x g for 1 min, the samples were incubated at 25°C for 75 min. The samples were then stamped with 10 μL of DS and incubated for 25 min before reading absorbance at 642 nm.

1536-well Z-factor analysis and compound library screen were accomplished largely as described for 384-well plates. Initial screen and Z-factor determination was performed in a final concentration of 5.5% dimethylsulfoxide. For 1536-well assays NUNC clear plates were used (ThermoFisher Scientific; Waltham, MA). For the compound library, the diverse set of known biologically active compounds, The Spectrum Library (MicroSource; Gaylordsville, CT), was chosen. Each component was dispensed as 1.8 μL samples into each well using a FlexDrop (PerkinElmer; Waltham, MA). To develop the plates, 1.8 μL of DS were stamped in quadrants using the Microlab Star liquid handling robot. After a 25 min incubation, the plates were analyzed using an EnVision plate reader (PerkinElmer; Waltham, MA) at 642 nm absorbance.

ALPHA-Screen Counter-Screen of RGS4.

Chemical labeling of RGS4 was performed using biotinamidohexanoic acid N-hydroxy succinimide ester (Sigma Aldrich; St Louis, MO). The reaction was carried out at a molar ratio of 3 : 1 (label : protein) for 3 h at 4°C

in 50 mM HEPES at pH 8 and 100 mM NaCl, similar to as previously described [57]. The reaction was then quenched with 10 μL of 1 M glycine for 10 min at 4°C. The free label was then separated from the desired protein using a YM-10 centrifugal concentrator. Final concentration of RGS4 was determined by 280 nm absorbance of the sample.

To prepare RGS4 for analysis using the ALPHA-Screen assay, RGS4 constructs were first labeled in a 1440 μL sample, diluted in Assay Buffer (AB 20mM HEPES at pH 8, 100 mM NaCl, 0.1% Lubrol, 1% bovine serum albumin), containing 60 nM RGS4, 14.4 μL streptavidin ALPHA-Screen beads (Perkin-Elmer; Waltham, MA). The sample was then incubated for 30 min, on ice, prior to dilution with AB to 2880 μL. In duplicate, 20 μL of each compound at 120 μM was plated across a white 384-well plate (ThermoFisher Scientific; Waltham, MA). 20 μL RGS4 was then plated into each well and the samples were incubated at 19°C for 30 min prior to the addition of GST-$G\alpha_o$. The final concentrations for RGS4 and compound will be 20 nM and 40 μM respectively.

GST-$G\alpha_o$ was prepared for the assay by creating a 1440 μL labeling reaction, diluted in AB, containing 3 nM GST-$G\alpha_o$, 10 μM GDP, and 14.4 μL anti-GST ALPHA-Screen Beads(Perkin-Elmer; Waltham, MA). The sample was incubated for 30 min on ice. A 40 μL sample was then removed and diluted with 40 μL AB; this is the positive control. The remaining 1400 μL is then diluted with 1400 μL AB supplemented with AMF (5 μM $AlCl_3$, 5 mM

$MgCl_2$, 5 mM NaF) to a final volume of 2800 µL. 20 µL of each sample was then dispensed into the each well. The final concentration of the GST-$G\alpha_o$ will be 0.5 nM.

Following the addition of both GST-$G\alpha_o$ and biotinylated Δ51-RGS4, the plates were incubated at 19°C for 1 hr prior to reading using the Synergy 2 plate reader.

Mass Spectrometry Analysis

RGS4(WT) was treated for 30 min at room temperature in MGB with a 2 fold excess of compound (1 µM protein : 2 µM compound). Samples were then diluted 1:10 and analyzed using a LC-ESI-IT-TOF (Shimadzu; Tokyo, JP) according to previous methods [59].

Isothermal Titration Calorimetry Analysis

Samples were analyzed using a MicroCal VP-ITC (GE Lifesciences; Uppsala, Sweden). Assays consisted of 50 µM protein in the sample cell and 500 µM compound in the injection well, suspended in matching MGB buffer. Assays consisted of twenty 18 µL injections for a final protein : compound ratio of 1: 2. Between each injection, samples were monitored for 180 s. Data was analyzed using provided Origin Software (GE Lifesciences; Uppsala, Sweden.)

Data Analysis.

Data were analyzed using Prism analysis software (Graphpad Software; La Jolla, CA). Initial malachite green assay optimization was accomplished by comparing the fit of both straight line and hyperbolic functions. The fit that mostly closely resembled the data was used to represent the data. IC_{50} values for each compound were determined by fitting the data to a sigmoidal curve, which was used to calculate the IC_{50} value.

Results

Optimization of Malachite Green Assay.

The initial focus of these experiments was to determine optimal conditions for the malachite green assay. A wavelength scan of 40 µL of 10 µM Na_3PO_4 at pH 7.5 developed for 50 min with 10 µL DS yielded an intense signal peak at 642 nm, with a secondary peak at 436 nm (Figure 3.2). These peaks coincide closely with the reported literature values of 630 nm and 425 nm [84]. Initial concentrations for each of the components were determined as a ratio of 200 nM RGS4 to 5 µM $G\alpha_i$ based on previously reported ratios [67]. In a time-course evaluation of different concentrations of $G\alpha_i$, higher concentrations of $G\alpha_i$ were excluded due to rapid saturation of the assay, even in the absence of RGS4. Lower concentrations of Gαi proved too slow and provided a small signal window even at 110 min leading to the selection of 5

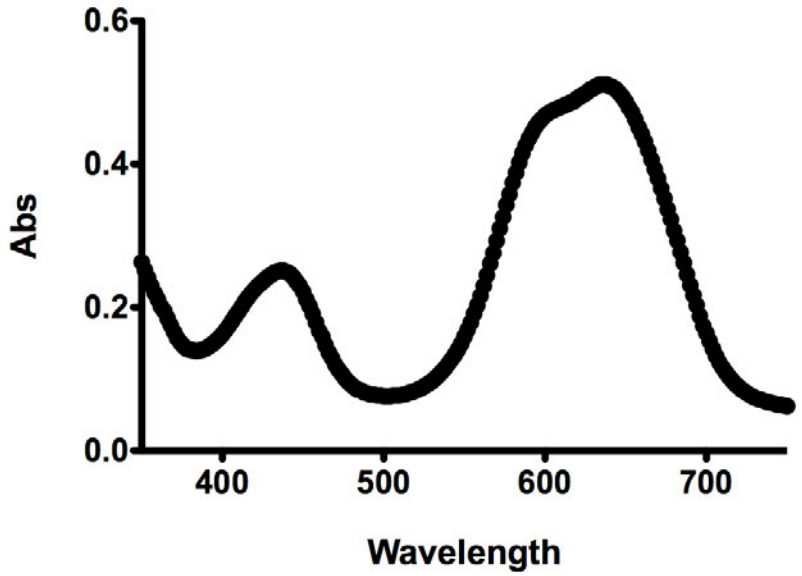

Figure 3.2 Wavelength Scan of 10 μM Na_3PO_4. Using 10 μM Na_3PO_4 as a control, a wavelength scan of the absorbance of the system was evaluated to determine the optimal wavelength for detection. Two peaks were detected with local maxima at 436 nm and 642 nm. Image shown is the representative of n=3 experiments.

μM as the optimal final concentration of $G\alpha_i$, as shown in Figure 3.3a. An added benefit of the higher $G\alpha_i$ concentration is the detection of its intrinsic GTPase activity, marked as open circles in Figure 3.3a, which allows for an internal control to detect compounds that inhibit $G\alpha_i$ rather than the RGS protein. Having selected 5 μM $G\alpha_i$ as the optimal concentration, we compared a variety of RGS4 concentrations. As shown in Figure 3.3b, both 200 nM was excluded due to rapid saturation of the assay. Similarly, the rates of reaction at concentrations of 50 and 100 nM RGS4 proved too slow for our HTS application, generating a similar signal window 1 h slower than those at 200

Figure 3.3 Optimization of Malachite Green Assay for RGS4. (a) Increasing concentrations of $G\alpha_i$, 1 μM to 20 μM final, were compared using final concentrations of 200 nM RGS4 and 300 μM GTP. Absorbance at 642 nm was read every 10 min. Each sample was graphed as with 200 nM RGS4 (closed symbols) or without (open circles). GTP only (300 μM final) control wells were used for background subtraction. (b) Increasing concentrations of RGS4, from 50 to 400 nM final, were compared using $G\alpha_i$ at 5 μM final, and 300 μM GTP. Absorbance at 642 nm was read every 10 min. GTP only (150 μM final) control wells were used for background subtraction. (c) Increasing concentrations of the GTP, from 50 to 600 μM final, were compared using RGS4 (200 nM) and $G\alpha_i$ (5 μM), final concentrations. Samples were read at 642 nm absorbance every 10 min. Data shown is the average of n=3 experiments.

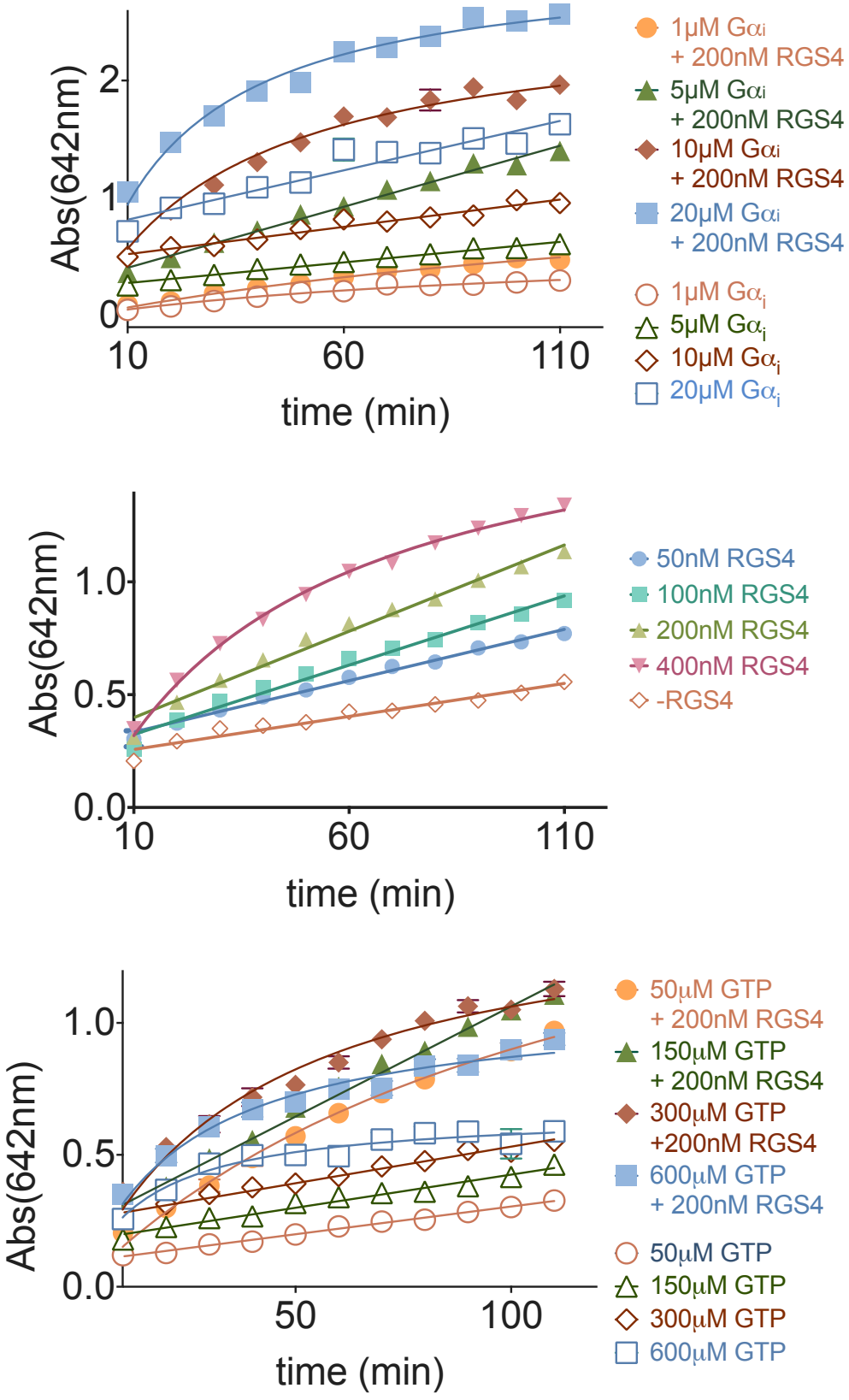

Figure 3.3 -- continued

nM RGS4 under the same conditions. The final component for optimization, GTP concentration, was evaluated using the selected concentrations of 200 nM RGS4 and 5 μM $G\alpha_i$, as shown in Figure 3.3c. Higher concentrations of GTP generated increasingly high background, saturating the system early, preventing the development of the large signal window seen previously. For lower concentrations, 50 μM GTP showed substrate depletion as the reaction progressed. Due to similar results between both 150 μM and 300 μM GTP, The lower concentration of 150 μM GTP was selected due to the reduced background signal. From this optimization, the ideal concentrations for RGS4 were determined to be 200 nM RGS4, 5 μM $G\alpha_i$, and 150 μM GTP. For comparison, various RGS8 concentrations were challenged against the optimized $G\alpha_i$ and GTP concentrations of RGS4, Figure 3.4a, and, as previously reported in literature, RGS8 was about twice as potent a GAP as RGS4, developing a similarly sized signal window with about half as much protein [92]. For comparison outside the R4 family, a RZ/A family member: RGS17, was similarly explored. As previously reported in literature, more RGS17 was required to generate a similar signal window, Figure 3.4b, due to its weak interaction with $G\alpha_{i1}$ [99]. To confirm the value of this now optimized assay, a comparison of RGS4 with and without 10 μM CCG-50014, a potent inhibitor of RGS4, was used to determine a Z-factor of 0.8, as shown in Figure 3.5a [92].

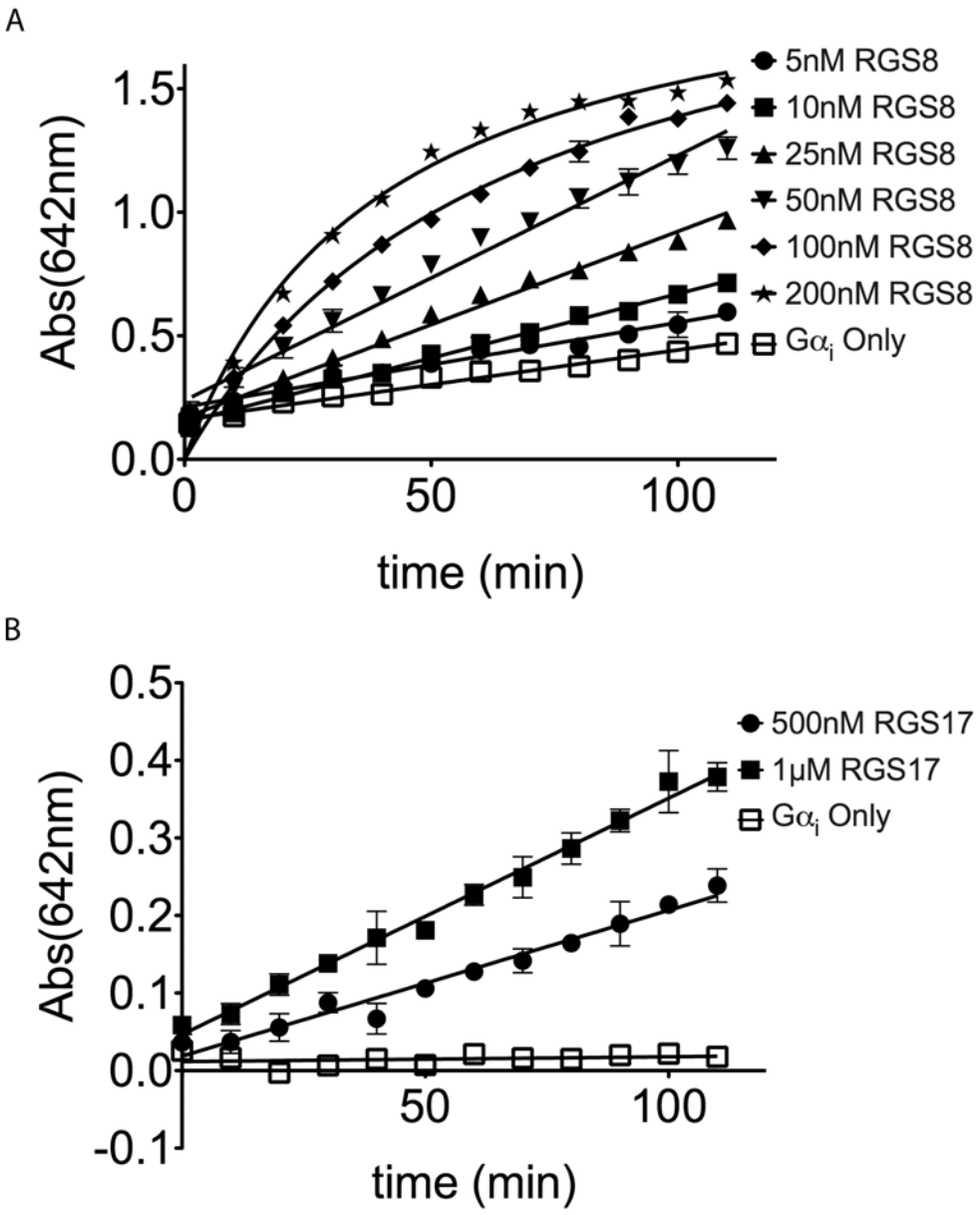

Figure 3.4 Characterization of Malachite Green Assay with RGS8 and RGS17. (a) Increasing concentrations of RGS8 from 5 nM final to 200 nM final, represented as closed symbols, show signal about equal to 2 x the concentration of RGS4, similar to as shown in literature [77]. For comparison, 5 μM final $G\alpha_i$ was included, represented by open symbols. GTP only (150 μM final) control wells were used for background subtraction. (b) Using a $G\alpha_i$ double mutant protein with an accelerated K_{off} for GDP exchange and decrease K_{cat} for GTPase activity we can monitor the effect of RGS17 on the intrinsic GTPase activity of the $G\alpha_i$ subunit. GTP only (300 μM final) wells were used for background. Data shown are the average of n=3 experiments.

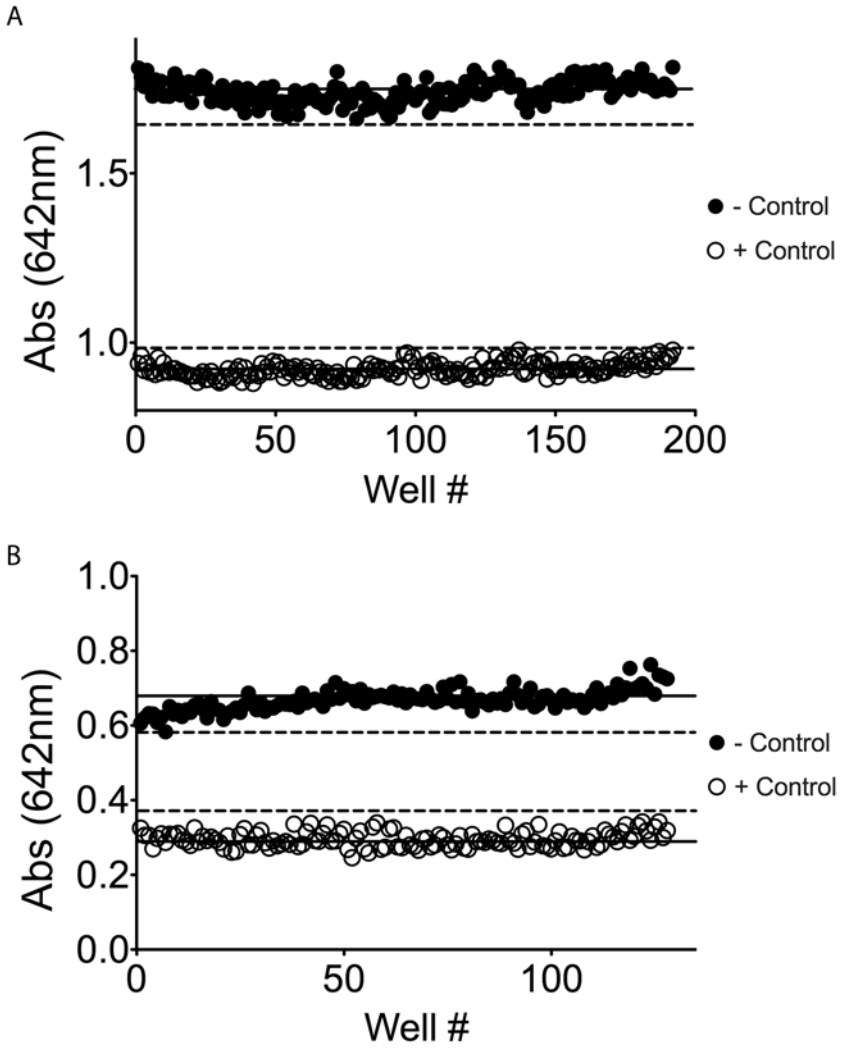

Figure 3.5 Determination of the Z-factor for 384-well and 1536-well assay. (a) In a 384-well plate, 192 wells were used as a negative control (buffer only), marked as closed circles. 192 wells were used as positive controls and were treated with CCG-50014, a potent RGS4 inhibitor, (10 μM final) marked as open circles [92]. The solid lines represent the mean for the negative and the positive control (1.74 and 0.92 respectively). The dashed lines marks the 3 standard deviation cut off for both the positive and negative control (standard deviation of 0.033 and 0.021 respectively). (b) This assay was conducted in 5.5% DMSO, same as HTS. In a 1536-well plate, 128 wells received buffer, negative control (closed symbols) and the remaining 128 wells received 10 μM final CCG-50014, positive control (open symbols). The solid lines represent the mean value for the negative control and the positive control (0.67 and 0.30 respectively). The dashed lines marks the 3 standard deviation cut off for both the positive and negative control (standard deviation of 0.028 and 0.021 respectively). The data shown is representative of one screen.

HTS Screen.

Following initial characterization of the assay, the assay was optimized for use in a 1536-well HTS format. Maintaining identical concentrations to the development of the assay in 384-well format, the miniaturized assay yielded a Z-factor of 0.6, Figure 3.5b. A screen of the Spectrum library was performed in two 1536-well plates and a final concentration of 40 μM for each compound. Compounds were determined to be hits if they were greater than 3 standard deviations from the mean negative control values. From this initial screen of 2320 compounds, 59 compounds (2.5%) were determined to be hits, Figure 3.6a and Figure 3.6b. While this would normally be considered an exceedingly high initial hit rate, the Spectrum Library consists of large set of known biologically active compounds [104].

Hit Confirmation and Counter-Screen.

Initial hits were confirmed by single point malachite green assay at 40 μM compound. Of the initial 59 compounds, 7 compounds fell within 3 standard deviations of the negative control, Figure 3.7a, leaving 52 compounds (2.2%). The assay was followed up with an interference assay designed to test for inhibition of the detection method using 50 μM Na_3PO_4 at pH 7.5 to mimic the maximum detectable released P_i by the assay. This control would detect compounds that either interrupt the detected complex or reduce the molybdate resulting in peak shift outside of the desired

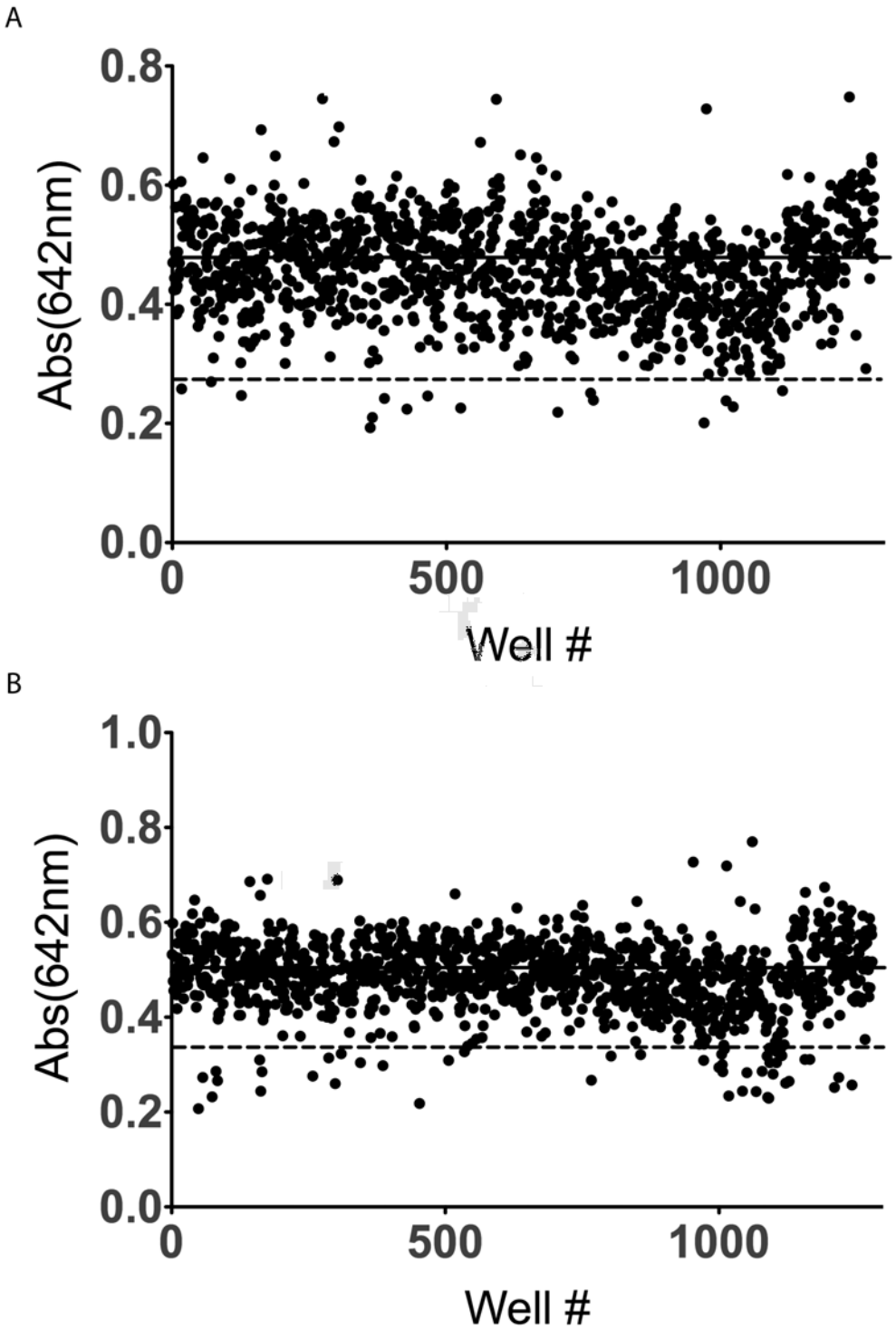

Figure 3.6 High Throughput Screen of Spectrum Library. Solid line represents mean negative control. Dashed line represents 3 standard deviations from control and consideration as a hit. (a) In plate one, 16 compounds were identified as hits. (b) In plate 2, an additional 43 compounds were identified. Image shown is the representative of one screen.

wavelength. One compound was found to disrupt the assay (Figure 3.7b). Compounds that increased the predicted absorbance were carried through, as they would indicate false negatives in the assay. A counter-screen focusing on the intrinsic GTPase activity of the $G\alpha_i$ mutant followed (Figure 3.7c). Utilizing the known GTPase activity of the $G\alpha_i$ mutant, this assay identified compounds that inhibited the $G\alpha_i$ subunit rather than the RGS protein. This assay, conducted at 40 μM compound, identified 5 compounds that interfered with the assay due to the compound falling 3 standard deviations below the negative control, bringing the total to 45 compounds (1.6%) of the screened library. ALPHA Screen was utilized as an orthogonal assay to confirm each of the remaining compounds as hits, Figure 3.8a. ALPHA Screen has been successfully used to assay RGS-G-protein interactions in literature [91]. The ALPHA-Screen assay functions by measuring the amount of stable complex formed between the RGS protein and the Gα subunit using the transition state mimic GDP-AlF_4^-. This orthogonal assay eliminated 15 compounds, leaving 30 compounds or 1.3% of the total compounds screened. Finally, compounds were challenged against the RGS4(Δ7) mutant in the malachite green phosphate detection assay, with the desire of eliminating thiol-modifiers similar to those previously discovered in HTS campaigns against RGS4 [59]. Of the 30 compounds remaining, only 13 compounds also inhibited the RGS4(Δ7) mutant (Figure 3.8b).

Figure 3.7 Single Point Hit Confirmation and Control Screens. (a) Single point hit confirmation assay was an analysis of each of the initial hits in a 384-well format (40 μM final for each compound). 7 compounds fell within 3 standard deviations of the negative control and were excluded from further analysis. (b) Phosphate control assay was a comparison of each compound's (40 μM final) ability to inhibit the assay itself, containing 50 μM phosphate instead of protein. Dashed line represents 3 standard deviations from the negative control. 1 compound fell below 3 standard deviations and was excluded from further analysis. (c) At 40 μM final for each compound, the $G\alpha_i$ control assay evaluated each compound for inhibition of $G\alpha_i$ (5 μM final). The dashed line represents 3 standard deviations below the negative control. 5 compounds fell below 3 standard deviations and were excluded from further analysis. Filled bars represent compounds retained to following experiments. Open bars represent compounds excluded from further analysis. Data shown are representative of one counter screen.

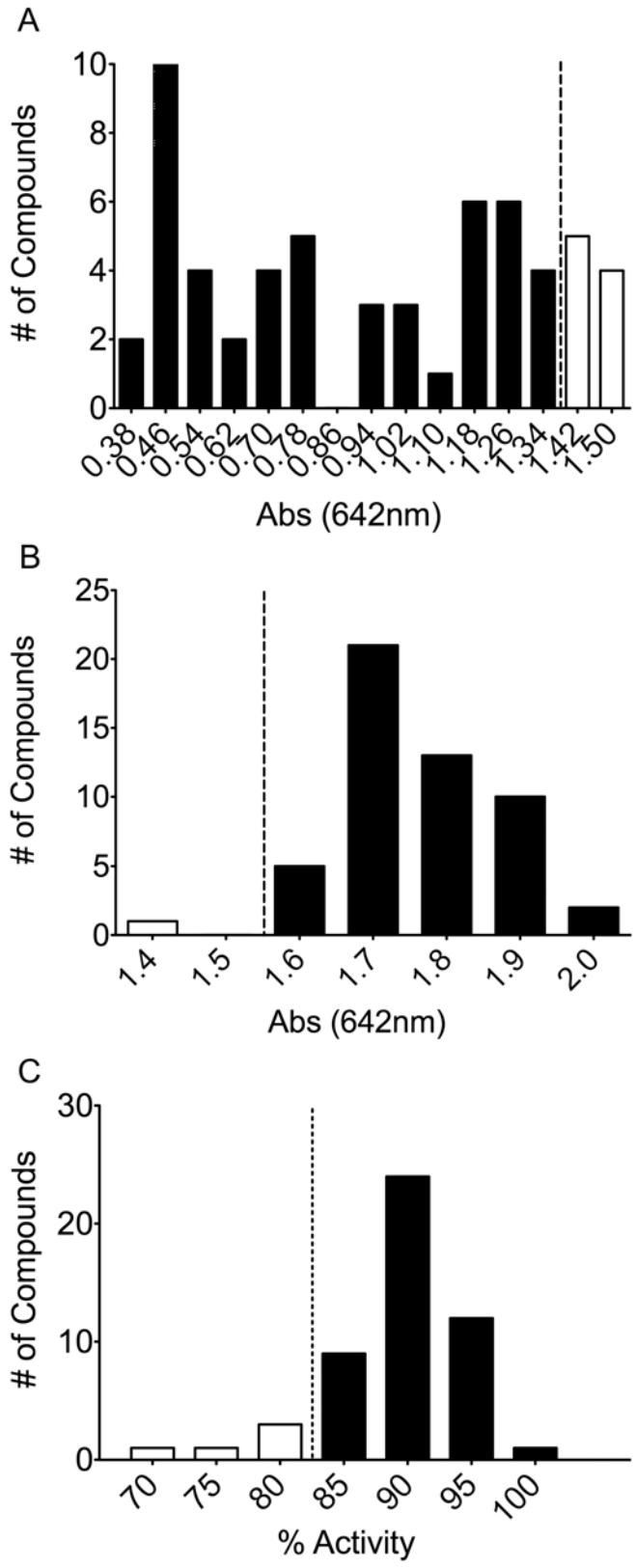

Figure3.7 -- continued

Characterization of Confirmed Compounds.

The activity of each of the 13 remaining compounds was assayed by generating concentration-response curves against RGS4 as well as the RGS4(Δ7) mutant. Figures 3.9a and 3.9b shows the 4 compounds selected for future analysis. UI-5 (Figure 3.10a) had an IC_{50} of 126 μM and 454 μM against the RGS4(WT) and RGS4(Δ7) respectively. The most potent compound, UI-1590 (Figure 3.10b), had an IC_{50} of 724 nM against RGS4(WT) and an IC_{50} of 88 μM against RGS4(Δ7). Finally, two structurally similar compounds, UI-1907 (Figure 3.10c) and UI-2034 (Figure 3.10d), had IC_{50} values of 16 μM and ~269 mM against RGS4(WT), respectively. Against the RGS4(Δ7) mutant, the compounds had IC50 values of 51 μM and 181 μM, respectively. Each of the hit compounds were far less potent against the RGS4(Δ7) mutant than RGS4(WT), similar to what has been reported in literature [77]. The 4 selected compounds were analyzed by mass spectrometry. Of the compounds analyzed, UI-5, UI-1907, and UI-2034 showed no covalent modification of RGS4(WT) (Figure 3.11a, Figure 3.11c, and Figure 3.11d respectively). UI-1590 covalently modified RGS4, appearing as a novel peak of +460 in Figure 3.11b. Each of the 4 compounds were then evaluated for binding to both Δ51-RGS4(WT) and $G\alpha_{i1}$(RTO) using isothermal titration calorimetry (ITC). The compound UI-5, shown in Figure 3.12a, bound directly to RGS4(WT) with an affinity of 580 nM and very poor or indeterminable binding to $G\alpha_{i1}$(RTO), shown in Figure 3.12b. Evaluation of

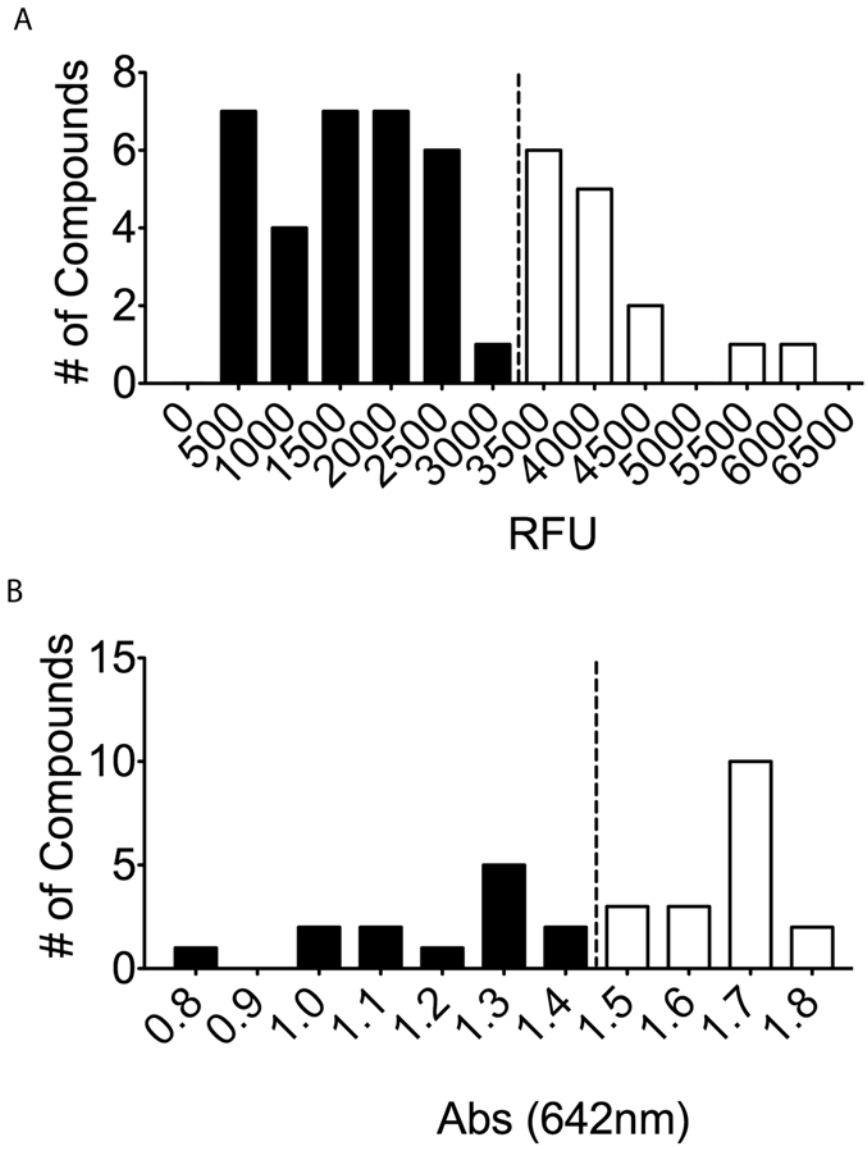

Figure 3.8 ALPHA-Screen orthogonal assay and RGS4(Δ7) counter screen. (a) At 40 μM final for each compound, this assay was used to confirm each compound as an inhibitor of RGS4 (20 nM final) through another assay. The dashed line represents the cutoff, 3 standard deviations from negative control. 15 compounds fell within 3 standard deviations of the negative control and were excluded from further analysis. (b) This single point assay, at 40 μM compound, was used to confirm activity of each compound against the RGS4(Δ7) mutant (200 nM final). The dashed line represents 25% inhibition, the cutoff for compounds carried forward. 18 compounds failed to inhibit the RGS4(Δ7) mutant of RGS4 and were excluded from further analysis. Filled bars represent compounds were retained for further analysis. Open bars represent compounds excluded from further analysis. Image shown is the representative of one counter screen.

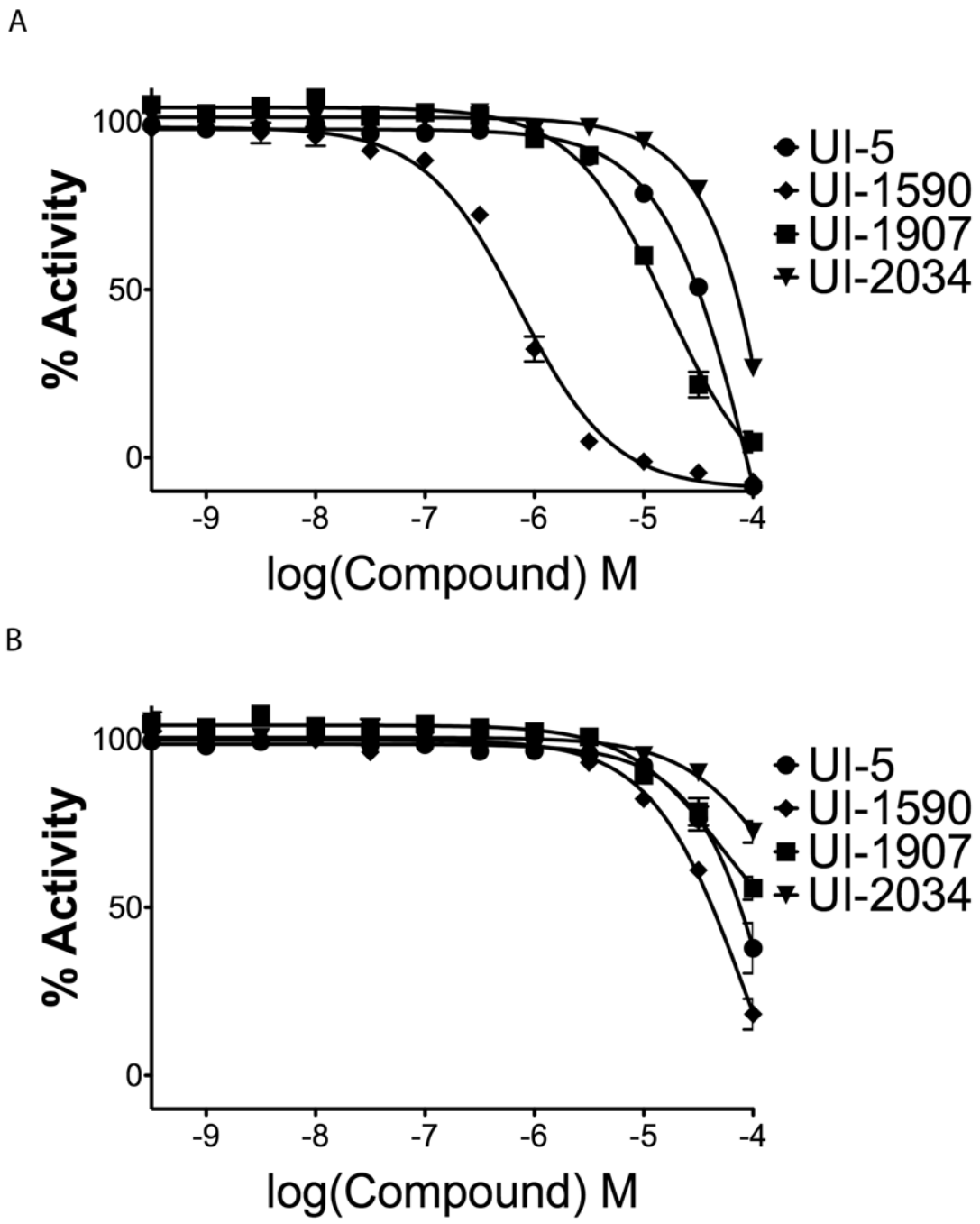

Figure 3.9 Dose-response anaylsis of UI-5, UI-1590, UI-1907, UI-2034. (a) Inceasing concentrations of compound challenged against RGS4(WT), 200 nM final, in the malachite green assay. (b) The same compounds were compared against the RGS4(Δ7) mutant. All compounds have marked lower potency against the RGS4(Δ7) than the RGS4(WT). Image shown is the average of n=3 experiments.

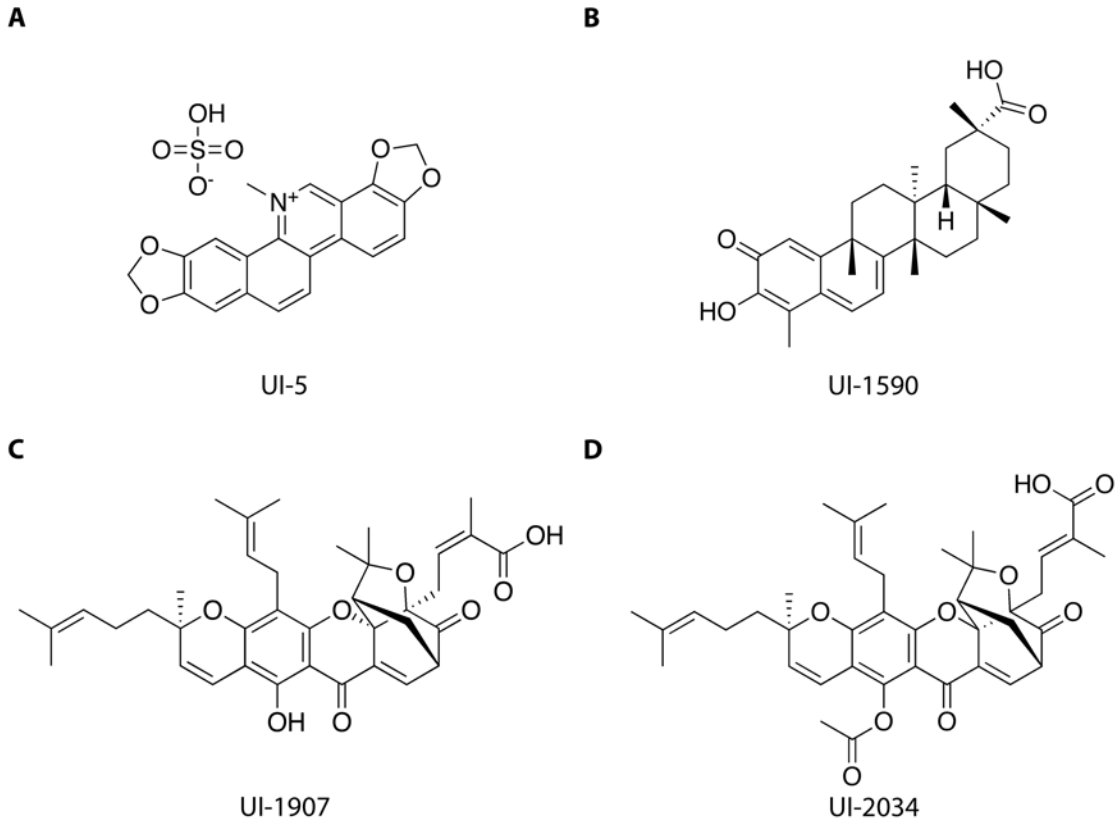

Figure 3.10 Structure of identified Compounds. (a) UI-5, also known as sanguinarium sulfate. (b) UI-1590 is the pre-therapeutic anti-cancer compound celastrol [72]. (c) UI-1907 is gambogic acid. (d) UI-2034, acetyl-isogambogic acid, is an analogue of UI-1907.

UI-1590 revealed no specific binding to either RGS4(WT) or $G\alpha_{i1}$, shown in Figure 3.13a and Figure 3.13b. The raw ITC data indicates that the modification, shown to be covalent, is due to spontaneous modification upon interaction, rather than specific binding. This long lag between injection and return to baseline is most likely the result of nonspecific covalent interactions between the compound and the protein. Both UI-1907 and UI-2034 were not evaluated due to poor solubility of each of the compounds in the assay buffer.

Figure 3.11 MS Analysis of Compound Treatment. RGS4(WT) was treated with 2 fold excess of each compound and analyzed for adduct formation using Mass Spectrometry. For each sample left side shows untreated spectra and the right side shows treated spectra. (a) RGS4(WT) treated with UI-5. No adduct detected. (b) RGS4(WT) treated with UI-1590. 1 adduct detected (+460 m/z). (c) RGS4(WT) treated with UI-1907. No adduct detected. (d) RGS4(WT) treated with UI-2034. No adduct detected. Images shown are representative of n=3 experiments.

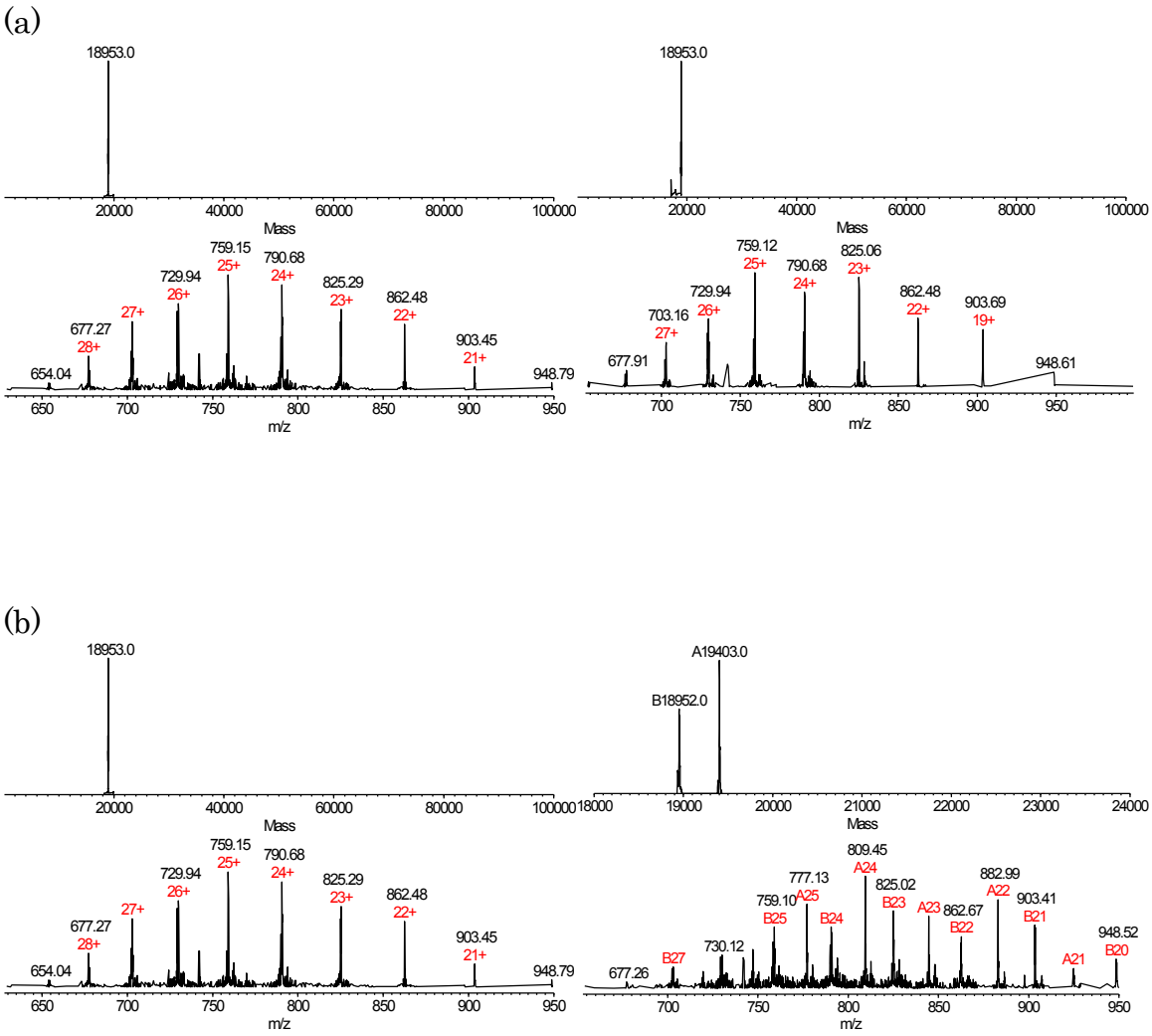

Figure 3.11 -- continued

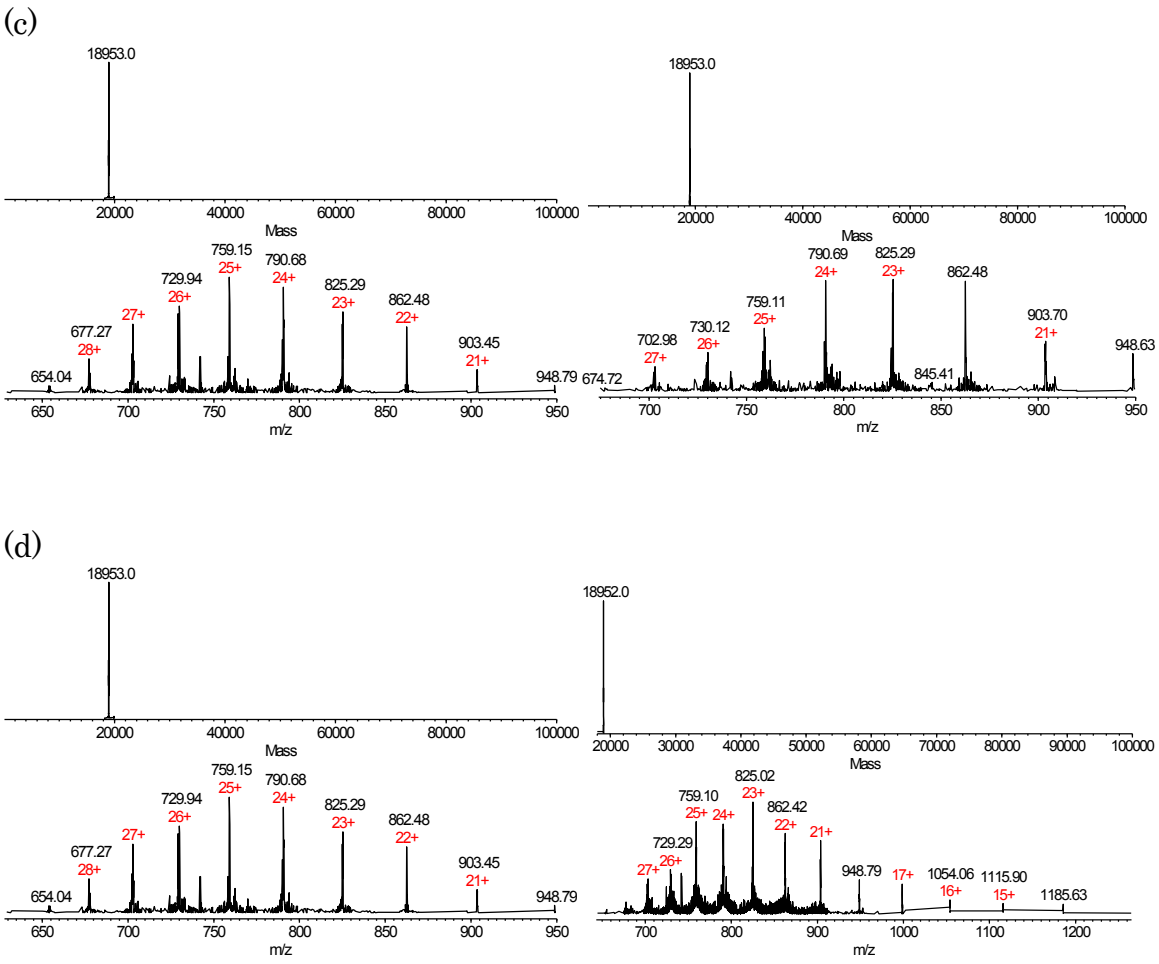

Figure 3.11 -- continued

Discussion

RGS proteins are interesting targets due to their role in modulating G-protein signaling. Previous work identifying inhibitors of R4 family RGS proteins have centered on the disruption of the high affinity RGS – Gα interaction observed in the presence of AlF_4^-, which mimics the transition state of GTP bound to a Gα subunit [77,91]. While valid methods for determination of RGS inhibitors, the transition state mimic generated by AlF_4^- generates an RGS - Gα protein : protein interaction with approximately 50-fold higher than basal affinity [35-36]. The objective of developing this assay was to generate an assay for measuring steady state protein activity that would be economical, fast, easy to use, and adaptable to members of other RGS protein families. The assay developed met each of those criteria.

The initial setup for the assay, for each 1536-well plate, was 1.5 h, which includes incubation steps for the production of free phosphate, allowing the assay to be conducted in highly parallel fashion. Using a colorimetric dye for readout is straightforward and can be accomplished on the simplest of plate readers in absorbance mode. Speed is also essential, and the total read time for each 1536-well plate was only 8 minutes, though this is plate-reader dependent. Perhaps most important is that this assay ameliorates a major concern in high throughput screening – the presence of library compounds that may absorb at a wavelength critical for the assay's readout. In the case

Figure 3.12 ITC Analysis of UI-5. ITC analysis of RGS4(WT) and Gαi1 binding of UI-5. (a) 50 μM RGS4(WT) was treated with 14 μL injections of 500 μM UI-5. UI-5 was found to bind to exactly 1 binding site on RGS4(WT). Above shows the raw heat traces and below the integrated peak intensity. UI-5 bound with a Kd of 580 nM. (b) 50 μM $G\alpha_{i1}$(RTO) was treated with 14 μL injections of 500 μM UI-5. UI-5 was found to not significantly bind to $G\alpha_{i1}$(RTO). Above shows the raw heat traces and below the integrated peak intensity. The data shown are representative of n=3 experiments.

(a)

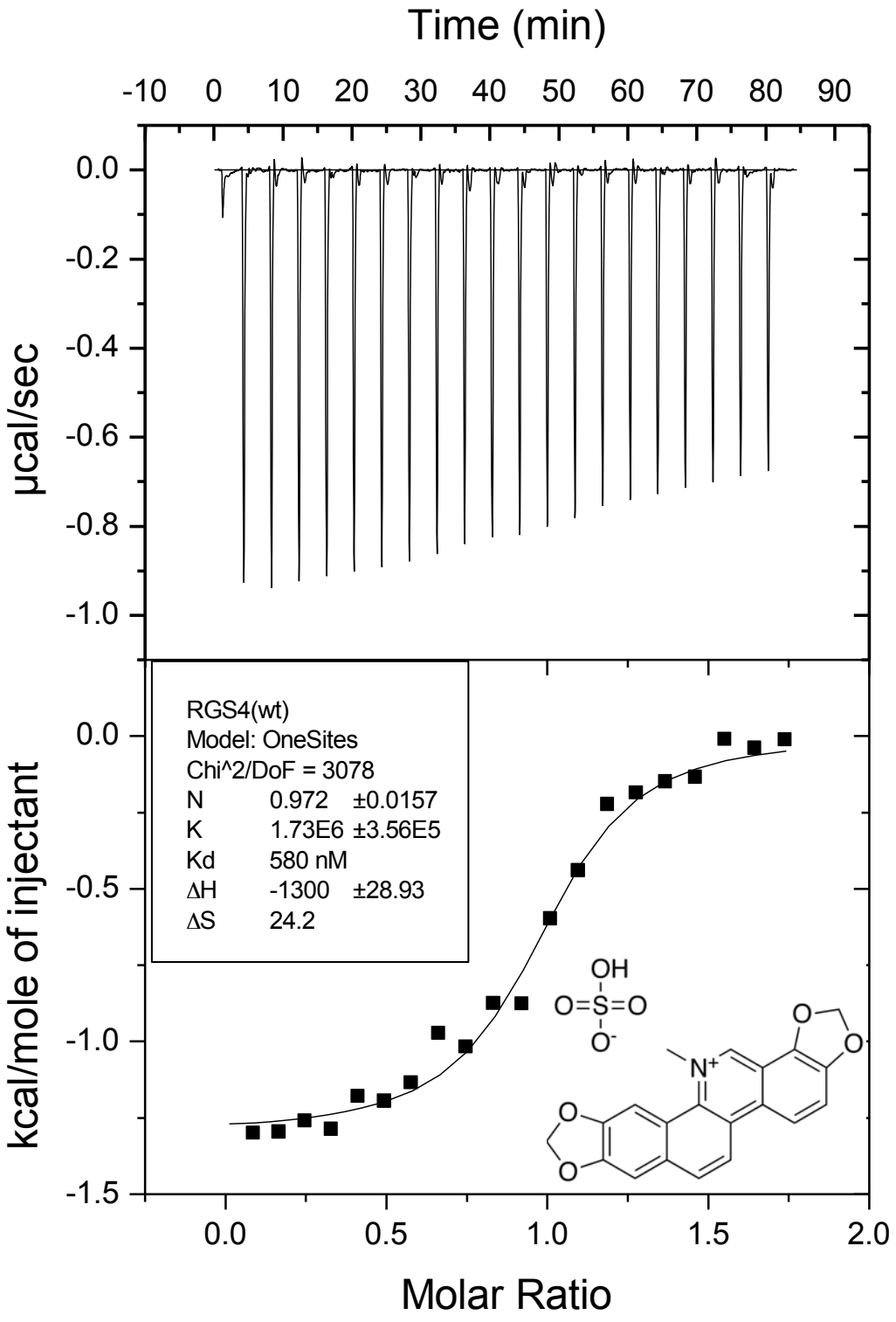

Figure 3.12 -- continued

(b)

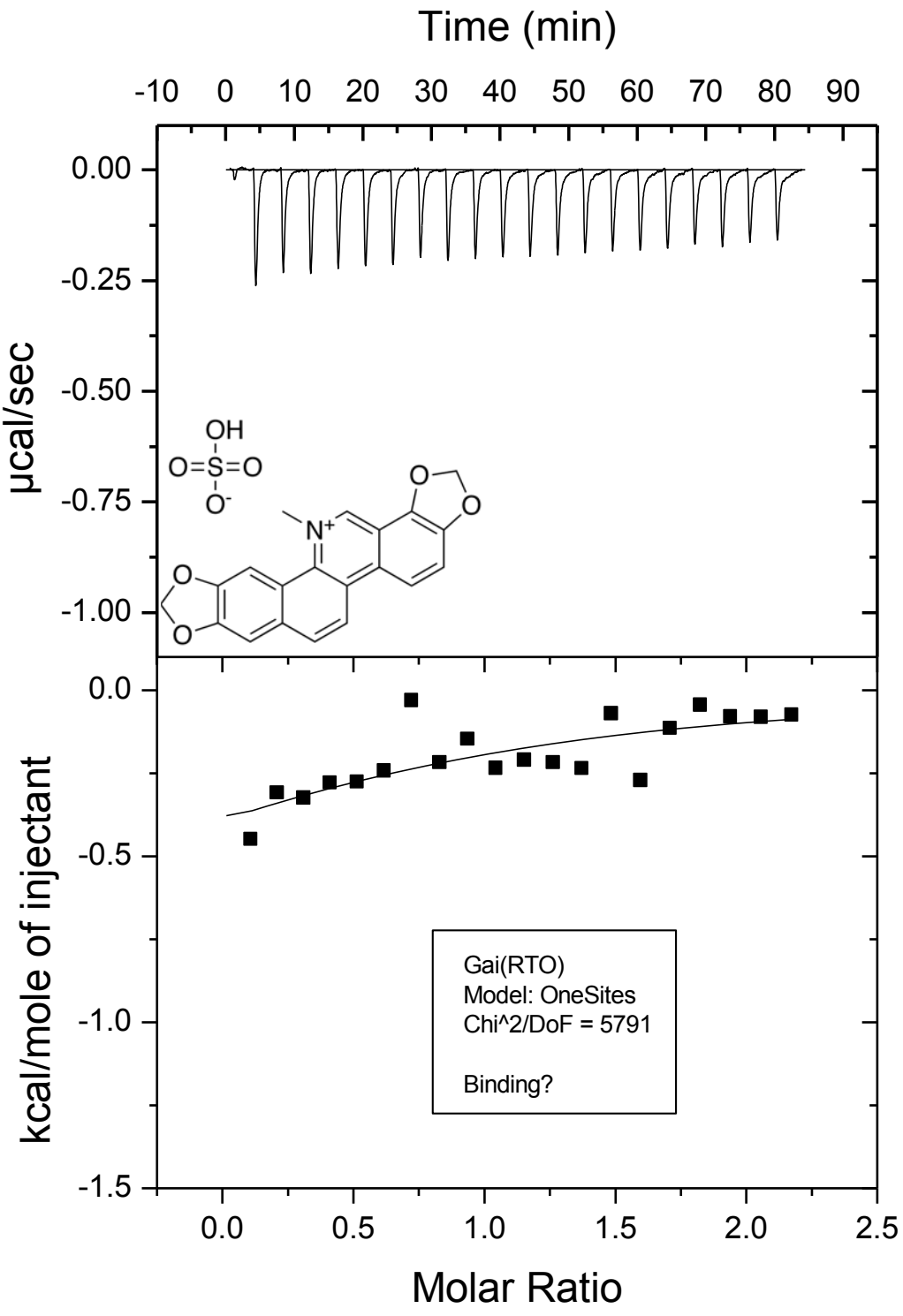

Figure 3.12 -- continued

of this malachite green assay, the primary wavelength for the absorption read of the assay is at 642 nm, however, a secondary peak is also present at 436 nm, which provides a second readout to help discriminate compounds that may interfere with the primary readout at 642 nm. The absorbance at 436 nm is lower intensity than that at 642 nm, however it is quite usable as a secondary, confirmatory readout – and one that can be run on the same sample as the primary read (Figure 3.2 and Figure 3.14).

After careful characterization of the constraints of the assay itself, we moved to a small-scale, proof-of-concept screen using a small molecule library of 2320 compounds (MicroSource; Gaylordsville, CT), summarized in Figure 3.15. The initial results for the 2320 compound library yielded an initial hit rate of 2.5% (59 compounds) that inhibited (by at least 3 standard deviations below the negative control) RGS-mediated GAP activity. RGS-mediated GAP activity is indicated by an increase in free P_i, generated by hydrolysis of GTP, available to complex with malachite green and increase absorbance at 642nm. An initial triage included the exclusion of hit compounds that interfered with the assay by directly inhibiting the chemical reactions of the assay readout or inhibiting $G\alpha_i$ itself reduced this hit rate to approximately 2.0%. 7 compounds failed to inhibit RGS4 greater than 3 standard deviations from the negative control in the initial hit confirmation assay using 40 μM compound. One compound was found to interfere with the malachite green

Figure 3.13 ITC Analysis of UI-1590. ITC analysis of RGS4(WT) and Gαi1 binding of UI-1590. For each panel, above shows raw heat traces and below the integrated peak intensity. (a) 50 μM RGS4(WT) was treated with 14 μL injections of 500 μM UI-1590. UI-1590 does not specifically bind to RGS4(WT). (b) 50 μM $G\alpha_{i1}$(RTO) was treated with 14 μL injections of 500 μM UI-1590. UI-1590 was found to not significantly bind to $G\alpha_{i1}$(RTO). The data above are representative of n=3 experiments.

(a)

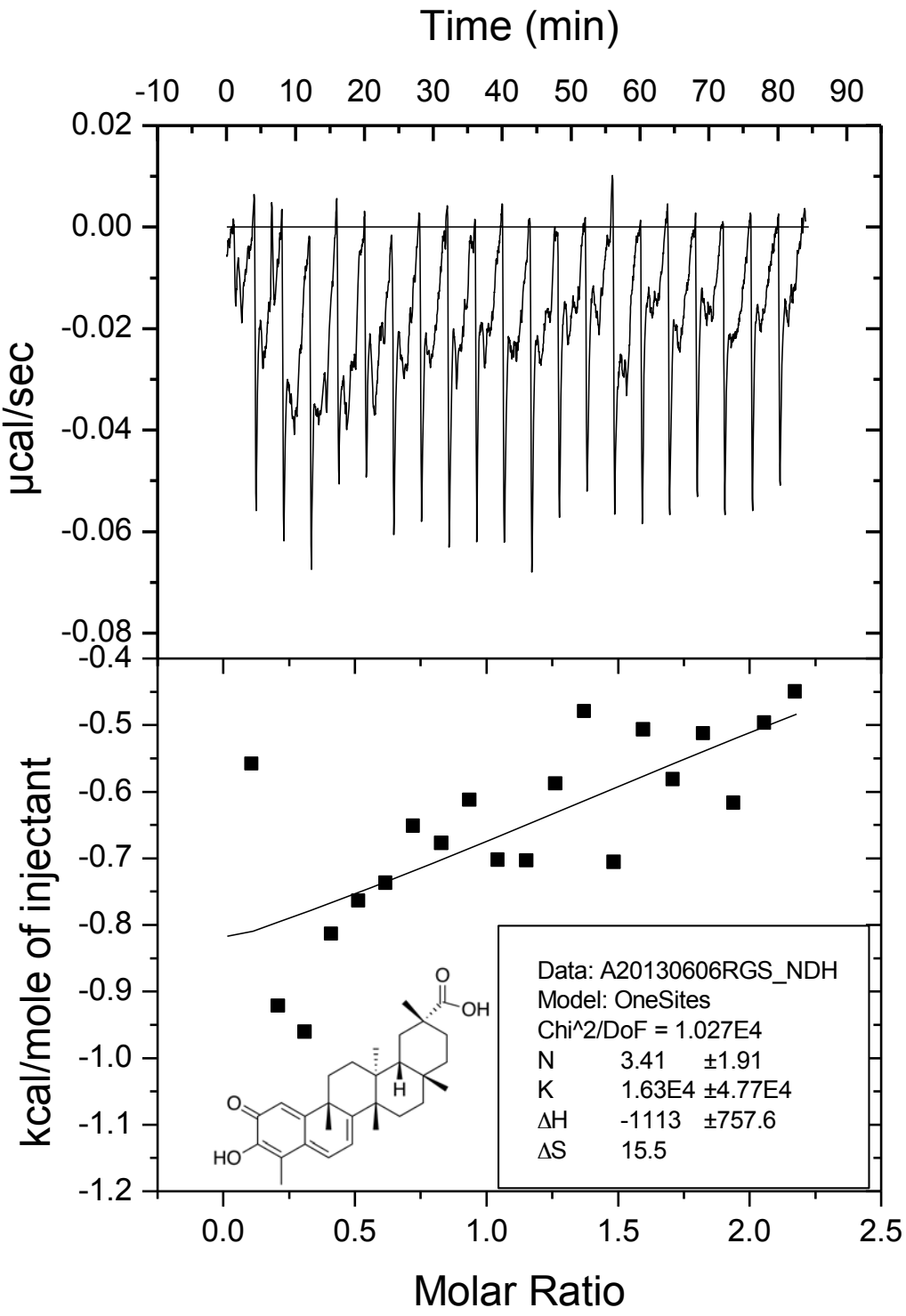

Figure 3.13 -- continued

(b)

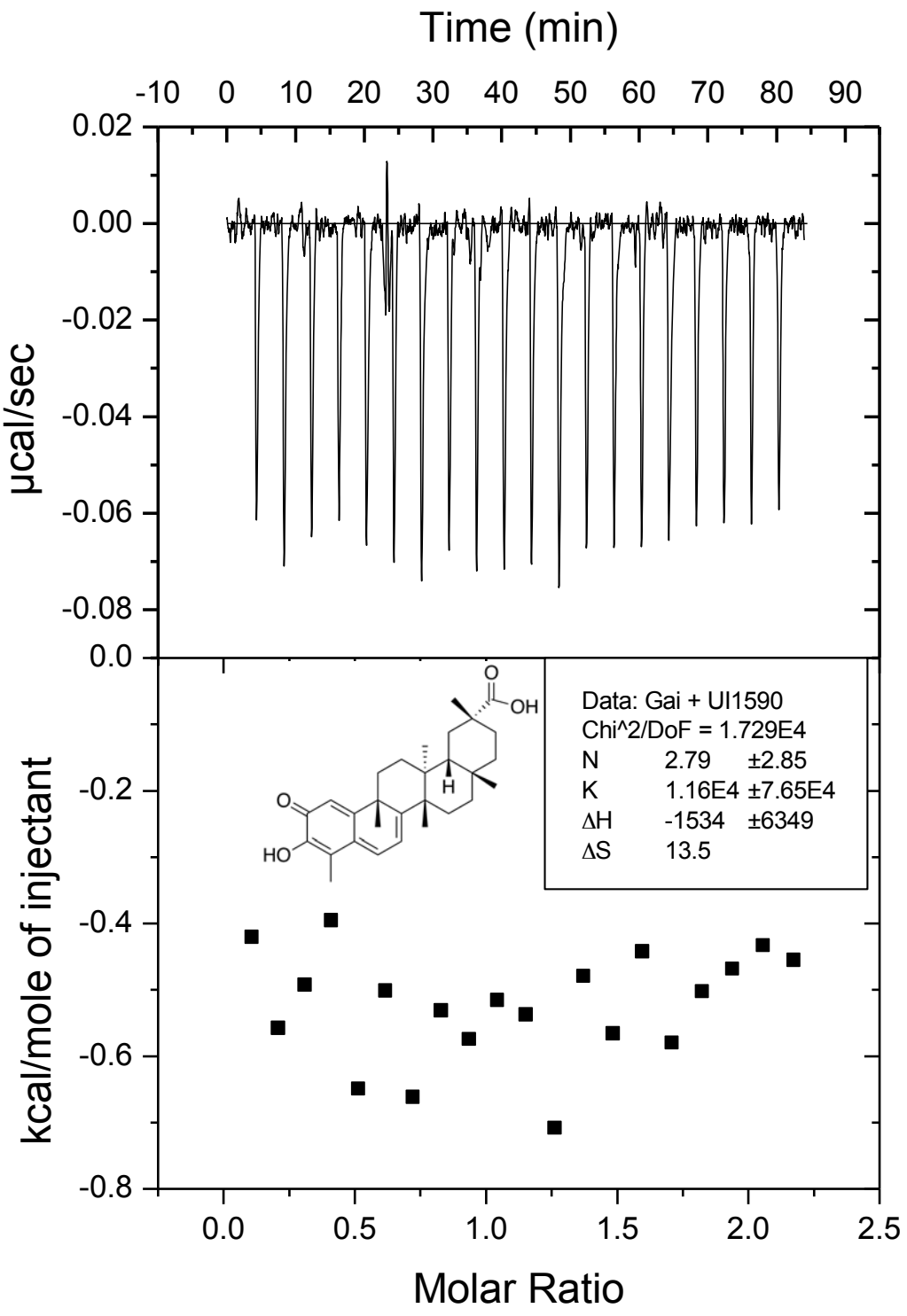

Figure 3.13 -- continued

assay directly, as shown when challenged in an assay containing only 50 μM PO_4, (greater than 3 standard deviations from the negative control). Finally, an additional 5 compounds were found to inhibit the intrinsic GTPase activity (greater than 3 standard deviations from the negative control) of the $G\alpha_i$ subunit alone. A second, confirmatory screen of the initial hit compounds was performed using an orthogonal assay, ALPHA Screen (Perkin Elmer; Waltham, MA), further reduced this to a hit rate of 1.3% [91]. A Single point ALPHA Screen, using the same concentration as the initial screen,

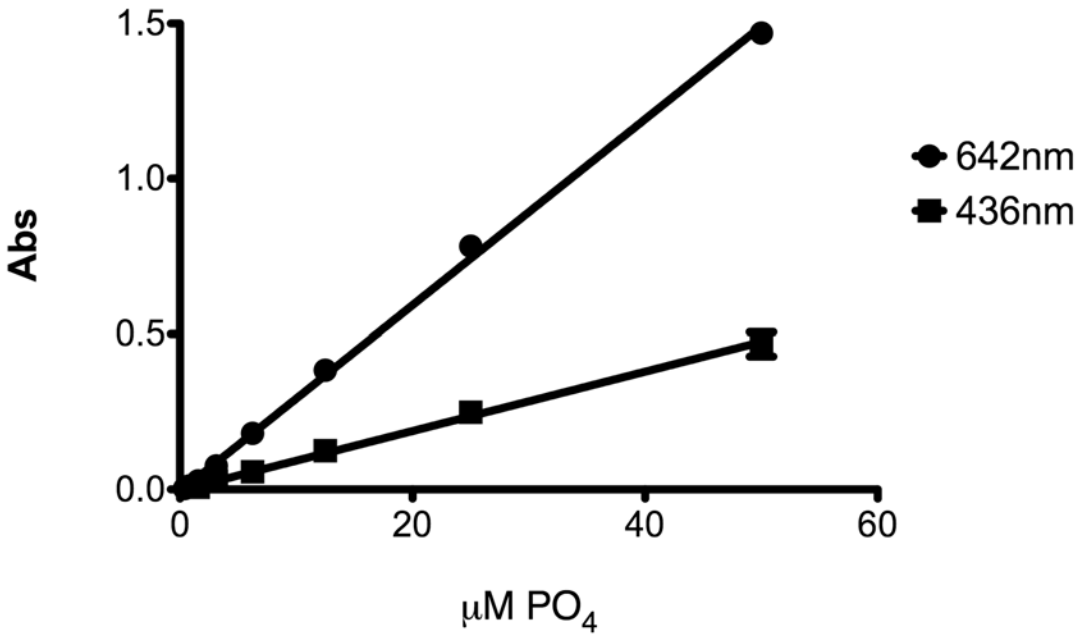

Figure 3.14 Linear Range Determination for 642nm and 436nm Absorbance Peak. The two selected peaks, 642 nm and 436 nm, were evaluated using ½ dilutions of Na3PO4 from 50 μM to 0.4 μM. The peak at 642 nm had a three fold greater response to Na_3PO_4 than the peak at 436 nm at equivalent concentrations. The image shown is representative of n=3 experiments.

eliminated an additional 15 compounds that failed to inhibit at least 3 standard deviations from the positive control. Of the 31 compounds only 13, 0.6% of all compounds screened, were shown to inhibit the RGS4(Δ7) construct (Figure 3.8b) greater than 25% from the control. The RGS4(Δ7) mutant was used as a filter to avoid thiol-modifiers similar to compounds already identified previously [58-59]. These compounds identified in the screen described here were shown to be weaker inhibitors of the RGS4(Δ7) mutant versus the wild type construct.

Each of the compounds demonstrates inhibition of RGS4. Some of the more potent compounds identified, such as UI-587 and UI-662, contain covalent cysteine and free amine chemical functionalities similar to those that have been discovered in other screens against RGS4 [58-59]. Interestingly, two very similar compounds, UI-1907 and UI-2034, were determined to be weak inhibitors of RGS4 and the RGS4(Δ7). Also identified in this screen is a series of compounds with a quinone functionality, UI-1775, UI-1925, UI-2144, UI-2202, UI-2231, and UI-2249. One of these compounds was the most potent inhibitor of the RGS4(Δ7) mutant, UI-2144. With IC_{50} values from 20 - 30 μM, UI-1775, UI-2144, UI-2202, and UI-2249 represent some of the most potent compounds reported for the RGS4(Δ7) mutant [77]. Certain compounds, UI-587 and UI-992, inhibited both RGS4 and the RGS4(Δ7) mutant equally. We expected UI-587 to inhibit both equally due to its potential mechanism of action including the modification of free amines.

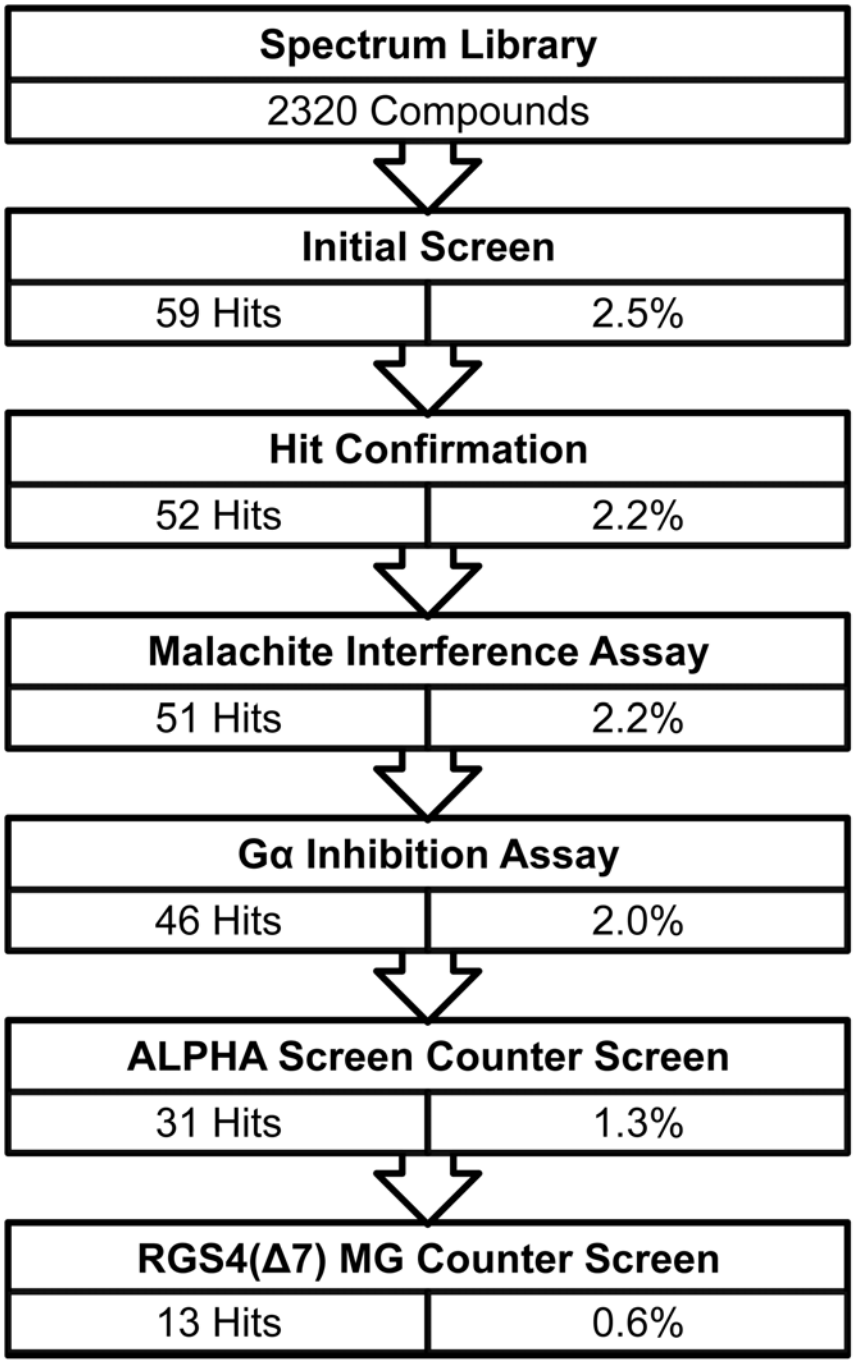

Figure 3.15 Pilot screen results for Spectrum Library. From the 2320 compound library, 59 compounds (2.5%) were considered hits. 52 of those compounds were confirmed in a single point assay. 6 compounds were found to inhibit either the assay or the $G\alpha_i$ directly, leaving 46 compounds (2.0%). An additional 15 compounds were removed for failing the ALPHA Screen orthogonal assay. And finally, 18 compounds were found to not inhibit RGS4(Δ7) at least 25% in the single point counter screen, leaving 13 compounds (0.6%).

Several of the compounds identified in this screen represent interesting structures, such as UI-5 and UI-1590, and warrant additional investigation, as their mode of action in inhibiting RGS4 is not readily apparent. The most potent compound, UI-1590, is the anticancer drug celastrol which has been studied extensively in both cellular models as well as rodent models, with minor toxicity shown in vivo [105-106]. Compounds excluded from further analysis are mentioned in the Appendix.

The development of this assay provides a new method for evaluating RGS proteins and their interactions with G-proteins. Steady-state analysis of RGS activity will allow for more accessible interpretations of compound effects on RGS G-protein interactions. ^{32}P liberation assays represent the only well used method for determining the effect of RGS proteins on the rate of GTP hydrolysis. This malachite green assay is capable of almost completely replacing that assay due to its ease of use as well as cost. The mutant used in this assay, $G\alpha_{i1}$, is capable of being used with a variety of RGS proteins beyond the R4 family, such as the RZ family [107]. Perhaps most importantly, this assay has been shown to be usable with another R4 family member, RGS8, as well as an RZ family member, RGS17. This is promising in that this simple assay should be greatly beneficial for the study of a wide variety of RGS proteins and perhaps other GAPs. Further affording potential for impact in the study of other RGS proteins, the mutations used to generate the mutant G-protein are translatable to a variety of other G-

proteins. In $G\alpha_q$, R183C functions very similarly to the mutation R178M in $G\alpha_{i1}$ [108]. The corresponding mutation in $G\alpha_{i2}$, R179C, also ablates intrinsic GTPase activity [109]. This highly conserved residue has been shown to be capable of mutation to remove intrinsic GTPase rate but maintain sensitivity to RGS proteins [110]. Similar conserved mutations exist for the rapid exchange of GDP for GTP. One example is the F332A in $G\alpha_t$, which increases the exchange rate by 150 times [111]. Similar conserved residues could be determined in other G-proteins, allowing for expansion of this assay to many more RGS proteins.

In conclusion, we developed a simple, easy to use, and low cost assay for the evaluation of the GAP activity of a variety of RGS proteins. This study shows that this colorimetric assay is both robust and readily miniaturized for HTS application. The dual absorbance peak of the assay, 642 nm and 436 nm, allows for an in well counter-screen to include compounds that may have been lost due to absorbance at the primary reading wavelength. The slow but detectable intrinsic GTPase rate of the mutant $G\alpha_i$ allows for a simple counter screen to remove compounds that interfere with the assay by direct inhibition of the $G\alpha_i$ construct. This assay has the potential to be expanded to encompass a variety of RGS protein families and increase the number of available tools to study this interesting family of proteins.

CHAPTER IV

TRANSCRIPTIONAL REGULATION OF RGS4 DURING OXIDATIVE STRESS

Introduction

Parkinson's disease (PD) is a progressive neurodegenerative disorder associated with the selective loss of dopaminergic neurons in the substantia nigra. A majority of PD cases are idiopathic [7]. A major risk factor for PD is age of onset, affecting over 2% of patients over 60 [1]. It is understood that aging increases the vulnerability of dopaminergic neurons due to the breakdown of normal cellular processes [64]. These sensitized cells may be affected by exposure to environmental toxins such as herbicides, pesticides, and several natural toxins have been linked to PD [65-66]. This toxic insult is believed to have a causal relationship with most idiopathic cases of PD, through oxidative stress [14].

Oxidative stress is evidenced in the substantia nigra of PD patients through increased levels of oxidation adducts on proteins, such as dopamine derived quinones and lipid peroxidation products, and DNA, with common products being 8-oxoguanine and 2-hydroxyadenine [112-113]. Oxidative stress occurs in cells when the formation of reactive oxygen species (ROS) overpowers reductive mechanisms in the cells. Another important component

of oxidative stress is the depletion of a main antioxidant, free glutathione (GSH) from cells. In PD patients GSH levels are reduced 40-50% in the substantia nigra [114]. This may arise from a variety of sources such as the aforementioned environmental toxins and, in particular within dopaminergic neurons, the biosynthetic pathway for dopamine generation.

Dopaminergic neurons are intrinsically sensitive to perturbation of the balance of reductive and oxidative reactions within the cell due to the production of dopamine. One of the markers of dopaminergic neurons, tyrosine hydroxylase, is known to produce hydrogen peroxide (H_2O_2) [115]. In addition, monamine oxidase, involved in the metabolism of dopamine, produces H_2O_2 during its enzymatic cycle [116]. This direct load of ROS endemic to dopaminergic cells is believed to sensitize these cells to oxidative stress. Beyond the biosynthetic pathways involving dopamine, its metabolites are also problematic. Excess dopamine in the cytoplasm can be both enzymatically, by monoamine oxidase, and spontaneously converted to 3,4-dihydroxyphenylacetaldehyde (DOPAL) [117]. The reactive quinone metabolite of DOPAL is both capable of directly adducting nucleophilic sites as well as producing the ROS $O_2^{\cdot -}$ when activated with O_2. DOPAL may also functionally inhibit dopamine transport, exacerbating the situation, and deregulating the electron transport chain within mitochondria [118]. This internal distress in dopaminergic neurons may in turn illicit a response from surrounding immune cells, microglia.

Microglia are activated in response to injury or toxic insult and function to eliminate cell debris within the brain [119]. When activated, microglia produce a variety of ROS, such as H_2O_2, nitric oxide, and superoxide [86]. Activated microglia, contributing ROS, aggravate the already stressed neurons, thereby promoting stress responses in the targeted and surrounding neurons and perpetuating a cycle of neurodegeneration in the substantia nigra [119]. The released ROS can function to activate additional pathways within the neurons.

Oxidative stress and the variety of lipid peroxidation products generated from ROS interacting with lipid membranes affect various signaling pathways. ROS treatment has been shown to induce protein expression as well as act as a mediator of receptor signaling [120-121]. Similarly direct receptor activation is possible through covalent modification of lipid peroxidation products, such as 4-hydroxy-2-nonenal [122]. Another target of lipid peroxidation products has been shown to be Regulator of G-protein Signaling 4 (RGS4) (Monroy et al; unpublished data).

RGS4 has previously been implicated in PD [30,55]. RGS4 contains 5 isoforms. Isoforms 1 and 2 express the same 205 amino acid protein. Isoform has been shown to have a cAMP-responsive element binding protein 1 (CREBP1) binding site while isform 2 has a steroidogenic factor 1 (SF1). Isoform 3 codes for a long form of RGS4 with a added N-terminus, of 97 amino acids. The candidate promoter region of isoform 3 has a CCAAT/

enhancer binding protein beta (CEBPB), CREBP1, and a interferon-stimulated response element (ISRE). Isoform 4 codes for a truncated form of RGS4, lacking a majority of the RGS domain. Isoform 4 shares its candidate promoter region with isoform 1. Isoform 5 codes for a truncated form of RGS4, lacking the first 18 amino acids. The candidate region for isoform 5 contains several promoters, including human zinc finger protein (ZF35) [48]. A description of each isoform mRNA construct is shown in Figure 4.1. While loss of D_2 receptor signaling has been shown to modulate RGS4 expression, the diverse promoter regions for the various isoforms of RGS4 may serve to control RGS4 expression in response to various stimuli, such as oxidative stress. We hypothesized that oxidative stress would modulate specific isoforms of RGS4 within a neuron.

To test this hypothesis we evaluated the effect of oxidative stress directly in cultured neurons. We exposed two cell lines, SH-SY5Y (neuroblastoma derived cell line) and HCN-1A (isolated cortical neurons from a megalencephaly patient), to H_2O_2 at varying concentrations to simulate oxidative stress within the cells. By western blot we show increased concentration of RGS4 within both the SH-SY5Y and the HCN-1A. Evaluation of RGS4 mRNA expression however showed no significant change in RGS4 splice variant expression.

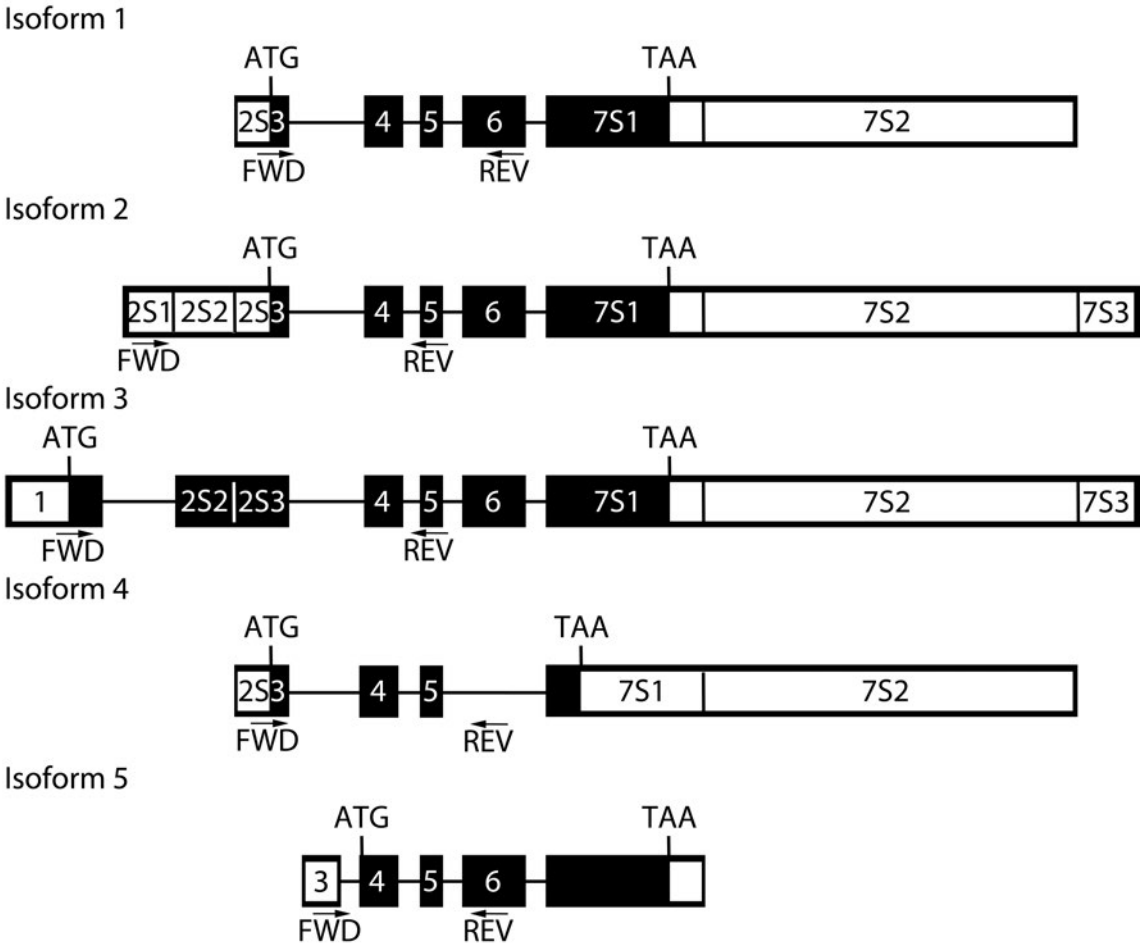

Figure 4.1 RGS4 Isoform qPCR Map. For isoform 1, the forward primer is located in exon 2S3 and the reverse primer anneals to exon 6. The resulting PCR product is 275 bp. For isoform 2, the forward primer anneals to exon 2S1 and the reverse primer anneals to exon 5. The resulting amplicon is 395 bp long. For isoform 3, the forward primer anneals to exon 1 and the reverse primer anneals to exon 5. The resulting amplicon is 476 bp. For isoform 4, the forward primer anneals to exon 2S3 and the reverse primer spans both exon 5 and exon 7S1. The resulting amplicon is 152 bp. For isoform 5, the forward primer anneals to exon 3 and the reverse primer anneals to exon 6. The resulting amplicon is 265 bp.

Experimental Procedures

Cell Culture and Treatment.

SH-SY5Y cells were obtained from ATCC (Manassas, VA). The cells were grown as an adherent monolayer, with small clumps, in T-75 tissue culture flasks in a 1 : 1 mix of high glucose DMEM (11965: Life Technologies; Carlsbad, CA) and F12 (11765: Life Technologies; Carlsbad, CA) mediaD7777 DMEM (Sigma-Aldrich; St Louis, MO) supplemented with 0.5% of 100x L-Glutamine, 0.5% 100x sodium pyruvate, 10% fetal bovine serum (Fisher Scientific; Waltham, MA), and 1% penicillin / streptomycin (Life Technologies; Grand Island, NY). After reaching confluence, SH-SY5Y cells were washed with twice phenol free media and treated with increasing concentrations of H_2O_2 (Sigma-Alderich; St Louis, MO), from 0 - 250 μM, in phenol free media without fetal bovine serum. Following a 1.5 h incubation at 37°C, stressing media was removed and cells were washed with PBS. Cells were lysed in Lysis Buffer (10 mM KH_2PO_4 pH 7.5 and 0.1% Triton X-100) and homogenized using a Sonic Dismembrator (Fisher Scientific; Waltham, MA). Samples were cleared by centrifugation at 13,000 x g for 15 min and the supernatant was collected. Crude protein concentration was determined by DC protein assay (Bio-Rad; Hercules, CA) for use in later experiments. For mRNA experiments, cells were resuspended in 1 mL of Trizol (Life

Technologies; Carlsbad, CA) for every well in a 6-well dish. RNA extraction was carried out according to manufacturer's protocol.

HCN-1A cells were also obtained from ATCC (Manassas, VA). The culture was grown as an adherent monolayer in T-25 tissue culture flasks in D7777 DMEM (Sigma-Aldrich; St Louis, MO) supplemented with1.5 g / L sodium bicarbonate, 10% fetal bovine serum (Fisher Scientific; Waltham, MA), and 1% penicillin / streptomycin (Life Technologies; Carlsbad, CA). Cells were stressed and harvested as described previously for SH-SY5Y cells.

SDS-PAGE and Western Blotting.

50 μg samples were loaded onto SDS-PAGE gels for analysis by western blot. Samples were transferred to Immobilon-P transfer membrane (Millipore; Billerica, MA) according to established protocols, and the membrane was then blocked, overnight, using tris buffered saline Tween-20 (TBST; 50 mM Tris pH 7.4, 150 mM NaCl, 0.1% Tween-20) supplemented with 3% bovine serum albumin (BSA). To detect RGS4, samples were probed for 4 h at 4°C using U1079 (rabbit anti-RGS4) at a 1 : 10 000 dilution in 3% BSA TBST. The blot was then probed at room temperature using a 1 : 20 000 dilution of goat anti-rabbit secondary, conjugated to horseradish peroxidase (Protein Biosystems; Pelham, Alabama), for 1.5 h. The blot was developed using 2 mL WestPico chemiluminescent substrate (Thermo Scientific,

Waltham, MA) and imaged using a UVP Biospectrum Imaging system (Upland, CA).

Real Time PCR

After RNA extraction with Trizol, RNA pellet was resuspended in 20 μL of nuclease free water. RNA concentration was determined by absorbance at 260nm using a Take 3 Plate (Biotek; Winooski, VT) in a Synergy 2 (Biotek; Winooski, VT). 1 μg of RNA was converted to cDNA using an Applied Biosciences Reverse Transcription kit (Life Technologies; Carlsbad, CA). For each reaction, a mixture of 3 components was made and diluted to 18 μL. The three components are 10 μL iQ SYBR Green Supermix (BioRad; Hercules, CA), 1.4 μL of cDNA stock, and 1.2 μL 50 mM $MgCl_2$. To complete the reaction, 2 μL of 2.5 μM primer mix, for a final concentration of 250 nM, is added to appropriate samples. For isoform 1, the forward primer used was 5'-CCG-GCT-TCT-TGC-TTG-AGG-AGT-G-3' and a reverse primer 5'-AGA-TCT-TTT-TGG-CCT-TGG-GAC-TT-3'. To identify isoform 2, the forward primer 5'-ATG-CGT-CAG-TCT-TTT-CTT-CCT-ATC-TCT-T-3' and the reverse primer 5'-CAG-CCC-ATT-TCT-TGA-CTT-CCT-CTT-3' was used. For isoform 3, the forward primer 5'-TGA-TCC-TGC-CAG-CTC-CCT-TTT-G-3' and the reverse primer 5'-CAG-CCC-ATT-TCT-TGA-CTT-CCT-CTT-3' was used. For isoform 4, the forward primer 5'-CCG-GCT-TCT-TGC-TTG-AGG-AGT-G-3' and the reverse primer 5'-AAT-CCA-GGT-TCA-CAT-TCA-TGA-CTA-ATC-3' was used.

For isoform 5, the forward primer 5'-GAC-GGG-CAT-ATA-AAG-GCT-TCT-CAG-GT-3' and the reverse primer 5'-GGG-ACT-TAG-TTT-AGA-TGG-TGA-TTT-GA-3' was used. As a control, glyceraldehyde 3-phosphate dehydrogenase (GAPDH) was analyzed using the forward primer 5'-GAG-TCA-ACG-GAT-TTG-GTC-GT-3' and the reverse primer 5'-AAT-GAA-GGG-GTC-ATT-GAT-GG-3'. The location of each of these primers annealing site and amplicon length are described in Figure 4.1. For the qPCR reaction, the sample was first melted at 95°C for 2 min. The PCR cycle consisted of 10 s at 95°C, followed and by 30 s at 62°C and finally 30 s at 72°C repeated for 40 cycles. To determine primer efficiency, a log dilution series of cDNA sample was created and qPCR was run as previously described.

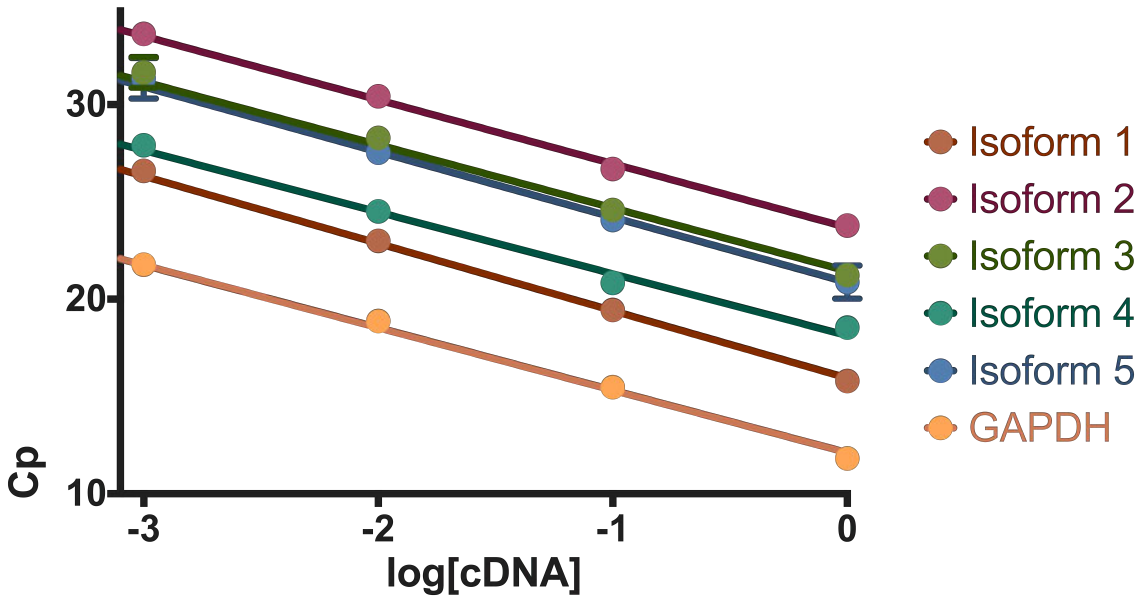

Figure 4.2 RGS4 qPCR Primer Validation. Serial log dilution of SH-SY5Y cell lysate. All primers have usable efficiencies between 90% and 110%. Image is a representative of n=1 experiments.

Data Analysis

For analysis, samples were first compared to the internal control GAPDH. The result, called ΔCp, was then compared between treated and untreated samples for significant changes in protein expression. Statistical analysis completed using PRISM graphing software (Graphpad Software; La Jolla, CA).

Results

Primer Validation

Each isoform primer pair was evaluated for efficiency in the qPCR reaction. As shown in Figure 4.2, each of primer pairs maintained an acceptable efficiency, between 90% - 110%. The longer amplicons, isoform 2 and isoform 3. had slightly higher then desired efficiencies while the smaller amplicons, isoform 1 and isform 5, had lower than desired efficiencies. The smallest, isoform 4, had the greater variance than the others reducing the overall determined efficiency. The overall efficiencies of the isoforms was acceptable for use in qPCR and carried forward for use in examining RGS4 expression in the selected cell lines.

SH-SY5Y cells were stressed with 100 μM H_2O_2 for 1.5 h before analysis. Cell lysate was analyzed by western blot for changes in RGS4 expression in response to H_2O_2 treatment. RGS4 protein was enriched in

treated cells as opposed to mock treated controls, shown in Figure 4.3a. Following this, mRNA expression of RGS4 was examined. As shown in Figure 4.3b, no significant induction of RGS4 occurred in stressed cells.

Table 4.1 Evaluation of Specific RGS4 Isoform Primer Pair qPCR Efficiencies.

Target	Slope	Efficiency*
Isoform 1	-3.459	94.5%
Isoform 2	-3.279	101.8%
Isoform 3	-3.243	103.4%
Isoform 4	-3.170	106.8%
Isoform 5	-3.353	98.7%
GAPDH	-3.326	99.8%

*Efficiency = (10^(-1/slope)-1)*100.

The experiments were repeated using the HCN-1A cell line. H_2O_2 was titrated from 0 - 250 μM and then prepared for analysis by western blot. As shown in Figure 4.4a, RGS4 was enriched in H_2O_2 stressed cells compared to actin, used as a control. After treatment with 100 μM H_2O_2 for 1.5 h, cells were prepared for analysis by Trizol RNA extraction. Using qPCR, cDNA from stressed cells was analyzed for changes in expression, relative to the

house keeping gene GAPDH. As shown in Figure 4.4b, RGS4 mRNA expression was not significantly induced after stressing with H_2O_2.

Discussion

ROS, such as H_2O_2, are common components of oxidative stress and the inflammatory response. In PD, oxidative stress is an important component involved in the degeneration of dopaminergic neurons in the substantia nigra [112]. These particular dopaminergic neurons are particularly sensitive to oxidative insult from exogenous sources due to the abundance of dopamine and the enzymes required for dopamine synthesis, which put a heavy oxidative load on those cells. ROS production can be induced from a variety of exogenous sources within the brain as well. The neuroinflammatory response in microglia can result in the release of ROS in response to cellular distress [123].

ROS has been shown to modulate a variety of signaling pathways, and even be integral to some of these pathways [121]. Recently RGS4 has been linked to the motor symptoms of PD [30]. Induction of RGS4, through dopamine depletion, has been shown to modulate cholinergic signaling [55]. Through analysis of RGS4 expression in various cell lines, we show that RGS4 levels in cells can be modulated by oxidative stress.

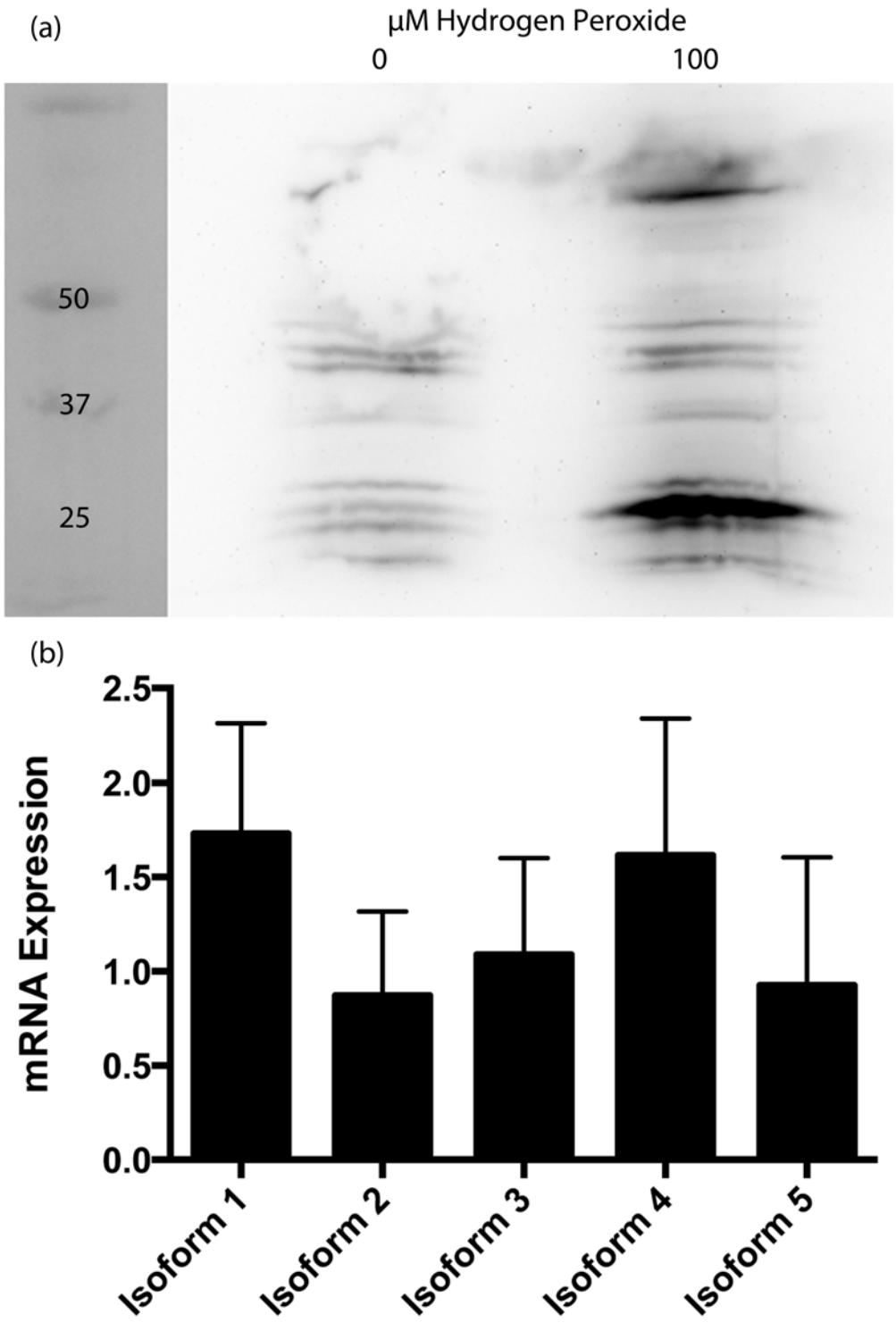

Figure 4.3 RGS4 Expression in Stressed SH-SY5Y Cells. (a) SH-SY5Y cells treated with H_2O_2 for 1.5 h, RGS4 was significantly induced. The dark band corresponds to 26 kDa band which represents RGS4 isoform 1 or 2. (b) In qPCR analysis of Stressed SH-SY5Y no significant increase in expression of any isoform was detected. Image is representative of n=3 experiments.

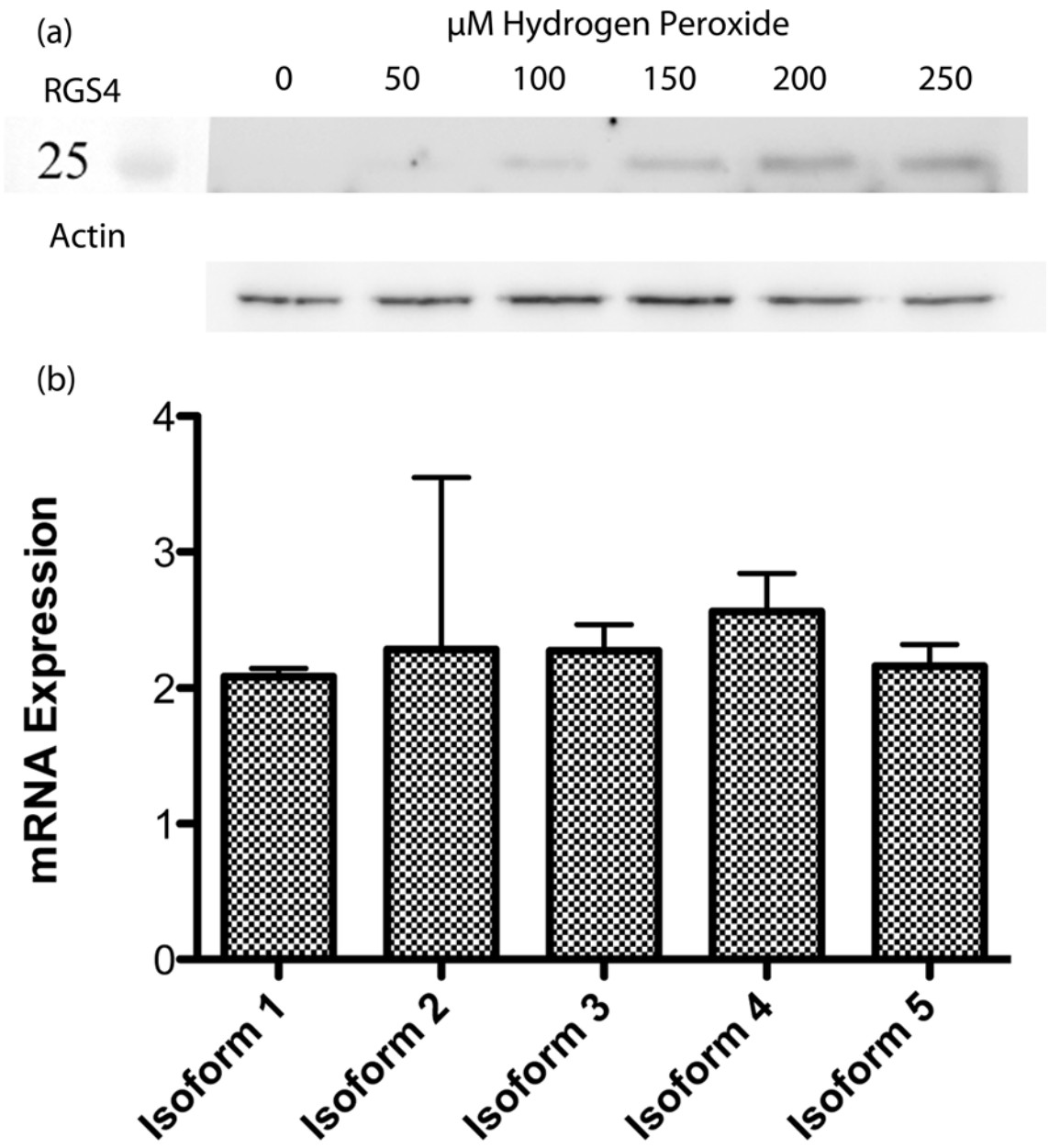

Figure 4.4 RGS4 Expression in Stressed HCN-1A Cells. (a) In response to increasing amounts of H_2O_2 exposure, HCN-1A cells become enriched in RGS4. The loading control, actin, provides confirms equivalent levels of protein loaded for analysis. (b) after 100 μM exposure for 1.5 h to H_2O_2, cells were assayed using qPCR for changes in expression of RGS4 isoforms, in relation to GAPDH. No significant changes in RGS4 mRNA were observed. Image is representative of n=3 experiments.

Initially we set out to detect changes in RGS4 levels in neuronal cell lines. Western blot analysis of RGS4 was used to determine RGS4 regulation in response to oxidative stress in both SH-SY5Y and HCN-1A cell lines. In both cell lines, RGS4 appeared to be enriched when the cells were exposed to H_2O_2. This trending increase in RGS4 will likely significantly affect GPCR signaling, similar to the enrichment observed upon dopamine depletion [55]. This enrichment of RGS4 was further investigated using qPCR. In both cell lines, no significant enrichment of RGS4 mRNA was detected. This implies that the method of regulation is related to translation of RGS4 mRNA or, more likely, inhibition of the degradation pathway of RGS4.

In conclusion, we have identified another potential mechanism for RGS4 enrichment in PD patients. Specifically, we have shown that oxidative stress, mediated by the ROS H_2O_2, can enrich RGS4 within these neuronal cell lines. This phenomenon is however not related to changes in mRNA expression, as we have shown. The mechanism for increase in RGS4 may be due to disruption of proteasomal degradation, in which RGS4 is targeted to by N-end rule ubiquitinylation target [124]. Oxidative stress is well known to inhibit the proteasome directly [125]. This increased RGS4 in striatal neurons can contribute to the aberrant signaling described previously. Excess RGS4 from oxidative stress may describe late stage RGS4 expression in PD patients where oxidative stress is high.

CHAPTER V

CONCLUSIONS

Parkinson's disease (PD) is a complex neurodegenerative disorder. The cognitive deficits of PD are believed to be caused by Lewy body formation, large protein aggregates formed within the cytoplasm of neurons within the substantia nigra [3]. The motor symptoms of PD are related to dopaminergic cell loss [6]. The link between RGS4 and the motor symptoms of PD has recently been highlighted in a mouse model of PD [30]. In this mouse model, 6-OHDA, a selective neurotoxic agent for dopaminergic neurons, was used to induce PD [29]. In this model, genetic deletion of RGS4 ablated the motor symptoms associated with PD [30]. In a similar model, reserpine, a potent VMAT2 inhibitor, was used to deplete dopaminergic signaling. In striatal neurons, the effective antagonism of the D_2 dopamine receptor resulted in induced RGS4 mRNA expression. This enrichment of RGS4 within the striatal neurons resulted in deregulation of the receptor by the M_4 muscarinic autoreceptor [55]. The resulting deregulation of these cholinergic interneurons are believed to mediate the motor symptoms of PD through M_1 muscarinic receptor mediated inhibition of medium spiny neurons. While depletion of D_2 receptor signaling through dopamine depletion represents a major component of RGS4 regulation during PD, we evaluated the role of oxidative stress in modulating RGS4.

Oxidative stress is an important component of PD progression. In the substantia nigra, toxic insult to the particularly sensitive dopaminergic neurons can result in the subsequent activation of microglia. Activated microglia results in the direct release of pro-inflammatory cytokines, nitric oxide, and superoxide [86]. The release of reactive oxygen species (ROS), such as superoxide and hydrogen peroxide, onto these stressed neurons may play a role in augmenting RGS4 signaling within the neurons. One common product of lipid peroxidation during oxidative stress is the formation of reactive lipids such as 4-hydroxy-2-nonenal (4HNE). 4HNE has been shown previously to directly stimulate receptors, such as inducing Ca^{2+} release from channel transient receptor potential anrkyrin 1 (TRPA1) [122]. The sensitivity of RGS4 to thiol modification and its relative importance to neuronal signaling makes it an ideal target for investigation as a target for 4HNE [59,55]. We evaluated RGS4 modification by 4HNE using a variety of techniques and showed that RGS4 can be modified as well as inhibited by 4HNE through modification at cysteine residues.

First, we determined the capability of 4HNE to modify RGS4 within cells. In HEK293T cells, 4HNE modification on RGS4 was readily detected by immunoprecipitation. The proximal location of RGS4 to the plasma membrane in neuronal cells, due to the N-terminal amphipathic helix, and the accumulation of 4HNE at the plasma membrane, due to lipophilicity, provides the opportunity for compound protein interaction [43,73]. To identify

target residues of 4HNE, MS analysis of purified protein was performed. 4HNE is capable of modifying cysteine, histidine, and lysine residues [87]. We confirmed that modification of RGS4 occurred at cysteine residues by mutation of cysteine residues, generating a cysteine null construct (RGS4(Δ7)), and comparing states of modification by LC/MS. To determine which cysteine residues were being modified, we evaluated RGS4(WT) modification by tryptic digest followed by LC/MS. The result was modification predominately at 3 residues: cysteine 71, 148 and 183. Of these, cysteine 148 is a modification site previously reported to inhibit RGS4 binding to its native binding partner a Gα subunit [59]. A steady state malachite green based assay was used to measure 4HNE modification on RGS4 GTPase activating protein (GAP) activity. 4HNE modification was found to substantially inhibit RGS4(WT) but not the cysteine null mutant. This inhibition by 4HNE may act to attenuate RGS4 activity and therefore ablate RGS4 induced Parkinsonian motor symptoms.

From this we identified RGS4 as a new potential target for 4HNE modification during oxidative stress. This study confirms that RGS4 is susceptible to modification at cysteine residues by endogenous reactive molecules. Specifically, thiol-modifying biomolecules like 4HNE can regulate RGS4 through its unique allosteric modulation site, cysteine 148. This may be an internal protective mechanism for disease states where oxidative stress is a strong component, such as PD. Additionally, the steady state assay

developed to analyze the effect of 4HNE modification may serve other applications.

The steady state assay developed to interrogate RGS4 activity can be a very powerful tool to study RGS proteins. Previous methods for identifying RGS protein inhibitors focused on disruption of the high affinity RGS - Gα interaction in the presence of GDP-AlF_4^-, a transition state mimic of GTP hydrolysis in the Gα subunit [77,91]. Using this transition state, while valid, is not a good mimic of actual affinity, as this interaction is 50-fold higher than basal affinity [56,36]. Aside from this method, two other methods exist for assaying RGS activity. The first, single turnover, is quite laborious, low throughput, and requires the use of ^{32}P [68]. The second (Transcreener), while rapid enough for high throughput screening (HTS), is quite expensive as it utilizes antibodies [67]. We set out to develop a economical, fast, and easy to use assay that may be adapted to different RGS family members. This malachite green based assay we developed met each of those criteria.

The initial setup of the assay, for a 1536-well plate, was 1.5 h. This setup includes long incubation steps for the release of free phosphate as well as color development, allowing for this assay to be performed in a highly parallel fashion. The usage of a colorimetric dye for a readout is a straightforward assay that may be used on even the simplest of plate readers. The dual peak nature of this colorimetric dye defeats one of the most common problems of HTS, the presence of library compounds which absorb at a

wavelength critical to the assay's readout. The principal peak occurs at 642 nm, and the secondary peak, about 1/3 the intensity, occurs at 436 nm, Despite its lower signal, the 436 nm peak is still usable as a secondary readout. To prove the usefulness of this assay, a small 2320 compound library was used to challenge the conditions crafted for the assay. From the initial screen, 59 compounds (2.5%) were hits. Internal controls for the assay, including hit confirmation, 50 μM phosphate and Gα subunit alone assay, eliminated 7, 1 and 5 compounds, respectively, in the initial triage. The remaining 46 compounds were challenged against both an orthogonal assay, ALPHA-screen, and RGS4(Δ7) inhibition assay. Each of these assays eliminated 31 and 13 hits, respectively. RGS4(Δ7) was used to eliminate compounds whose mechanism of action related to thiol modification. The remaining compounds were then categorized based on pharmacophore. Several compounds were eliminated for either high structural symmetry and difficulty synthesizing, obvious covalent mechanism, or core quinone structure (Appendix A). The remaining compounds UI-5, UI-1590, UI-1907, and UI-2034 were evaluated using the malachite green assay, MS, and ITC if available. All of the identified compounds were more potent against RGS4(WT) than with the cysteine null construct, RGS4(Δ7). The steady state assay developed successfully functioned as a reliable HTS assay.

The development of this assay provides a new method for evaluating RGS proteins. Steady state analysis of RGS activity allows for more

accessible evaluation of compound activity on RGS - G-protein interactions. This method is significantly more accessible when compared to the current gold standard of ^{32}P single turnover assays to evaluate RGS protein GAP activity. The malachite green assay can almost completely replace this assay due to its lower cost and ease of use. The currently developed $G\alpha_{i1}$(RTO) is capable of interacting with RGS proteins beyond R4 family members, to include RZ [107]. This assay can be expanded by performing equivalent point mutations on other Gα subunits. In $G\alpha_q$, R183C mutations functions similar to R178M in $G\alpha_{i1}$ [108]. Similarly in $G\alpha_{i2}$, the corresponding mutation is R179C [109]. In Gαt, F332A functions simliar to A326S [111]. Similar residues may be determined for other Gα subunits to expand this assay to many more RGS proteins.

Finally, we evaluated the effect of ROS during the inflammatory response in neurodegenerative disorders such as PD. ROS is an important component in the loss of dopaminergic neurons in the substantia nigra [112]. ROS is known to modulate a variety of signaling pathways, and even be integral to some pathways [121]. While RGS4 induction through dopamine depletion can modulate cholinergic signaling [55]. We set out to determine whether ROS, using H_2O_2, can modulate RGS4 expression similar to dopamine depletion using reserpine.

Initially we set out to detect RGS4 expression changes in neuronal derived cell lines. In both SH-SY5Y, a neuroblastoma cell line, and HCN-1A,

megalencephaly cortical neurons, showed significantly enriched RGS4 when analyzed by western blot after treatment with H_2O_2. This change likely has a similar affect as dopamine depletion [55]. To further investigate this enrichment of RGS4, both cell lines were examined by qPCR. No change in mRNA expression implies augmentation of the degradation pathway. RGS4 is targeted by the N-end rule ubiquitination pathway and ROS can directly interfere with proteasome activity [124]. This is the most probable mechanism for RGS4 enrichment during oxidative stress.

In this thesis I examined the role of oxidative stress modulation of RGS4. This modulation may play an important role in mediating the motor symptoms of PD. During oxidative stress, the initial formation of 4HNE adducts on RGS4 would effectively ablate RGS4 activity in affected neurons. The disruption of protein degradation observed during oxidative stress, would later overpower this subtle loss of RGS4 activity. This proposed mechanism would indicate a temporal effect of oxidative stress on RGS4 activity. Initially oxidative stress would be protective but prolonged stress would enrich RGS4. This would indicate that sudden oxidative insults would be mitigated by this effect from developing PD motor symptoms and represents a novel protective mechanism for PD motor symptoms.

The novel assay developed for monitoring RGS4 is a major achievement for research on RGS proteins. While this assay takes considerably longer than established assays involving AlF_4^- mediated Gα

subunit transition state, this assay monitors steady state GTPase activating protein (GAP) activity [91]. Previous methods for assaying RGS protein GAP activity were either laborious or expensive. Traditionally this was performed using low throughput methods involving ^{32}P labeled GTP and requiring careful timing for reproducible results [39]. The method developed utilizes malachite to detect free phosphate formation and takes advantage of a rapid turnover mutant of Gαi1 to slow the reaction down and allow for easier manipulation of the assay [67,84]. Recently a new method for determining GAP activity was developed. This method uses antibodies to detect GTP turnover and as a result is exceedingly expensive [67]. The assay described in this thesis is relatively inexpensive in comparison to current methods [69]. This assay is easily adapted to evaluating other RGS proteins.

In conclusion, oxidative stress modulation of RGS4 represents a novel mechanism for symptom progression in PD. Specifically, enrichment of RGS4 during oxidative stress in neuroinflammation may lead to the onset of parkinsonian motor symptoms. Inhibition of RGS4 by lipid peroxidation products may serve to mask these effects under mild stressful conditions. The new compounds identified as RGS4 inhibitors may have implications in treating the motor symptoms of PD.

APPENDIX: OTHER IDENTIFIED HIT COMPOUNDS

Listed here are compounds identified as RGS4 inhibitors in the malachite green HTS assay. Each of the compounds was excluded based on predicted toxicity and specificity concerns. Among those excluded were highly symmetrical structures that are difficult to synthesize (Figure A.1), have known covalent adduction as the mechanism of action (Figure A.2), and primarily quinone structures (Figure A.3). We excluded these compounds due to the desire to find compounds that expanded beyond the known mechanisms of action against RGS4 [59].

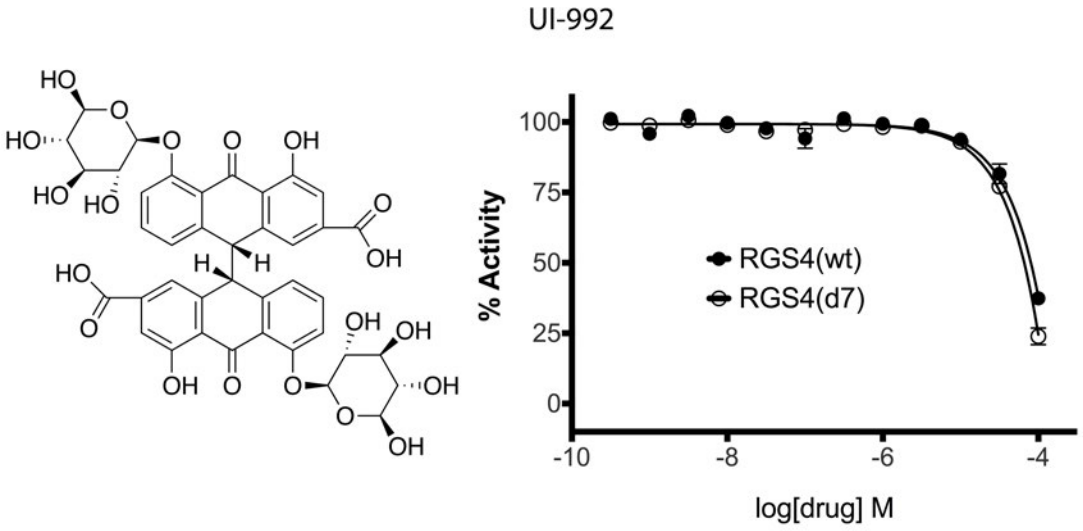

Figure A.1 Hits Excluded Due to High Symmetry and Difficulty Synthesizing. Compound UI-992 was excluded due to its high symmetry and difficulty to synthesize. It had a predicited IC50 of 297 mM againt RGS4(WT) and an IC50 of 364 mM against RGS4(Δ7).

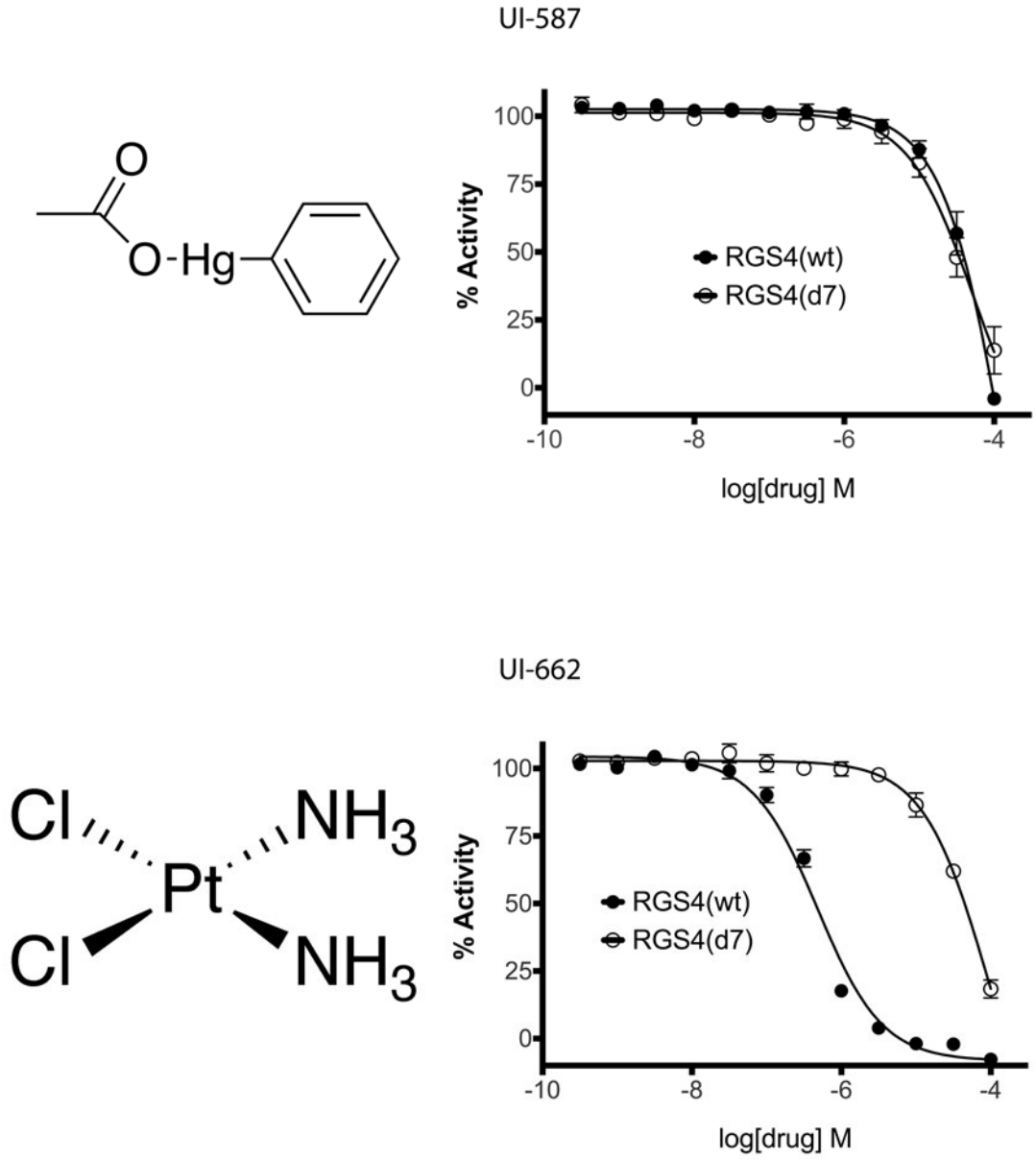

Figure A.2 Compounds Excluded Due to Known Adduct Forming Mechanism of Action. Both UI-587 and UI-662 were excluded due to known covalent adduction as their mechanism of action. UI-587 had a predicted IC_{50} of 169 μM against RGS4(WT) and an IC_{50} of 51 μM against RGS4(Δ7). UI-662 had a predicted IC_{50} of 480 nM against RGS4(WT) and an IC_{50} of 93 μM against RGS4(Δ7).

Figure A.3 Compounds Excluded Due to Quinone Structure. UI-1775, UI-1925, UI-2144, UI-2202, UI-2231, and UI-2249 were excluded due to pharmacophore being a quinone. UI-1775 had a predicted IC_{50} of 8.6 μM against RGS4(WT) and an IC_{50} of 266 μM against RGS4(Δ7). UI-1925 had a predicted IC_{50} of 74 μM against RGS4(WT) and an IC_{50} of 82 μM against RGS4(Δ7). UI-2144 had a predicted IC_{50} of 8 μM against RGS4(WT) and an IC_{50} of 29 μM against RGS4(Δ7). UI-2202 had a predicted IC_{50} of 3.1 μM against RGS4(WT) and an IC_{50} of 20 μM against RGS4(Δ7). UI-2231 had a predicted IC_{50} of 4 μM against RGS4(WT) and an IC_{50} of 68 μM against RGS4(Δ7). UI-2249 had a predicted IC_{50} of 320 nM against RGS4(WT) and an IC_{50} of 21 μM against RGS4(Δ7).

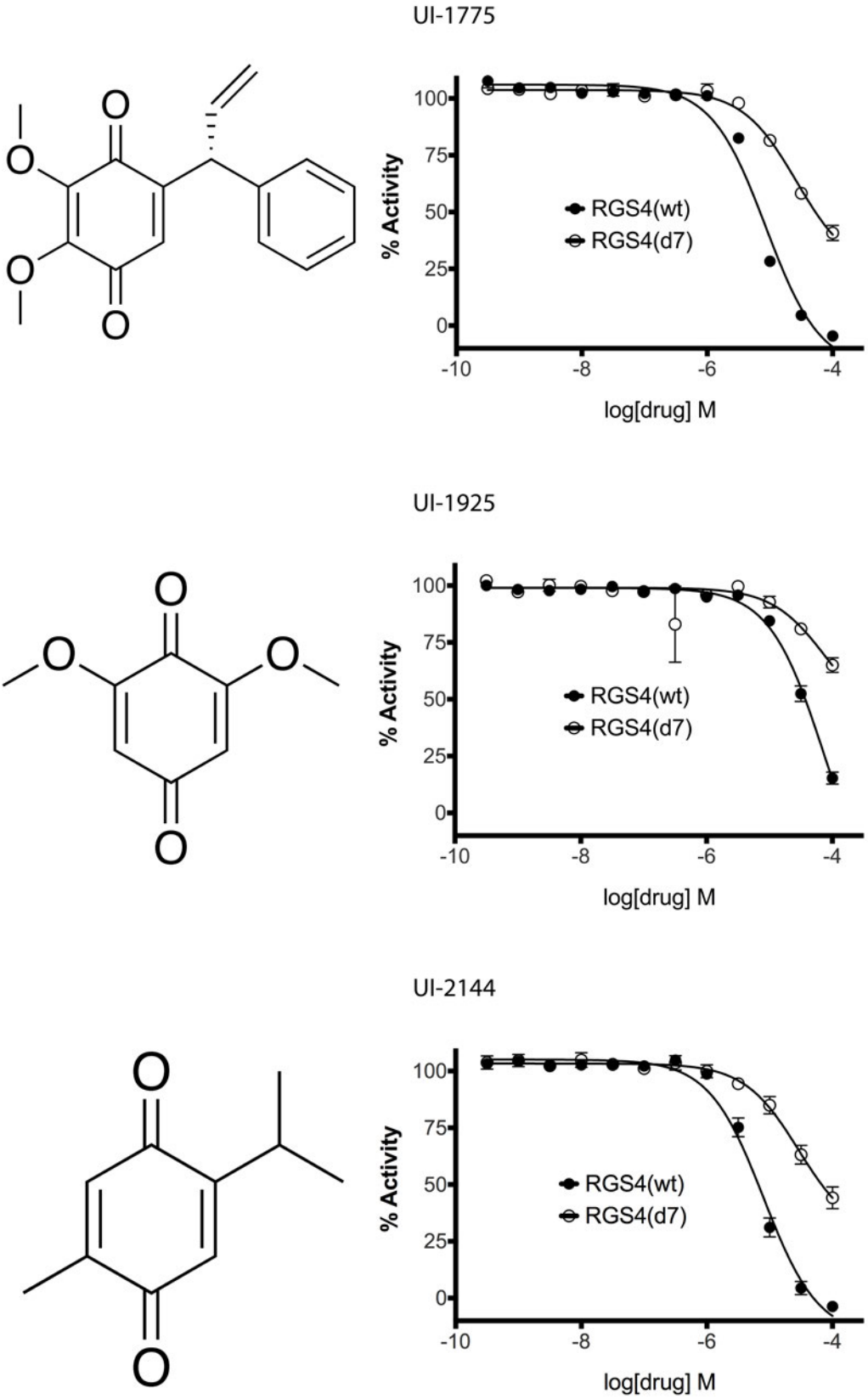

Figure A.3 -- continued

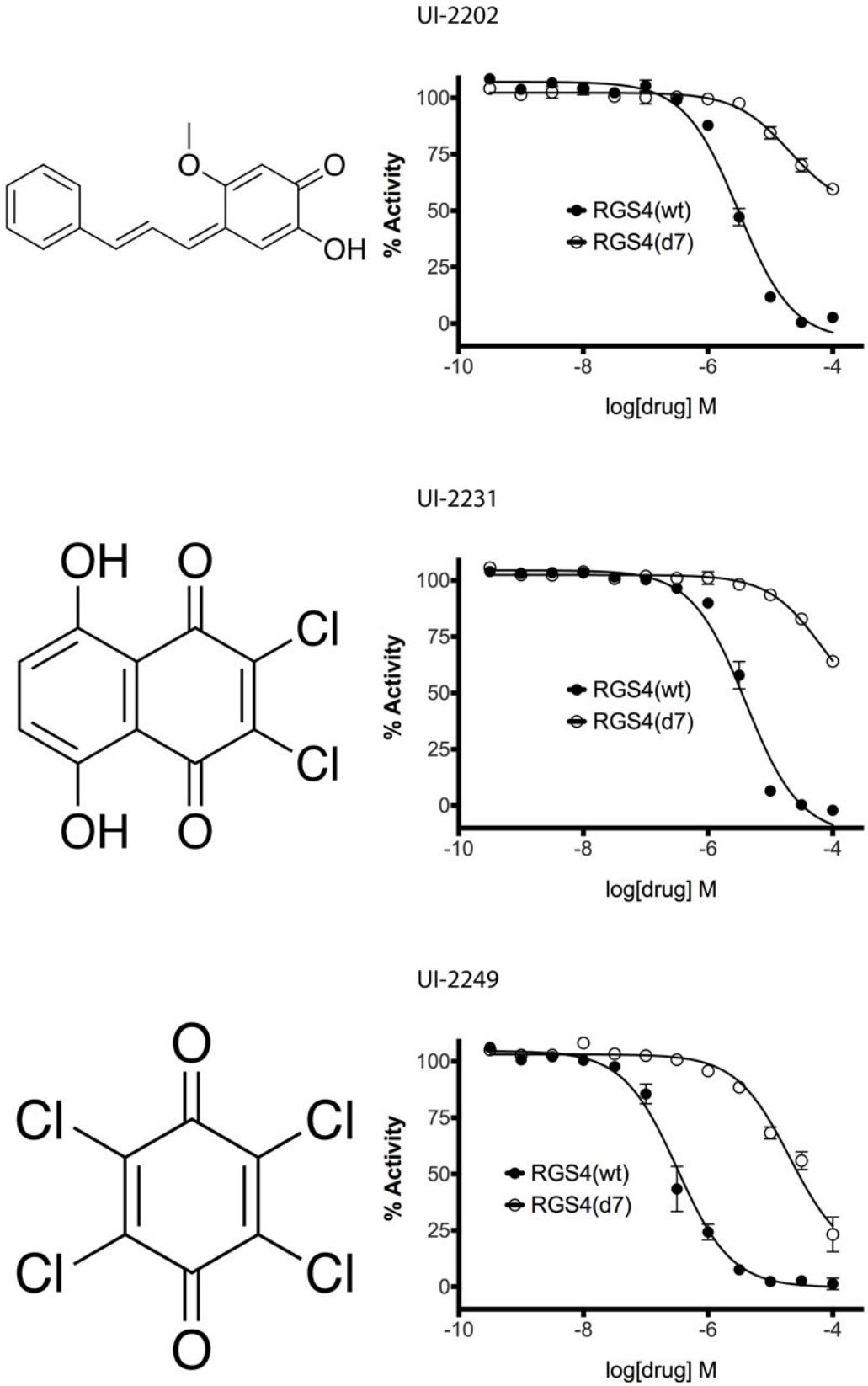

Figure A.3 -- continued

REFERENCES

1. Thomas B, Beal MF (2007) Parkinson's disease. Hum Mol Genet 16 Spec No. 2: R183–R194.

2. Parkinson J (2002) An essay on the shaking palsy. 1817. The Journal of Neuropsychiatry and Clinical Neurosciences. 14: 223–236.

3. McKeith IG, Dickson DW, Lowe J, Emre M, O'Brien JT, et al. (2005) Diagnosis and management of dementia with Lewy bodies: third report of the DLB Consortium. Neurology 65: 1863–1872.

4. Braak H, Del Tredici K, Rub U, de Vos R, Jansen Steur E, Braak E (2003) Staging of brain pathology related to sporadic Parkinson's disease. Neurobiol Aging 24: 197–211.

5. Fearnley J, Lees A (1991) Aging and Parkinson's disease: substantia nigra regional selectivity. Brain 114: 2283–2301.

6. Obeso JA, Rodriguez-Oroz MC, Chana P, Lera G, Rodriguez M, et al. (2000) The evolution and origin of motor complications in Parkinson's disease. Neurology 55: S13–S20 discussion S21–S23.

7. Farrer M (2006) Genetics of Parkinson disease: paradigm shifts and future prospects. Nat Rev Genet. 7(4): 306–318.

8. Polymeropoulos M, Lavedan C, Leroy E, et. al. (1997) Mutation in the alpha-synuclein gene identified in families with Parkinson's disease. Science 276(5321): 2045–2047.

9. Leroy E, Boyer R, Auburger G, et. al. (1998) The ubiquitin pathway in Parkinson's disease. Nature 395(6701): 451–452.

10. Kitada T, Asakawa S, Hattori N, et. al. (1998) Mutations in the parkin gene cause autosomal recessive juvenile parkinsonism. Nature 392(6676):605–608.

11. Zimprich A, Biskup S, Leitner P, et. al. (2004) Mutations in LRRK2 cause autosomal-dominant parkinsonism with pleomorphic pathology. Neuron 44(4): 601–607.

12. Valente E, Abou-Sleiman P, Caputo V, et. al. (2004) Hereditary early-onset Parkinson's disease caused by mutations in PINK1. Science 304(5674): 1158–1160.

13. Bonifati V, Rizzu P, Squitieri F (2003) DJ-1 (PARK7), a novel gene for autosomal recessive, early onset parkinsonism. Neurol Sci 24(3): 159–160.

14. Hwang O (2013) Role of oxidative stress in Parkinson's disease. Exp Neurobiol 22: 11–17.

15. Krüger R, Kuhn W, Müller T, Woitalla D, Graeber M, et al. (1998) Ala30Pro mutation in the gene encoding alpha-synuclein in Parkinson's disease. Nat Genet 18: 106–108.

16. Zimprich A, Biskup S, Leitner P, Lichtner P, Farrer M, et al. (2004) Mutations in LRRK2 cause autosomal-dominant parkinsonism with pleomorphic pathology. Neuron 44: 601–607.

17. Moore DJ, Dawson TM (2008) Value of genetic models in understanding the cause and mechanisms of Parkinson's disease. Curr Neurol Neurosci Rep 8: 288–296.

18. Conway K, Harper J, Lansbury P (1998) Accelerated in vitro fibril formation by a mutant alpha-synuclein linked to early-onset Parkinson's disease. Nat Med 4(11): 1318–1320.

19. Shimura H, Hattori N, Kubo S, et. al. (2000) Familial Parkinson disease gene product, parkin, is a ubiquitin protein ligase. Nat Genet 25(3): 302–305.

20. Canet-Aviks R, Wilson M, Miller D, et. al. (2004) The Parkinson's disease protein DJ-1 is a neuroprotective due to cysteine-sulfinic acid-driven mitochondrial localization. Proc Natl Acad Sci U S A 101(24): 9103–9108.

21. Dauer W, Przedborski S (2003) Parkinson's disease: mechanisms and models. Neuron 39: 889–909.

22. Erickson J, Eiden L, Hoffman B (1992) Expression cloning of a reserpine-sensitive vesicular monoamine transporter. Proc Natl Acad Sci U S A 89(22): 10993–10997.

23. Fon E, Pothos E, Sun B, et. al. (1997) Vesicular transport regulates monoamine storage and release but is not essential for amphetamine action. Neuron 19(6): 1271–1283.

24. Langston JW, Ballard P, Tetrud JW, Irwin I (1983) Chronic Parkinsonism in humans due to a product of meperidine-analog synthesis. Science 219: 979–980.

25. Cohen G (1984) Oxy-radical toxicity in catecholamine neurons. Neurotoxicology 5: 77–82.

26. Day BJ, Patel M, Calavetta L, Chang LY, Stamler JS (1999) A mechanism of paraquat toxicity involving nitric oxide synthase. Proc Natl Acad Sci USA 96: 12760–12765.

27. Betarbet R, Sherer TB, MacKenzie G, Garcia-Osuna M, Panov AV, et al. (2000) Chronic systemic pesticide exposure reproduces features of Parkinson's disease. Nat Neurosci 3: 1301–1306.

28. Duty S, Jenner P (2011) Animal models of Parkinson's disease: a source of novel treatments and clues to the cause of the disease. Br J Pharmacol 164(4) 1357–1391.

29. Martin GE, Myers RD, Newberg DC (1976) Catecholamine release by intracerebral perfusion of 6-hydroxydopamine and desipramine. Eur J Pharmacol 36: 299–311.

30. Lerner TN, Kreitzer AC (2012) RGS4 is Required for Dopaminergic Control of Striatal LTD and Susceptibility to Parkinsonian Motor Deficits. Neuron 73: 347–359.

31. Bjarnadóttir TK, Gloriam DE, Hellstrand SH, Kristiansson H, Fredriksson R, et al. (2006) Comprehensive repertoire and phylogenetic analysis of the G protein-coupled receptors in human and mouse. Genomics 88: 263–273.

32. Schoenlein R, Peteanu L, Mathies R, Shank C (1991) The first step in vision: femtosecond isomerization of rhodopsin. Science 254: 412–415.

33. Arshavsky V, Pugh E (1998) Lifetime Regulation of G Protein-Effector Complex: Emerging Importance of RGS Proteins. Neuron 20: 11–14.

34. He W, Cowan C, Wensel (1998) RGS9, a GTPase accelerator for phototransduction. Neuron 20(1): 95–102.

35. Berman DM, Kozasa T, Gilman AG (1996) The GTPase-activating Protein RGS4 Stabilizes the Transition State for Nucleotide Hydrolysis. J Biol Chem 44: 27209–27212.

36. Tesmer JJG, Berman DM, Gilman AG, Sprang SR (1997) Structure of RGS4 Bound to AlF4−-Activated Giα1: Stabilization of the Transition State for GTP Hydrolysis. Cell 89: 251–261.

37. Hollinger S, Hepler JR (2002) Cellular regulation of RGS proteins: modulators and integrators of G protein signaling. Pharmacol Rev 54: 527–559.

38. Hepler JR (1999) Emerging roles for RGS proteins in cell signalling. Trends Pharmacol Sci 20: 376–382.

39. Berman D, Gilman A (1998) Mammalian RGS Proteins: Barbarians at the Gate. J Biol Chem 273: 1269–1272.

40. Zheng B, De Vries L, Gist Farquhar M (1999) Divergence of RGS proteins: evidence for the existence of six mammalian RGS subfamilies. Trends Biochem Sci 24: 411–414.

41. Chatterjee T, Eapen A, Kanis A, Fisher R (1997) Genomic organization, 5'-flanking region, and chromosomal localization of the human RGS3 gene. Genomics 45(2): 429–433.

42. Bansal G, Druey KM, Xie Z (2007) R4 RGS proteins: regulation of G-protein signaling and beyond. Pharmacol Ther 116: 473–495.

43. Srinivasa SP, Bernstein LS, Blumer KJ, Linder ME (1998) Plasma membrane localization is required for RGS4 function in Saccharomyces cerevisiae. Proc Natl Acad Sci USA 95: 5584–5589.

44. Drenan RM, Doupnik CA, Jayaraman M, Buchwalter AL, Kaltenbronn KM, et al. (2006) R7BP augments the function of RGS7*Gbeta5 complexes by a plasma membrane-targeting mechanism. J Biochem 281: 28222–28231.

45. Kimple RJ, Kimple ME, Betts L, Sondek J, Siderovski DP (2002) Structural determinants for GoLoco-induced inhibition of nucleotide release by Galpha subunits. Nature 416: 878–881.

46. Bernard ML, Peterson YK, Chung P, Jourdan J, Lanier SM (2001) Selective interaction of AGS3 with G-proteins and the influence of AGS3 on the activation state of G-proteins. J Biochem 276: 1585–1593.

47. Nunn C, Mao H Chidiac P, Albert P (2006) RGS17/RGSZ2 and the RZ/A family of regulators of G-protein signaling. Semin Cell Dev Biol 17(3):390–399.

48. Ding L, Mychaleckyj JC, Hegde AN (2007) Full length cloning and expression analysis of splice variants of regulator of G-protein signaling RGS4 in human and murine brain. Gene 401: 46–60.

49. Zhang S, Watson N, Zahner J, Rottman JN, Blumer KJ, et al. (1998) RGS3 and RGS4 are GTPase activating proteins in the heart. J Mol Cell Cardiol 30: 269–276.

50. Erdely HA, Lahti RA, Lopez MB, Myers CS, Roberts RC, et al. (2004) Regional expression of RGS4 mRNA in human brain. Eur J Neurosci 19: 3125–3128.

51. Owen VJ, Burton PB, Mullen AJ, Birks EJ, Barton P, et al. (2001) Expression of RGS3, RGS4 and Gi alpha 2 in acutely failing donor hearts and end-stage heart failure. Eur Heart J 22: 1015–1020.

52. Soundararajan M, Willard F, Turnbull, et. al. Structural diversity in the RGS domain and its interaction with heterotrimeric G protein alpha-subunits. Proc Natl Acad Sci U S A 105(17): 6457–6462.

53. Gold SJ, Han M-H, Herman AE, Ni YG, Pudiak CM, et al. (2003) Regulation of RGS proteins by chronic morphine in rat locus coeruleus. Eur J Neurosci 17: 971–980.

54. Gu Z, Jiang Q, Yan Z (2007) RGS4 Modulates Serotonin Signaling in Prefrontal Cortex and Links to Serotonin Dysfunction in a Rat Model of Schizophrenia. Mol Pharmacol. 71(4): 1030–1039.

55. Ding J, Guzman JN, Tkatch T, Chen S, Goldberg JA, et al. (2006) RGS4-dependent attenuation of M4 autoreceptor function in striatal cholinergic interneurons following dopamine depletion. Nat Neurosci 9: 832–842.

56. Berman DM, Wilkie TM, Gilman AG (1996) GAIP and RGS4 Are GTPase-Activating Proteins for the Gi Subfamily of G Protein α Subunits. Cell 86: 445–452.

57. Roman DL, Talbot JN, Roof RA, Sunahara RK, Traynor JR, et al. (2007) Identification of Small-Molecule Inhibitors of RGS4 Using a High-Throughput Flow Cytometry Protein Interaction Assay. Mol Pharmacol 71: 169–175.

58. Roof RA, Roman DL, Clements ST, Sobczyk-Kojiro K, Blazer LL, et al. (2009) A covalent peptide inhibitor of RGS4 identified in a focused one-bead, one compound library screen. BMC Pharmacol 9: 9.

59. Roman DL, Blazer LL, Monroy CA, Neubig RR (2010) Allosteric Inhibition of the Regulator of G Protein Signaling-Gα Protein-Protein Interaction by CCG-4986. Mol Pharmacol 78: 360–365.

60. Gold S, Ni Y, Dohlman H, Nestler E (1997) Regulators of G-protein signaling (RGS) proteins: region-specific expression of nine subtypes in rat brain. J Neurosci 17: 8024–8037.

61. Schwendt M, Gold S, McGinty J (2006) Acute amphetamine down-regulates RGS4 mRNA and protein expression in rat forebrain:distinct roles of D1 and D2 dopamine receptors. 96(6): 1606–1615.

62. de Rover M, Lodder J, Kits K, et. al. (2002) Cholinergic modulation of nucleus accumbens medium spiny neurons. Eur J Neurosci 16(12): 2279–2290.

63. Grillet N, Pattyn A, Contet C, et. al. Generation and Characterization of Rgs4 Muatnt Mice. Mol Cell Biol 25(10): 4221–4228.

64. Obeso JA, Rodriguez-Oroz MC, Goetz CG, Marin C, Kordower JH, et al. (2010) Missing pieces in the Parkinson's disease puzzle. Nat Med 16: 653–661.

65. Corrigan FM, Murray L, Wyatt CL, Shore RF (1998) Diorthosubstituted polychlorinated biphenyls in caudate nucleus in Parkinson's disease. Exp Neurol 150: 339–342.

66. Richardson JR, Shalat SL, Buckley B, Winnik B, O'Suilleabhain P, et al. (2009) Elevated serum pesticide levels and risk of Parkinson disease. Arch Neurol 66: 870–875.

67. Zielinski T, Kimple AJ, Hutsell SQ, Koeff MD, Siderovski DP, et al. (2009) Two Gαi1 Rate-Modifying Mutations Act in Concert to Allow Receptor-Independent, Steady-State Measurements of RGS Protein Activity. J Biomol Screen 14: 1195–1206.

68. Mukhopadhyay S, Ross EM (1999) Rapid GTP binding and hydrolysis by Gq promoted by receptor and GTPase-activating proteins. Proc Natl Acad Sci USA 96: 9539–9544.

69. Monroy CA, Mackie DI, Roman DL (2013) A High Throughput Screen for RGS Proteins Using Steady State Monitoring of Free Phosphate Formation. PLoS ONE 8: e62247.

70. Gottlieb RAR (2011) Cell death pathways in acute ischemia/reperfusion injury. J Cardiovasc Pharmacol Ther 16: 233–238.

71. Yao JK, Keshavan MS (2011) Antioxidants, redox signaling, and pathophysiology in schizophrenia: an integrative view. Antioxid Redox Signal 15: 2011–2035.

72. Siems W, Grune T (2003) Intracellular metabolism of 4-hydroxynonenal. Mol Aspects Med 24: 167–175.

73. Uchida K (2003) 4-Hydroxy-2-nonenal: a product and mediator of oxidative stress. Prog Lipid Res 42: 318–343.

74. Blanc EME, Kelly JFJ, Mark RJR, Waeg GG, Mattson MPM (1997) 4-Hydroxynonenal, an aldehydic product of lipid peroxidation, impairs signal transduction associated with muscarinic acetylcholine and metabotropic glutamate receptors: possible action on G alpha(q/11). J Neurochem 69: 570–580.

75. Neubig RR, Connolly MP, Remmers AE (1994) Rapid kinetics of G protein subunit association: a rate-limiting conformational change? FEBS Lett 355: 251–253.

76. Young KH, Wang Y, Bender C, Ajit S, Ramirez F, et al. (2004) Yeast-Based Screening for Inhibitors of RGS Proteins. Meth Enzymol 389: 277–301.

77. Roman DL, Ota S, Neubig RR (2009) Polyplexed Flow Cytometry Protein Interaction Assay: A Novel High-Throughput Screening Paradigm for RGS Protein Inhibitors. J Biomol Screen 14: 610–619.

78. Siedlecki AM, Jin X, Thomas W, Hruska KA, Muslin AJ (2011) RGS4, a GTPase activator, improves renal function in ischemia-reperfusion injury. Kidney Int 80: 263–271.

79. Schwab SG, Wildenauer DB (2009) Update on key previously proposed candidate genes for schizophrenia. Curr Opin Psychiatry 22: 147–153.

80. Davydov IV, Varshavsky A (2000) RGS4 Is Arginylated and Degraded by the N-end Rule Pathway in Vitro. J Biol Chem. 275(30): 22931–22941.

81. Kapust RB, Tözsér J, Fox JD, Anderson DE, Cherry S, et al. (2001) Tobacco etch virus protease: mechanism of autolysis and rational design of stable mutants with wild-type catalytic proficiency. Protein Eng 14: 993–1000.

82. Shankaranarayanan A, Thal DM, Tesmer VM, Roman DL, Neubig RR, et al. (2008) Assembly of High Order Gαq-Effector Complexes with RGS Proteins. J Biol Chem 283: 34923–34934.

83. Sternweis PC, Robishaw JD (1984) Isolation of Two Proteins with High Affinity for Guanine Nucleotides from Membranes of Bovine Brain. J Biol Chem 259: 13806–13813.

84. Baykov AA, Evtushenko OA, Avaeva SM (1988) A Malachite Green Procedure for Orthophosphate Determination and Its use in Alkaline Phosphatase-Based Enzyme Immunoassay. Anal Biochem 171: 266–270.

85. Elkon H, Melamed E, Offen D (2004) Oxidative stress, induced by 6-hydroxydopamine, reduces proteasome activities in PC12 cells: implications for the pathogenesis of Parkinson's disease. J Mol Neurosci 24: 387–400.

86. Zhang P, Hatter A, Liu B (2007) Manganese chloride stimulates rat microglia to release hydrogen peroxide. Toxicol Lett 173: 88–100.

87. Doorn JA, Petersen DR (2002) Covalent modification of amino acid nucleophiles by the lipid peroxidation products 4-hydroxy-2-nonenal and 4-oxo-2-nonenal. Chem Res Toxicol 15: 1445–1450.

88. Gudermann T, Nürnberg B, Schultz G (1995) Receptors and G proteins as primary components of transmembrane signal transduction. J Mol Med 73: 51–63.

89. Gilman AG (1987) G Proteins: Transducers of Receptor-Generated Signals. Annu Rev Biochem 56: 615–649.

90. Berman DM, Gilman AG (1998) Mammalian RGS Proteins: Barbarians at the Gate. J Biol Chem 273: 1269–1272.

91. Mackie DI, Roman DL (2011) Development of a Novel High-Throughput Screen and Identification of Small-Molecule Inhibitors of the Gα-RGS17 Protein-Protein Interaction Using AlphaScreen. J Biomol Screen 16: 869–877.

92. Blazer LL, Zhang H, Casey EM, Husbands SM, Neubig RR (2011) A Nanomolar-Potency Small Molecule Inhibitor of Regulator of G-Protein Signaling Proteins. Biochemistry 50: 3181–3192.

93. Chidiac P, Markin VS, Ross EM (1999) Kinetic Control of Guanine Nucleotide Binding to Soluble Gαq. Biochem Pharmacol 58: 39–48.

94. Ingi T, Krumins AM, Chidiac P, Brothers GM, Chung S, et al. (1998) Dynamic Regulation of RGS2 Suggests a Novel Mechanism in G-protein Signaling and Neuronal Plasticity. J Neurosci 18: 7178–7188.

95. Coleman DE, Berghuis AM, Lee E, Linder ME, Gilman AG, et al. (1994) Structures of Active Conformations of Giα1 and the Mechanism of GTP Hydrolysis. Science 265: 1405–1412.

96. Freissmuth M, Gilman AG (1989) Mutations of GSα Designed to Alter the Reactivity of the Protein with Bacterial Toxins. J Biol Chem 264: 21907–21914.

97. Posner BA, Mixon MB, Wall MA, Sprang SR, Gilman AG (1998) The A326S Mutant of Giα1 as an Approximation of the Receptor-bound State. J Biol Chem 273: 21752–21758.

98. Iiri T, Herzmark P, Nakamoto JM, Van Dop C, Bourne HR (1994) Rapid GDP release from Gsα in patients with gain and loss of endocrine function. Nature 371: 164–168.

99. Kodama T, Fukui K, Kometani K (1986) The Initial Phosphate Burst in ATP Hydrolysis by Myosin and Subfragment-1 as Studied by a Modified Malachite Green Method for Determination of Inorganic Phosphate. J Biochem 99: 1465–1472.

100. Bell RD, Doisy EA (1920) Rapid Colorimertric Methods for the Determination of Phosphorus in Urine and Blood. J Biol Chem 44: 55–67.

101. Itaya K, Ui M (1966) A New Micromethod for the Colorimetric Determination of Inorganic Phosphate. Clin Chim Acta 14: 361–366.

102.Blazer LL, Roman DL, Chung A, Larsen MJ, Greedy BM, et al. (2010) Reversible, Allosteric Small-Molecule Inhibitors of Regulator of G protein Signaling Proteins. Mol Pharmacol 78: 524–533.

103.Soundararajan M, Willard FS, Kimple AJ, Turnbull AP, Ball LJ, et al. (2008) Structural diversity in the RGS domain and its interaction with heterotrimeric G protein alpha-subunits. Proc Natl Acad Sci USA 105: 6457–6462.

104.Weisman JL, Liou AP, Shelat AA, Cohen FE, Guy RK, et al. (2006) Searching for New Antimalarial Therapeutics amongst Known Drugs. Chem Biol Drug Des 67: 409–416.

105.Hansen J, Bross P (2010) A Cellular Viability Assay to Monitor Drug Toxicity. Methods Mol Biol 648: 303–311.

106.Raja SM, Clubb RJ, Ortega-Cava C, Williams SH, Bailey TA, et al. (2011) Anticancer activity of Celastrol in combination with ErbB2-targeted therapeutics for treatment of ErbB2-overexpressing breast cancers. Cancer Biol Ther 11: 263–276.

107.Mao H, Zhao Q, Daigle M, Ghahremani MH, Chidiac P, et al. (2004) RGS17/RGSZ2, a Novel Regulator of Gi/o, Gz, and Gq Signaling. J Biol Chem 279: 26314–26322.

108.Conklin BR, Chabre O, Wong YH, Federman AD, Bourne HR (1992) Recombinant Gqα. J Biol Chem 267: 31–34.

109.Wong YH, Federman A, Pace AM, Zachary I, Evans T, et al. (1991) Mutant α subunits of Gi2 inhibit cyclic AMP accumulation. Nature 351: 63–65.

110.Krumins AM, Gilman AG (2002) Assay of RGS Protein Activity in Vitro Using Purified Components. Meth Enzymol 344: 673–685.

111.Marin EP, Krishna AG, Sakmar TP (2001) Rapid Activation of Transducin by Mutations Distant from the Nucleotide-binding Site. J Biol Chem 276: 27400–27405.

112.Girotto S, Sturlese M, Bellanda M, Tessari I, Cappellini R, et al. (2012) Dopamine-derived quinones affect the structure of the redox sensor DJ-1 through modifications at Cys-106 and Cys-53. J Biol Chem 287: 18738–18749.

113.Nakabeppu Y, Tsuchimoto D, Yamaguchi H, Sakumi K (2007) Oxidative damage in nucleic acids and Parkinson's disease. J Neurosci Res 85: 919–934.

114.Riederer P, Sofic E, Rausch WD, Schmidt B, Reynolds GP, et al. (1989) Transition metals, ferritin, glutathione, and ascorbic acid in parkinsonian brains. J Neurochem 52: 515–520.

115.Haavik J, Almas B, Flatmark T (1997) Generation of Reactive Oxygen species by Tyrosine Hydroxylase: A Possible Contribution to the Degeneration of Dopaminergic Neurons? J Neurochem 68(1): 328–332.

116.Sandri G, Panfili E, Ernster L (1990) Hydrogen peroxide production by monoamine oxidase in isolated rat-brain mitochondria: its effect on glutathione levels and Ca2+ flux. Biochim Biophys Acta 1035(3): 300–305.

117.Burke W, Li S, Chung H, et. al. (2004) Neurotoxicity of MA metabolites of catecholamine neurotransmitters: role in neurodegenerative diseases. Neurotoxicology 25: 101–115.

118.Lee CS, Han JH, Jang YY, Song JH, Han ES (2002) Differential effect of catecholamines and MPP(+) on membrane permeability in brain mitochondria and cell viability in PC12 cells. Neurochem Int 40: 361–369.

119.Qian L, Flood PM, Hong J-S (2010) Neuroinflammation is a key player in Parkinson's disease and a prime target for therapy. J Neural Transm 117: 971–979.

120.Zhang Y, Yang J-H (2013) Activation of the PI3K/Akt pathway by oxidative stress mediates high glucose-induced increase of adipogenic differentiation in primary rat osteoblasts. J Cell Biochem [Epub ahead of print].

121.Pomytkin IA (2012) H2O2 Signalling Pathway: A Possible Bridge between Insulin Receptor and Mitochondria. Curr Neuropharmacol 10: 311–320.

122.Cao D-S, Zhong L, Hsieh T-H, Abooj M, Bishnoi M, et al. (2012) Expression of transient receptor potential ankyrin 1 (TRPA1) and its role in insulin release from rat pancreatic beta cells. PLoS ONE 7: e38005.

123.Członkowska A, Kohutnicka M, Kurkowska-Jastrzebska I, Członkowski A (1996) Microglial reaction in MPTP (1-methyl-4-phenyl-1,2,3,6-tetrahydropyridine) induced Parkinson's disease mice model. Neurodegeneration 5: 137–143.

124.Bodenstein J, Sunahara RK, Neubig RR (2007) N-terminal residues control proteasomal degradation of RGS2, RGS4, and RGS5 in human embryonic kidney 293 cells. Mol Pharmacol 71: 1040–1050.

125.Ishii T, Sakurai T, Usami H, Uchida K (2005) Oxidative modification of proteasome: identification of an oxidation-sensitive subunit in 26 S proteasome. Biochemistry 44: 13893–13901.